Gap Junction Protein Connexin 43 – an Unexpected Regulator of Brain Endothelial Permeability in Familial Cerebral Cavernous Malformations Type III.

By

Allison M. Johnson

A dissertation submitted in partial fulfillment
of the requirements for the degree of
Doctor of Philosophy
(Molecular and Cellular Pathology)
at the University of Michigan
2017

Doctoral Committee:

Associate Professor Anuska Andjelkovic Zochowska, Chair
Professor Richard F. Keep
Professor Celina G. Kleer
Professor Michael M. Wang

johnsam@umich.edu
ORCiD: 0000-0002-1425-9991

To Cameron, the best brother that anyone could ask for, my life-long protector and friend. You have shaped my life in so many ways. My accomplishments are your accomplishments.

Acknowledgments

First and foremost, I must thank my thesis advisor, Anuska Andjelkovic-Zochowska for all of the guidance throughout my graduate studies. I came into the lab lacking the confidence to pursue my own ideas but, through your unwavering support and encouragement, leave the lab as a confident, independent thinker and do-er. I am proud of how we turned a simple question about Cx43 into a whole body of work. I always felt like my ideas were valued and for that, I am forever grateful. And of course thank you to Svetlana Stamatovic, whose unique, imaginative, outside-of-the-box thinking about scientific questions in and out of the lab was truly inspiring. You helped me appreciate and find humor in the little things in life and I'll forever be curious about what conversations the birds are really having.

Thank you to the undergraduate students I had the opportunity to mentor during my graduate studies, including Anna Hu, Kaylee Witte and Jennifer Choi. In addition to providing assistance with my projects and being friendly faces to talk to, you also taught me the art of mentorship, opening my eyes to the difficulties and joys of being in a leadership position.

Thank you to my committee members: Richard Keep, Michael Wang and Celina Kleer. You all played central roles in the progression of my project from an initial set of questions to the body of work it is now. I am grateful for all of the input and questions during committee meetings and outside of them that made this thesis something that I can be proud of. In addition to the scientific contributions that you've made to this body of work, you also contributed greatly to my development as a confident speaker. Committee meetings provided a unique time for me to learn how to present to a group of experts while feeling, especially in the beginning, intimidated by the vast amount of knowledge contained in one room.

For that, I am truly grateful. Finally, I can only hope to one day pay forward the amount of time you all devoted to help make my thesis and professional development possible.

I'd also like to thank the Molecular and Cellular Pathology graduate program. Thank you to Laura Labut for an endless amount of quickly answered emails, always having the answers to everything and many more behind-the-scenes work that I'm not even aware of. Thank you to Zaneta Nikolovska-Coleska for your support throughout the ups and downs of my graduate studies and supporting the activities of the student group, without whom I would not have made it through graduate school with any amount of sanity. The pathology student group has been such a joy to be a part of, whether it is our student lunches, trivia nights, camping trips or kickball teams. The friendships I've made in this group have had an enormous impact on my professional and personal growth and I look forward to our continued support of each other in the next phases of our lives.

It goes without saying that I owe a debt of gratitude to my family. Thank you to my parents for providing me with an abundance of intellectual and character-building opportunities throughout my life. In addition to always supporting my academic interests, you've both invested time and money to help make me a well-rounded person with a love of sports, camping, travel, sewing and after much trial and error as a 16-year-old, how to properly use my car defroster. And of course, thank you to my brother Cameron, to whom this dissertation is dedicated, for all of the love and companionship since day 1. I will forever cherish the memories of our reconnaissance missions with Yellow Dog on the hill, Christmas Eve blanket forts, nighttime car rides with the music blasting and so many others. I am proud and grateful to have you as my brother and can't wait to see what the future holds for us! Thank you also to Laura, the sister I never had, for all of the phone calls, laughter and emotional support over the years. I can't believe it's been 10 years.

Finally, thank you to my amazing partner in crime, Brian. You have been a source of unwavering support and needed distraction over the past year. You have been, and continue to be, my biggest

cheerleader. I am so excited to start a new chapter of our lives together in Chicago, continue to be same-same but different people and celebrate in whatever the future has in store for us. Should we hug now?

Table of Contents

Chapter 4: Over-expression of the C-terminal Tail of Connexin 43 Regulates Brain Endothelial Cell Permeability

Chapter 5: Conclusions, Future Directions and Final Remarks

List of figures

List of Abbreviations

fCCM, familial Cerebral Cavernous Malformations
fCCM3, familial Cerebral Cavernous Malformations type III
NVU, neurovascular unit
ECs, endothelial cells
mBECs, murine brain endothelial cells
VEGF, vascular endothelial growth factor
TGF-b, transforming growth factor beta
ICAP1, integrin cytoplasmic domain-associated protein 1
KO, knockout
KD, knockdown
iEcKO, inducible endothelial-specific knockout mice
PDGF/PDGFR-β – platelet-derived growth factor (receptor) beta
BBB, blood-brain barrier
Cxs, connexins
Cx43, connexin of 43kDa
GJ, gap junction
GJIC, gap junction intercellular communication
HC, hemichannel
TJ, tight junction
ZO-1, zonula occludens 1
TEER, transendothelial electrical resistance
AJ, adherens junction
CCM3KD, siRNA-mediated knock down of *ccm3*
STRIPAK, Striatin-interacting phosphatase and kinase complex
GAP27, Cx43 GJ and HC inhibitor
GAP19, Cx43 HC inhibitor
LY, LuciferYellow
43-Cx43, 43kDa Cx43
20-Cx43, 20kDa Cx43 isoform
FL^{over}, full length Cx43-overexpressing mBECs
213^{over}, 20kDa Cx43 isoform overexpressing mBECs
FRET, forester resonance energy transfer
FRAP, fluorescence recovery after photo-bleaching
Gd-DTPA, gadolinium diethylenetriaminepentacetate

Abstract

Familial Cerebral Cavernous Malformations type III (fCCM3) is a disease of the cerebrovascular system caused by loss-of-function mutations in *pdcd10* (ccm3) that result in dilated capillary beds susceptible to hemorrhage. No effective pharmacologic treatment is available. Prior to hemorrhage, fCCM3 lesions are characterized by a hyperpermeable blood brain barrier (BBB) that is the key pathologic feature of fCCM3. We have identified that connexin 43 (Cx43), a gap junction (GJ) protein incorporated into the BBB junction complex, is upregulated in lesions of murine model of fCCM3 ($ccm3^{+/-}p53^{-/-}$). Importantly, we have found that Cx43 is highly expressed in developing lesions permeable to gadolinium diethylenetriaminepentacetate (Gd-DTPA) prior to hemorrhage. In murine brain endothelial cells (mBECs) *in vitro*, siRNA-mediated ccm3 knockdown (CCM3KD) upregulated Cx43 protein expression, increased GJ plaque size and GJ intracellular communication (GJIC) and increased barrier permeability. Barrier hyperpermeability was blocked by GAP27, a peptide inhibitor of Cx43 GJIC. Cx43 GJs appear to regulate permeability via effects on tight junction (TJ) formation. In particular, TJ protein ZO-1 preferentially accumulates as plaque-like structures at Cx43 GJs, only exhibiting fragmented ZO-1 staining at the TJs along the cell border. Inhibition of Cx43 GJs with GAP27 in CCM3KD cells restored ZO-1 to TJ structures and reduced plaque accumulation at Cx43 GJs. The TJ protein claudin-5 was also fragmented at TJs in CCM3KD cells, and GAP27 treatment lengthened TJ-associated fragments and increased transcellular claudin 5-claudin 5 interaction.

We have additionally identified that overexpression of Cx43 and its 20kDa isoform (20-Cx43) in mBECs alone recapitulates many aspects of CCM3KD cells, including increased GJIC, increased hemichannel activity and increased permeability. Full length and 20-Cx43-overexpressing cells also display fragmented ZO-1 TJ staining. Intriguingly we observe that mBECs overexpressing 20-Cx43 have altered

endogenous Cx43 and TJ gene transcription as well as a depletion of full length Cx43 from the chromatin-bound cellular compartment that mirrors CCM3KD cells. Overall, we demonstrate that Cx43 expression and GJIC in fCCM3 and Cx43 overexpressing cells regulate barrier permeability by a TJ-dependent mechanism. Importantly, Cx43 GJIC represents a potential target to pursue further in the search for pharmacologic fCCM3 treatments.

Chapter 1: Introduction

1.1 The Blood Brain Barrier

1.1.1 Functions of the Blood Brain Barrier

The blood brain barrier (BBB) was first described by Paul Ehrlich in a series of experiments in which dye injected into the circulatory system did not diffuse into the brain, while it could be seen in other organs of the body (1,2). Later observations determined that neurotoxic agents were only fatal when injected into the cerebrospinal fluid but not the circulatory system (2-4). Given the importance of neurological function to survival, the BBB serves as an evolved mechanism that prevents non-selective introduction of blood-borne material into the brain. Many levels of regulation exist to ensure competence of the barrier, including specialized neurovascular architecture and endothelial junctions. A vast number of diseases can cause primary or secondary BBB insufficiency, including inflammatory diseases that disrupt cellular homeostasis to promote leakage across the barrier, as in epilepsy or CNS vasculitis (5). Secondary pathologies of Alzheimer's disease and Parkinson's disease arise from insufficient clearance of toxic substances from the brain (5). Understanding the cellular mechanisms regulating barrier permeability in both homeostatic and disease states is of the utmost importance to the prevention and treatment of disease.

1.1.2 The neurovascular unit in development and homeostasis

The neurovascular unit (NVU) is comprised of endothelial cells (ECs) lining the neurovascular capillary beds and their supporting cell types, including pericytes and astrocytes, and the basement membrane (Fig 1.1.1). While ECs are the only cell type of the NVU to come in direct contact with the blood and represent the central gate keepers to the brain, the NVU is required in its entirety to allow adequate function of ECs

in the BBB. This section is intended to give a brief introduction to the important features of the NVU in development and homeostasis.

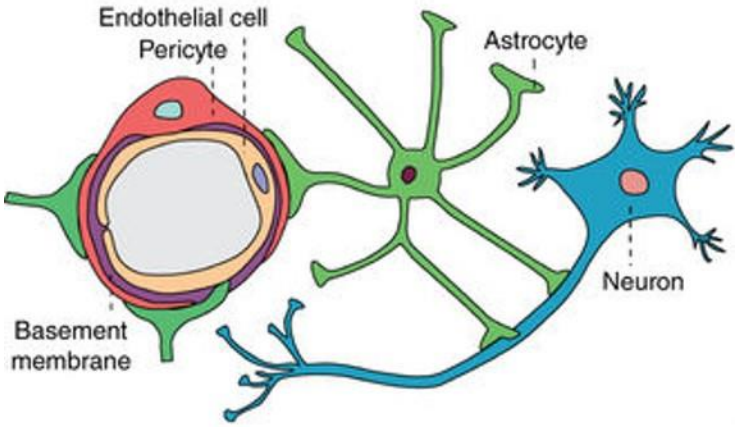

Figure 1.1.1. Structure of the neurovascular unit. Capillary beds of the NVU are lined by endothelial cells. Pericytes encircle endothelial cells at a ratio of approximately 1:4 pericyte:endothelial cell. Pericytes and endothelial cells are connected by junctions, including gap junctions, and share a basement membrane. Astrocytic endfeet attach to endothelial cells and pericytes, bridging the vessel to neurons. Adapted from Sweeney MD et al., *Nature* 2016.

Endothelium of the BBB are highly specialized and exhibit marked differences from endothelium lining the general circulatory system. Such specialized features include inhibition of pinocytosis and bulk transcytosis, both of which reduce the transport of material into and out of endothelial cells, termed transcellular permeability. Additionally, brain ECs have tighter regulation of leukocyte adhesion molecule expression, reducing the extravasation of immune cells (5). In addition to preventing transcellular permeability, brain ECs also express highly regulated junctional proteins that form such tight junctions between neighboring ECs that even ions can only pass through a selective mechanism based on tight junction strand pore formation (6,7). Junctional proteins form the other main feature of the BBB – prevention of paracellular permeability. The features of brain ECs that regulate the BBB at the cellular level are discussed in more detail in the next section.

Pericytes regulate blood flow through regulating vessel diameter via changes to the actin cytoskeleton (8). PDGFR-β and PDGF-β knockout (KO) mice lack brain pericytes and die due to CNS microhemorrhages (9). The cellular mechanism of this KO phenotype lies in the disrupted TJ presence and organization (10, 11). During development, nascent ECs produce PDGF-β, attracting pericytes to the sprouting vessel (12). Subsequently, secretion of TGF-β by both cell types promotes adhesion of pericytes to the growing vessel (13, 14). SMAD4 KO mice, lacking TGF-β receptor, are embryonic lethal and display

decreased TJ formation, vessel permeability and hemorrhage (15). The mechanism by which TGF-β promotes pericyte adhesion is through upregulation of N-cadherin on ECs. Notch signaling between pericytes and ECs also regulates the expression of N-cadherin and sphingosine-1 phosphate (S1P) intercellular signaling stimulates the transportation of N-cadherin to the EC plasma membrane (16). Deficiencies in any of these pathways result in BBB integrity defects as a consequence of lack of proper EC/pericyte interaction.

Astrocytes regulate the BBB through regulating the concentration of materials in the extracellular space between astrocytic endfeet and the EC basement membrane, including neurotransmitters, ions and water. Co-culture experiments suggest that astrocytes release soluble factors, including fibroblast growth factor 2 (FGF2) and interleukin-6 (IL-6), that promote maturation of BBB (17, 18). ECs grown in co-culture with astrocytes demonstrate more well-formed TJs and decreased monolayer permeability compared to ECs cultured by themselves (19). *In vitro* experiments suggest that astrocytes may also promote BBB formation through secretion of Ang-1, which activates Tie-2 receptors of ECs and leads to increased expression of TJ proteins (20). In addition to TJ protein expression, Ang-1, in conjunction with downstream activation of EC Ang-1 receptor AT-1, can regulate the accumulation of occludin in lipid rafts, and in this way, also contribute to EC barrier properties (21).

The basement membrane is composed of structural proteins and adhesion molecules secreted by NVU cells. Structural proteins including collagen IV, laminin and fibronectin, create the platform upon which cells of the NVU can interact (22). Adhesion molecules provide a docking station for those cells which express transmembrane adhesion molecule receptors, including integrins. β1-integrins are particularly important for the differentiation and stabilization of ECs and vessels in the mouse brain. β1-integrin deficiencies prevent interaction with laminin, thus preventing adhesion to the ECM and downstream signaling associated with β1-integrin stimulation, including expression of TJ protein claudin-5 (23). In addition, integrin binding promotes astrocytic activation of TGF-β that results in activation of

stabilization pathways preventing angiogenesis (24). Finally, in addition to structural and adhesion proteins in ECM, signaling molecules can also be secreted and trapped within the matrix, allowing for latent effects when they are activated or inhibited in particular conditions (25, 26).

Other key pathways in ECs contribute to BBB development and maturation in addition to support from NVU cell types. Angiogenesis occurs in part by the release of vascular endothelial growth factor (VEGF) from neuroprogenitor cells, stimulating the sprouting of capillaries from larger vessels (27-29). Endothelial VEGF receptor 2 (VEGFR2) plays a significant role in angiogenesis by activating the Ras-Raf-MEK pathway, PI3K-Akt pathway, and p38 MAPK–HSP27 pathway, leading to EC proliferation, survival and migration, respectively (30). The Wnt-β-catenin pathway is also involved in angiogenesis in development. Wnt7b-KO mice die of brain hemorrhage between E11-E13, and canonical Wnt signaling induces the expression of Glut1 transporter in the developing brain (31, 32). Additionally, accumulation of β-catenin enhances downstream signaling of VEGFR2, promoting further angiogenesis and sprouting (33). Beyond angiogenesis, barrier maturation occurs through the activation of sonic hedgehog (SHH). Shh-KO mice die between E11 and E13.5 due to BBB insufficiency (34). Assessment of TJ expression indicates significantly reduced expression of occludin and claudin-5 (34). KO mice of elements downstream of Shh also lead to embryonic lethality due to an inability to close the barrier and associated deficiency in TJ protein expression (34).

1.1.3 Endothelial cells and BBB occlusion

With the help of pericytes, astrocytes and other features of the NVU, ECs function as the gate keepers of the BBB by regulating highly selective transcellular and paracellular permeability in a manner distinct from ECs in the general circulatory system. Cerebrovascular ECs regulate transcellular permeability through mechanisms including active efflux, carrier-mediated transport (CMT), receptor-mediated transport (RMT) and the major facilitator superfamily of transport molecules, among others. Insufficiency or aberrant activation of systems regulating transcellular permeability can result in a

hyperpermeable BBB. For example, neurological defects in Alzheimer's and Parkinson's Disease are associated with alterations in active efflux, a process mediated by ATP-binding cassette (ABC) proteins on the luminal side of ECs that create ATP-driven pumps to promote the efflux of metabolites and other small molecules (35-37). While the majority of this dissertation will focus on the regulation of paracellular permeability, it is important to keep in mind that mechanisms regulating transcellular permeability are also paramount to BBB integrity and have been implicated in disease pathogenesis (35-41).

Paracellular permeability, the ability of molecules, blood and other cell types to pass between two ECs, is maintained by multiple junctional complexes including tight junctions (TJs) and adherens junctions (AJs) (Fig. 1.1.2). Tight and adherens junctions are organized in similar manners with different component proteins. Each junction complex includes transmembrane proteins that span the intercellular space and bind to their counterparts on neighboring endothelial cells. These *trans*-interactions, particularly those of

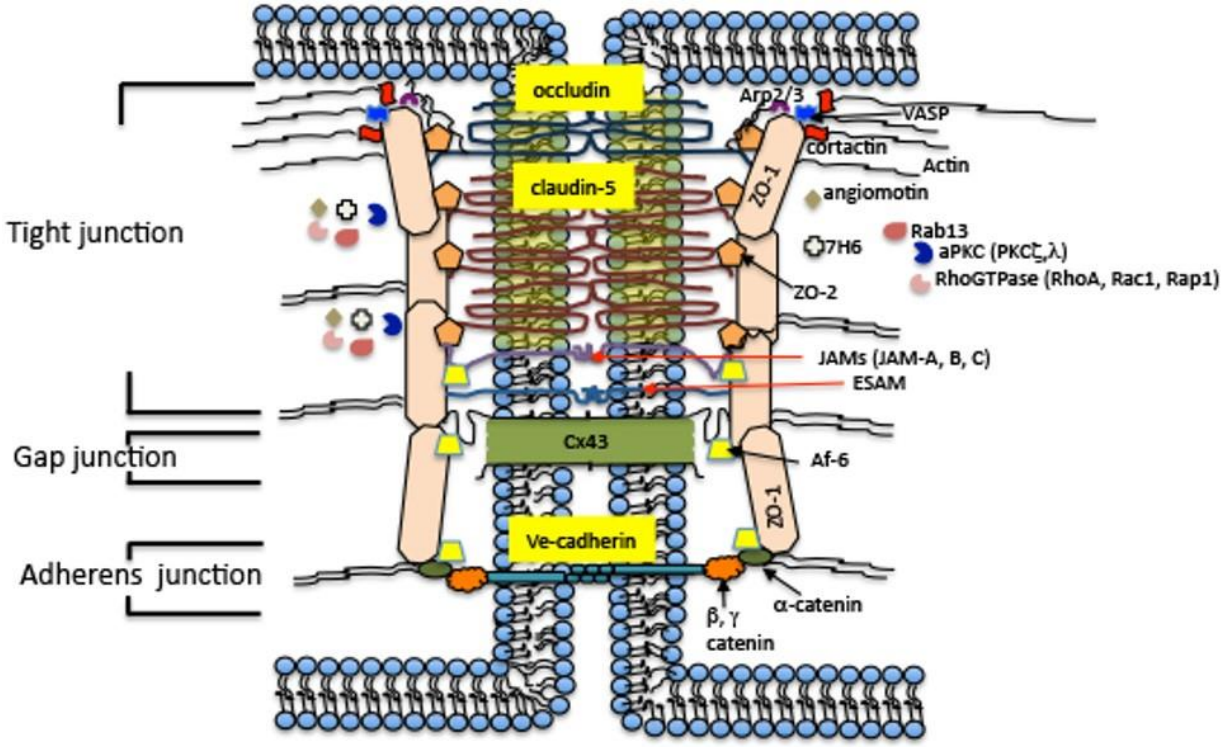

Figure 1.1.2. Endothelial junctions of the Blood Brain Barrier. Barrier occlusion is achieved through the function of junction complexes connecting neighboring endothelial cells. Transmembrane proteins Occludin and Claudin-5 comprise TJs, VE-Cadherin comprise Ajs, and Cx43 form GJ channels between cells. Transmembrane proteins are anchored to the cytoskeleton by adapter proteins including ZO-1. Adapted from Stamatovic et al., *Tissue Barriers*, 2016.

the TJs, serve as the principal mechanism by which the paracellular space is occluded. The transmembrane proteins of TJs and AJs are anchored to the actin cytoskeleton by scaffolding proteins. The expression and localization of each junctional component is coordinated by various cellular signals throughout development and homeostasis. Each junction is described in detail below.

Multiple transmembrane proteins can be found in TJs. Claudin-5 is the most abundantly expressed claudin in brain endothelia, with approximately 1000 fold greater mRNA expression compared to other claudins (42). Claudin-3 is also expressed in brain endothelial cells, however, it is much more abundant during embryonic development and less so in adult brain ECs (43). In addition to claudin-3's expression pattern, a role for claudin-3 in development is supported by the observation that it is inducible by Wnt/β-catenin signaling and potentially represents a mechanism by which alterations to the Wnt/β-catenin pathway reduces BBB integrity in development (44). Claudin-1 and claudin-12 are also expressed by brain ECs, however, their expression is low during homeostasis while high expression can be observed in disease states, such as claudin-1 following stroke (45). Importantly, while claudins-1, -3 and -5 are capable of forming homo- and hetero- *trans*-interactions, claudins-1, -3 or -5 knockout mice have demonstrated that claudin-5 is particularly important for barrier closure, dying shortly after birth due to brain edema, while other claudin-specific knockout mice have a functionally intact BBB (46).

In addition to claudins, occludin and junctional adhesion molecule (JAM) family members also comprise the transmembrane spanning portion of TJs. occludin and JAMs form homo *trans*-interactions bolstering the barrier, however, as with claudin-1, -3, and -12, occludin is not required for closure of the BBB indicated by intact TJ structures in occludin-KO mice (47). JAM proteins interact with integrins, providing additional BBB structural integrity, and also facilitate leukocyte extravasation (48, 49).

Zonula occludens -1 and -2 (ZO-1, ZO-2) are the core scaffolding proteins of the TJ complex in the brain. Each contain PDZ binding domains that enable interaction with transmembrane proteins, including claudins, occludin, and JAM-A, as well as others such as Gap Junction protein Connexin 43 (Cx43) (50, 51).

ZO proteins also contain an actin-binding region that allows direct interaction with F-actin (52). Additional actin-associated proteins, including cortactin, vinculin and VASP, co-localize and can be precipitated with ZO-1, suggesting additional mediators of ZO/actin cytoskeleton interaction (53, 54). ZO-1 is incorporated into AJs through interaction with α-catenin (55).

Adherens junctions are situated abluminal of TJs on the lateral membrane. Transmembrane proteins of AJs include cadherins, with VE-cadherin being the most abundantly expressed in brain ECs with low expression of N- and E-cadherin (56, 57). As with claudins and occludin of the TJs, cadherins also form *trans*-interactions to tether together neighboring ECs (55). Intracellular proteins of AJs included β- and α-catenin, p120 and plakoglobin (55). β-catenin facilitates the trafficking and insertion of cadherins into the membrane and upon phosphorylation, can signal for the endocytosis of cadherins (58). Following membrane insertion, cadherin-associated β-catenin can recruit α-catenin, and together this complex facilitates the anchoring of cadherins with the actin cytoskeleton via α-catenin (59). p120 catenin also anchors catenins to microtubules (60). AJs can be perturbed by rearrangements of the actin cytoskeleton mediated by GTPases Rho or Rac (61).

1.2 Gap Junction proteins

Until recently, TJs and AJs were the principal junctional complexes believed to regulate paracellular permeability in the BBB. However, all cell types of the NVU express functional gap junctions, and while barrier maintenance has not traditionally been ascribed to GJ or their component proteins, emerging studies have begun to uncover contributions to the BBB. Gap junctions will be discussed in brief below, with further details provided in chapters 2 and 4.

1.2.1 Canonical functions of connexins

Connexin (Cx) family members canonically function as gap junctions (GJs) or hemichannels (HCs). Several Cx family members have been identified and display tissue-specific expression (62). Cxs typically have four transmembrane-spanning domains with unstructured N- and C-terminal cytoplasmic tails, the

latter of which serves as the main regulator of Cx function (63; Fig. 1.2.1, left). Cx37, Cx40 and Cx43, named for their molecule weight of 37-, 40- or 43kDa, respectively, are expressed in brain endothelial cells (64, 65). Each Cx can form GJs or HCs following homo- or heterohexamerization and insertion into the plasma membrane (66, 67). GJs are formed by the aggregation of multiple Cx hexamers (termed a GJ plaque) and direct opposition of a neighboring cell GJ plaque (Fig. 1.2.1, right). The center of Cx hexamers function as a channel through which molecules of less than 1kDa can non-selectively pass from one cell cytosol to the other (63). Separately, the insertion of Cx hexamers into the plasma membrane that do not aggregate and do not directly oppose Cx GJ plaques on opposing cells function as HCs (Fig. 1.2.1, center). In a similar manner, the interior of HC Cx hexamers form a channel for the bi-directional, non-selective transport of molecules <1kDa, from cytosol to the extracellular space.

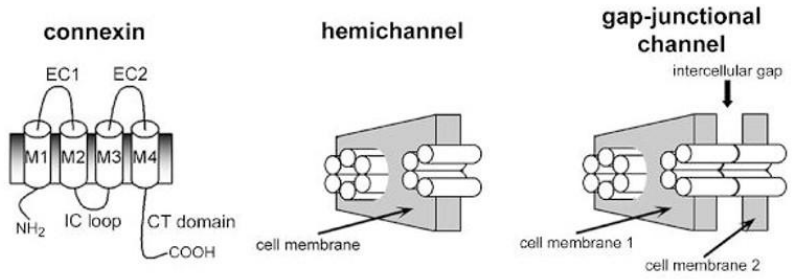

Figure 1.2.1 Connexin 43 structure and function. (Left) Cx43 is a transmembrane protein with 4 membrane-spanning domains (M1-M4), two extracellular loops (EC1-2), an intracellular loop (IC loop) and a c-terminal, cytoplasmic tail (CT domain) that serves as its main regulatory domain. Cx43 hexamerizes to from a channel structure that inserts into the cell membrane to form a hemichannel opposing the extracellular space (middle) or a gap junction that opposes another cells gap junction channel (right).

Given the non-selective passage of molecules through Cx channels, it is no surprise that channel opening is regulated at multiple levels, including phosphorylation and GJ plaque aggregation. The Cx C-terminal cytoplasmic tail (CT) regulates channel function at the membrane and its sequence varies widely among Cxs (63, 68). Cx43 is the most ubiquitously expressed and well-studied of the Cx family members, so knowledge Cx CT regulatory functions have been derived from the Cx43 CT, but are not necessarily representative of all Cxs, particularly with respect to phosphorylation sites and interacting kinases. Phosphorylation of Cx43 at S325/328/330 promotes GJ channel opening by inducing a conformation change by which the negatively charged CT interacts with

the positively charged cytoplasmic loop (CL) (69, 70). MAPK-driven phosphorylation of S279/282 result in the inhibition of channel opening through a proposed mechanism of releasing the CT from the CL (70, 71).

1.2.2 Connexin life cycle and turnover

In addition to phosphorylation events regulating channel opening, the delivery of Cxs to the membrane and assembly into GJ plaques also govern overall GJ and HC activity. The N-terminus of Cxs is essential for their oligomerization (72). Trafficking of connexins through the endoplasmic reticulum (ER), through the Golgi network and to the plasma membrane is dependent on their oligomerization state. While Cx37 and Cx40 hexamerize in the ER and this is required for trafficking to the Golgi and beyond, Cx43 is unique in its delayed oligomerization in the *trans*-Golgi network (73). It is not understood why this differential regulation exists, however, Cx43-specific chaperone protein, ERp29, has been identified as crucial to restrict Cx43 oligomerization in the ER (74). Cells lacking ERp29 do not express Cx43 GJs at their cell surface. Phosphorylation of S364/365 promotes the trafficking of Cx43 from the Golgi to the plasma membrane, while protein phosphatase 2A (PP2A) binds Cx43 in the Golgi to remove inhibitory phosphates (75, 76).

Connexin degradation represents the final level of GJ and HC activity regulation. Cx43 is reported to utilize both lysosomal and proteosomal degradation pathways. Protein kinase C-mediated phosphorylation of Cx43 at S368 targets Cx43 for disassembly for the GJ plaque and subsequent degradation (77, 78). This phosphorylation event promotes Cx43 ubiquitination by the E3 ubiquitin-protein ligase, Nedd4 (79, 80). In this proposed pathway, Eps15 binds ubiquitinated Cx43 and facilitates its internalization and degradation via the 26S proteasome (81). Cx43 can also be flagged for degradation in the endoplasmic reticulum (ER) in a process mediated by the ubiquitin-like protein, Cx43-interacting protein of 75kDa (CIP75) (82). Altered expression or function of Nedd4, Eps15, or CIP75 have been implicated in disease progression, including various cancers in which over-activation of Nedd4 leads to loss of Cx43 GJIC (83). Cx43 can also be degraded in a lysosome-dependent pathway. Lysosome inhibition

results in accumulation of Cx43 GJs and inhibition of Cx43 transport pathways results in the appearance of Cx43 in lysosomes (84). The specific signals regulating lysosomal degradation have not been described.

1.2.3 Channel independent functions of Cx43

In recent years an increasing number of studies have demonstrated channel-independent functions of Cx43 – functions that do not require the presence or activity of GJs or HCs. Connexin expression and GJIC is low or absent in many cancer cell lines, including breast cancer, prostate cancer, lung cancer and others, which prompted the study of how Cxs may regulate cell cycle progression or cell growth. One study observed that re-introduction and overexpression of Cx43 in a lung cancer cell line resulted in an increase in E-cadherin and blockage of cell cycle progression (85). An inhibition of cell cycle progression could also be seen with Cx43 overexpression in a hepatocellular carcinoma cell line (86). In both studies, no increase in GJIC was observed and exogenously-expressed Cx43 was localized to the cytosol, leading researchers to conclude that the function of Cx43 in cell cycle control is independent of its channel functions. Induction of otherwise Cx43 depleted cancer cells has also been implicated in cell migration and differentiation (87). Overexpression of Cx43 in MDA-MB-231 breast cancer cells reduced migration, however, high Cx43 expression in C6 glioma was determined to promote invasion, thus the functions of Cx43 in migration and other cancer phenotypes are likely cell-type specific (88). Many interacting proteins have been implicated in facilitating Cx43-dependent migration, including ZO-1, cadherin and cortical actin-binding protein, cortactin (88). Additionally, many studies have demonstrated that exogenous expression of the Cx43 C-terminal tail results in a plethora of phenotypes regulating both channel and channel-independent functions (89). Those studies are discussed in more detail in Chapter 4.

1.2.4 Connexins in disease

Mutations in Cx family members have been described in several diseases. Most prevalent is Oculodentodigital dysplasia (ODDD), in which mutations in the N-terminus of Cx43 prevent the formation of GJs (91). ODDD manifests in physical deformities of eyes, teeth and limbs, however a third of patients

also develop neuropathies. The contributions of endothelial Cx43 to these neuropathies has not been described, however, Cx43 deficiency in astrocytes contributes to neuron-coupling neuropathies observed in ODDD. Mutations in Cx37 and Cx40 have to been described in the literature to contribute to cardiac disease, particularly with electric coupling of cardiomyocytes and ascribed to dysregulated HC activity (91-93). Mutations in Cx37 and Cx40 that affect the neurovascular unit or BBB integrity have not been described.

Several recent studies have linked elevated Cx43 expression in endothelial cells to defective barrier properties in the lung and brain (94-96). Thrombin-induced elevation of Cx43 in lung endothelial was associated with increased permeability (94). siRNA-mediated decrease of Cx43 rescued this permeability defect. Additionally, increases in Cx43-mediated calcium signaling in brain endothelial *in vitro* can kill Cx43-normal neighboring cells (97). In general, alterations to calcium waves, particularly in astrocytes, can be detrimental to barrier integrity (95). What is lacking are studies examining the interaction between Cx43 GJs and brain endothelial TJs and AJs. Studies have demonstrated a reciprocal relationship between the expression of Cx43 and E-cadherin in development, and ZO-1 interacts with the CT of Cx43 to inhibit GJ plaque accretion and subsequent GJ intercellular communication (GJIC) (85, 98). A cohesive study of how or if Cx43 can affect permeability in a junction-mediated manner has not been performed.

Overall, proper expression and organization of junctional complexes, including tight, adherens and gap junctions are required to prevent the trans- or paracellular permeability of brain ECs. Unsurprisingly, defects in one or more junctional complexes are pathologic to BBB integrity in many diseases (5). One such disease, cerebral cavernous malformations (CCM), highlights the uniqueness of these complexes to the BBB and its integrity. In CCMs, mutations in proteins ubiquitously expressed throughout the body manifest exclusively in the cerebral vascular system. The study of CCMs offer insights not only to the treatment of human patients, but also to the basic biology of the BBB.

1.3 Cerebral cavernous malformations

Cerebral cavernous malformations (CCM) are characterized by cerebral vascular lesions in which capillary beds have become enlarged, dilated caverns with altered blood flow and insufficient BBB integrity. Patients experience a wide range of symptoms including stroke, seizure, focal neurological deficits and hemorrhage. CCM cases are categorized as sporadic or familial. Familial patients carry a heterozygous mutation for *krit1*, *ccm2* or *pdcd10* (fCCM1, 2,or 3) while sporadic patients (sCCM) are genetically normal at these loci. Intriguingly, while CCM proteins are ubiquitously expressed, CCM disease only manifests in the cerebrovascular system. While CCM has been clinically observed for a long time, identification of *krit1 (ccm1)*, *MGC4607* (*ccm2)*, and *pdcd10* (*ccm3*) has been relatively recent, with *ccm3* only being identified in 2005 (99, 100). Consequently, molecular pathways governing fCCM pathogenesis are still being defined and pharmaceutical options for treatment are lacking. Available treatment for patients include symptomatic management, surgical excision of lesions, or gamma knife surgery, all of which are not curative (101-104). For these reasons, the CCM field is focused on the identification of therapeutic targets.

1.3.1 CCM clinical disease

The overall prevalence of CCM disease in the general population is 0.1-0.5%. CCMs are the second most prevalent of vascular malformations (10-15%), following developmental venous anomalies (DVA). Of CCM patients, sporadic cases represent approximately 90% of all cases, while of the familial cases, fCCM1, 2, and 3 account for 56%, 33% and 6%, respectively (101). Sporadic patients present with a single lesion at variable age of onset. Many sporadic cases are identified as a result of diagnostic testing for an independent disease, given that lesion symptoms are highly dependent on their localization with the cerebrovascular system. Familial patients, on the other hand, have multiple lesions, with the central clinical difference between the three subtypes being age of onset. The majority of fCCM3 patients will experience lesion-related symptoms prior to age 10, while fCCM1 and fCCM2 patients will not experience

symptoms until age 20-40 years (101). The gold standard for lesion visualization, including identification permeable and/or hemorrhaged lesions, is T2*-weighted MRI imaging (Fig. 1.3.1) (101, 105).

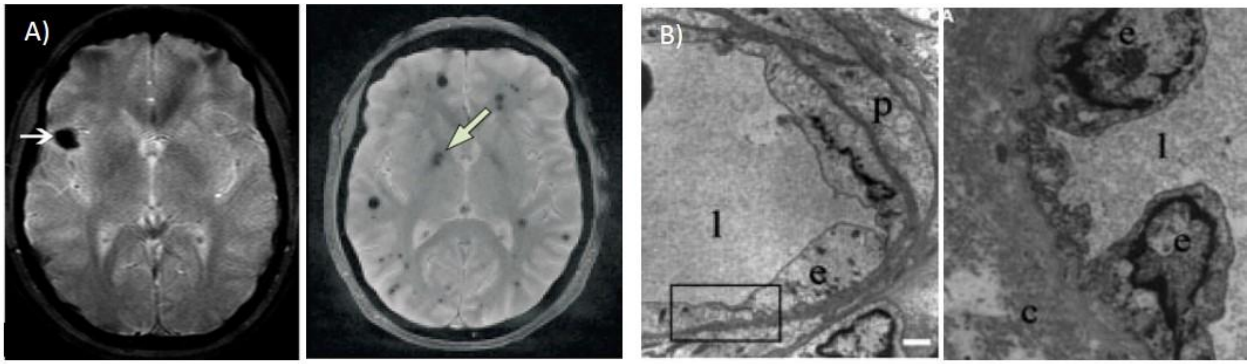

Figure 1.3.1. Lesions of Cerebral Cavernous Malformations. (A) Magnetic resonance imaging of patients with sporadic (left) and familial (right) CCM. Sites of hemorrhage are indicated by black spots. Sporadic patients typically only develop one lesion while familial patients develop multiple. (B) Electron micrographs of healthy (left) or CCM lesion (right) vessels. In healthy vessels, the vessel lumen (l) is surrounded by endothelial cells (e) with no intervening space between (boxed region). Pericytes (p) and basement membrane surround endothelial cells. In lesions, endothelial cells lose contact and the basement membrane is exposed to the lumen. Pericytes are often absent from lesions. Adapted from de Souza J et al., *Am J Neuroradiol* 2008 and (B) Clatterbuck RE et al., *J Neurol Neurosurg Physchiatry,* 2001.

The clinical course of fCCM disease shows great diversity between and among fCCM subtypes. Twenty three to fifty percent of patients present with seizure, 6-52% with headache, 20-45% with focal neurological defect and 9-56% percent with hemorrhage (101). Consistent with the greater severity of fCCM3 subtype, 53% of fCCM3 patients present with bleeding as the first symptom, while only 20-39% of fCCM1 and 2 patients present with bleeding (101). As hemorrhage represents the most dangerous of symptoms, hemorrhage prediction is of particular importance for clinicians. Lesion bleeding rates vary widely depending on study, as many studies do not differentiate between familial subtypes, but have been reported as high as 3.1% per individual per year (101). It is debated whether previous bleeds can affect future bleeds from the same lesion, with some studies finding that previous bleeds are the best predictor of future bleeds, while other studies do not find an association (101, 106).

The diversity of clinical outcomes for fCCM patients may be due to the genetics of the individual and of individual lesions. A two-hit hypothesis is widely accepted as the mechanism by which lesions are initiated (107, 108). Individuals inherit one *ccm* allele with a null mutation and acquire at some point,

whether in development or as an adult, a somatic mutation in the functional allele, rendering the cell(s) ccm null. Many germline mutations have been identified for *ccm1*, *ccm2* and *ccm3*, including non-sense, truncation and point mutations (109). Identified somatic mutations vary widely (110). Murine and cell cultures studies have not been performed to examine whether functional outcomes differ depending on the specific germline or acquired mutations.

The current treatment options for CCM patients are symptomatic treatment, surgical excision of lesions, gamma knife surgery, or most recently for fCCM1 and 2 patients, a RhoA inhibitor in clincial trials, fasudil (111). Surgical excision of lesion is both costly and of high risk for patients. In many cases, invasive procedures such as surgical excision or gamma knife surgery are not viable options for brain stem or otherwise inoperable lesions. Gamma knife surgery also frequently results in the development of new lesions surrounding the resected area, proposed to be due to gamma-induced second-hits to surrounding endothelia (104). The first pharmacologic treatment option, fasudil, for fCCM patients is targeted to overactive RhoA kinase identified in CCM pathogenesis (111). Currently in clinical trials, fasudil has been effective for fCCM1 and fCCM2 patients, but has had little effect for fCCM3 patients. Given the clinical differences that exist between fCCM3 and fCCM1/2 patients, as well as on-going efficacy studies with fasudil, gives strong evidence that the molecular mechanisms governing fCCM3 pathology are distinct from fCCM1 and 2 and demand further study.

1.3.2 Molecular mechanisms of CCM proteins

Given the clinical similarities, initial research into the molecular mechanisms of fCCM focused on the identification of a single molecular pathway regulated by all three CCM proteins. Each CCM protein has a distinct structure. CCM3 is most highly conserved evolutionarily compared to CCM1 and 2, with two distinct domains including four N-terminal helices that enable homodimerization and four C-terminal helices that resemble a focal adhesion targeting (FAT) domain (112). CCM1 contains a C-terminal FERM signaling domain, a phosphotyrosine-binding (PTB) domain and an N-terminal nuclear localization signal

and nuclear export signal (113-116). CCM2 also contains a PTB domain and harmonin homology domain (HHD) (117-118).

Initial studies identified that CCM1, 2, and 3 complex together and regulate cellular adhesion. Within the complex, CCM2 acting as a scaffolding protein, binding CCM1 and CCM3 at distinct sites (119, 120). The centrality of CCM2 is supported by studies assessing overlapping functions among the three CCM proteins, identifying that while loss of CCM1 does not heavily affect CCM3 functions and vice versa, loss of CCM2 affects the function of both CCM1 and 3. A key effector of this complex is the GTPase, Rap1 (Krev1). Activated Rap1, a regulator of cell polarity and integrin-mediated cell adhesion, binds to the FERM domain of CCM1 (121). The Rap1-bound CCM complex localizes to the peri-membrane space and enables interaction of CCM1 with β-catenin and VE-cadherin within AJs, though whether these interactions are direct or indirect is not well understood (122). Loss of CCM1 results in greater nuclear localization of β-catenin, thought to be a direct result of loss of CCM1 localization at the AJ (123). Nuclear localization of β-catenin can alter gene expression and is known to promote oncogenesis when over-activated (124). In addition to Rap1, integrin cytoplasmic domain-associated protein 1 (ICAP1) also binds CCM1 to regulate cell adhesion through an integrin-mediated mechanism (125). ICAP1 is a small protein that competes with the integrin-binding protein talin for binding sites on the cytoplasmic domains of integrin, in particular integrin-β1. ICAP1/integrin association negatively regulates cell adhesion while talin/integrin association is a positive regulator (126, 127). In physiologic conditions, CCM1 binds ICAP1 and sequesters it from integrins, allowing binding of talin and formation of integrin-mediated cell adhesion (128). Loss of CCM1 promotes the association with ICAP1 with integrin-β1 and disrupts cell adhesion.

In addition to pathways affecting AJs and integrin-mediated adhesion, the CCM1-CCM2-CCM3 complex also regulates actin cytoskeleton organization through RhoA. The PTB domain of CCM2 binds the E3 ubiquitin ligase SMAD ubiquitin regulatory factor 1 (SMURF1) (129). Canonically, SMURF1 is a negative regulator of the bone morphogenic pathway (BMP), but also functions as a negative regulator of RhoA

signaling (130). SMURF1 ubiquitinates RhoA, signaling for its proteosomal degradation (131). Loss of CCM2-SMURF1 binding renders SMURF1 unable to ubiquitinate RhoA and results in over-active RhoA signaling (129). Downstream effectors of RhoA include Rho-associated coiled coil forming kinase (ROCK) and mammalian homolog of *Drosophila* diaphanous (mDia) (132). While mDia positively regulates actin filament polymerization, ROCK is a positive regulator of myosin light chain (MLC)-mediated actin cross-linking (132, 133). Overactive ROCK, a consequence of loss of the CCM1-CCM2-CCM3 complex, results in increased stress fiber formation with downstream consequences to cell adhesion (134-137). Inhibition of overactive RhoA *in vitro*, in fCCM mouse models and clinical trials using fasudil improves cell adhesion, lesion burden and bleed rate in fCCM1 and fCCM2 (111).

Finally, endothelial to mesenchymal transition (EndMT) has recentaly been proposed as a principal mechanism in the pathogenesis of fCCM1. Researchers observed that loss of CCM1 in an endothelial-specific CCM1KO mouse model resulted in increased SMAD transcription factor activation downstream of BMP6 (138). Importantly, the authors of that study demonstrated that increased SMAD activation results in a decreased expression and localization of VE-cadherin to endothelial AJs and an increase in N-cadherin expression. This cadherin switch indicates a loss of cell specialization and in addition to loss of junction organization, results in loss of cell polarity and increased proliferation. EndMT has not been evaluated in fCCM2 or fCCM3 mouse models.

1.3.3 CCM3 and the STRIPAK complex

In vitro and *in vivo* evaluation of RhoA activation in CCM3 knockdown (CCM3KD) cells or CCM3 knockout (CCM3KO) mice has identified varying levels of RhoA activation. Current clinical trials using the RhoA inhibitor fasudil have not shown robust effects for fCCM3 patients. Proteomic studies have since provided an explanation for these observations. CCM3 has been identified as a member of the peri-membrane Striatin-Interacting Phosphotase and Kinase (STRIPAK) complex and it is estimated that the majority of CCM3 protein is bound to STRIPAK and not to the CCM1-CCM2-CCM3 complex (139). The

STRIPAK complex contains many phosphatases and kinases that produce wide-ranging cellular effects, including Golgi apparatus development, calcium sensing and cytoskeleton organization (140).

The function of CCM3 in the STRIPAK complex, particularly in the context of barrier maintenance, is still being evaluated. CCM3 is incorporated into STRIPAK following a conformational change that enables heterodimerization with GCKIII kinases including Stk4 and Mst4 (139, 141, 142). Studies in murine endothelial and non-endothelial cell lines have demonstrated that the CCM3-Stk4 interaction within the STRIPAK inhibits UNC13D, a protein required for calcium-dependent exocytic vesicle maturation and fusion with the membrane (143). Loss of CCM3 results in increased UNC13D fusion with the membrane and increased exocytosis. One study showed that CCM3 normally inhibits the secretion of angiopoietin 2 (ANGPT2) (144). ANGPT2 secretion is elevated in endothelial-specific CCM3KO mice and the study argues that this leads to destabilization of the endothelial barrier. In a separate study, CCM3 functions in the STRIPAK complex, in conjunction with Mst4, to regulate ERK1/2 activation (53). Loss of CCM3 increases ERK1/2 activation and double knockdown of CCM3 and Mst4 rescues this. This study suggests a CCM3-MST4-ERK1/2 signaling axis regulates barrier permeability via downstream effects on cortactin-mediated cytoskeletal and TJ organization.

Additional STRIPAK-independent CCM3 signaling pathways have been proposed to enable disease progression of fCCM3. These include a CCM1-CCM2-CCM3-MEKK3-Klf4 and CCM1-CCM2-CCM3-mTOR signaling axis. In the former, loss of CCM3 results in abnormally high MEKK3 activity that acts on Klf4 transcription factor to increase the transcription of Toll-like receptor 4 (TLR4) (145, 146). Recently, it was shown that fCCM3 disease severity can be linked to single nucleotide polymorphisms (SNPs) in TLR4, such that SNPs enabling higher expression of TLR4 lead to more severe disease (147). The downstream effects of this cellular pathway have not been well described in the context of CCM disease, however. A CCM1-CCM2-CCM3-mTOR axis reportedly regulates autophagosome component p62/SQSTM (149). Loss of

CCM1 or CCM3 results in overactive mTOR and accumulation of p62/SQSTM that inhibits autophagosome formation.

As evident, many functions of CCM proteins, whether in the CCM1-CCM2-CCM3 or through alternative complexes such as CCM3 in the STRIPAK, have been proposed. No central unifying theory exists, especially for CCM3, shy of the fact that barrier properties in fCCM patients, mouse models and cell culture systems are severely compromised. In part, the study of fCCM has been inhibited by the lack of adequate model systems. The advantages and disadvantages of current model systems will be discussed in detail in the following section.

1.3.4 fCCM model systems

Initial attempts to study fCCM using mouse models failed due to the unexpected embryonic lethality of global CCM1, 2 and 3 KO mice due to cardiovascular defects (149-151). CCM1 and CCM2 are required for the development of brachial arteries that attach the heart to the aorta, thus CCM1KO and CCM2KO mice die at E9.0 and E11.0, respectively, of severe circulatory defects (149, 150). CCM3KO mice die earlier in development at E8.0 due to defects in lumen development (151). One study has demonstrated that CCM3KO mice have reduced VEGFR2 signaling and this blocks angiogenesis in the developing embryo (152). Researchers attempted to avoid embryonic lethality with endothelial-specific CCMKO mice, however, these mice are also embryonic lethal (149-151). In the case of CCM3, Tie2-Cre Pdcd10l$^{ox/-}$ mice, an endothelial specific CCM3KO model, these mice die at E13.5 due to venous rupture and have enlarged cardinal veins (151). Neural and glial tissue-specific CCMKO mice are not embryonic lethal and born at expected ratios, however, these mice show low or no disease penetrance (153). Accordingly, inducible endothelial-specific KO mice is commonly used in mouse models of fCCM.

It is important to note that in the case of CCM3, multiple KO alleles have been developed and target different exons of ccm3. Slight differences in embryonic and adult phenotypes have been observed in inducible and non-inducible models employing these exons (151, 152). As noted in the clinical disease

section, the germline and somatic mutations that result in fCCM disease are vast and functional differences between mutation profiles have not been fully assessed. One study was able to demonstrate that C-terminal truncation mutations of CCM3 observed in fCCM3 patients can replicate VEGFR2 signaling defects *in vitro* (152). However, as a whole, Cre-mediated deletion of whole exons is not representative of patient mutations and comparisons between mouse models employing different alleles should be taken with caution.

Several tissue-specific and inducible CCMKO mouse models exist that have allowed researchers to avoid embryonic lethality as well as address a very important question in CCM disease – which cell type is required and sufficient for disease initiation? Inducible endothelial cell-specific CCM3KO (iEC-CCM3KO) mice utilize a cadherin-5 or PDGFβ promoter to drive Cre expression (151). Similar to human disease, iEC-CCM3KO mice develop multiple hemorrhagic lesions, however, these lesions are restricted to the cerebellum and eyes. Neural cell (Nestin-Cre), glial cell (GFAP-Cre), and neural progenitor cell (Emx1-Cre)-specific CCM3KO mice have also been created in an attempt to understand the role of CCM3 in particular cell types (153, 154). Neural and neural progenitor cell-specific CCM3KO mice do not develop fCCM3 disease, however, each were born with enlarged brains and in the case of neural cell-specific KOs, all mice died within three days of birth. Glial/astrocyte-specific CCM3KO mice also did not exhibit lesions typical of fCCM3 disease, but did exhibit enlarged brains and ventricles and died within a month of birth. Non-endothelial cell specific CCM3KO models have uncovered roles for CCM3 in development in particular cell types but have not led to specific insights into fCCM3 lesion initial or maturation other than the determination that CCM3 deficiencies in these cell types are not sufficient to cause CCM disease. However, it should be noted that given the early deaths of glial- and neural cell-specific CCM3KO mice, it is possible that these mice may have developed disease had they survived to adulthood.

Inducible CCM3KO models have many advantages and disadvantages. One of the more obvious problems with these models is the restriction of lesion appearance to the cerebellum. No explanation

exists for this observation. Second, the steps required for lesion initiation and maturation are not well understood. For example, it is not known whether a somatic hit occurs early in development, resulting in multiple cell (and/or cell types) with CCM deficiency or if a somatic mutation to a single mature cell is sufficient to initiate a lesion. Inducible KO models do not allow for acquisition of somatic mutation during development and result in CCM3 deficiency in all cells expressing Cre. These issues may confound the study of lesion initiation. When it comes to lesion maturation, it is not known whether maturation of lesions is dependent on growth or other factors in development or adulthood and how the contributions of surrounding cells may influence maturation. If developmental factors influence lesion maturation, it cannot be assessed by post-natal Cre induction. Additionally, Tamoxifen administration causes CCM3 deficiency and lesion initiation at a single time point, thus if lesion maturation is dependent on age or related factors, this model provides only a narrow window into the mechanisms of lesion maturation. Overall, induction of CCM3 deficiency at a particular time point in all Cre-inducible cells is not representative of the accepted model by which fCCM3 patients develop disease.

There now exist mouse models based on the two-hit hypothesis of fCCM. These models employ $ccm^{+/-}$ mice crossed with mice harboring mutations in the tumor suppressor genes Msh2 or p53. $Ccm^{+/-}$ $p53^{-/-}$ or $ccm^{+/-}msh2^{-/-}$ mice all develop fCCM disease that mirrors human disease very well (155, 156). These mice develop lesions indiscriminately throughout the brain and theoretically should overcome the lesion initiation and maturation issues faced by inducible KO models. Another advantage of the two-hit model is the acquisition of diverse somatic mutations instead of specific deletion of particular exons. Disadvantages, however, include that $msh2^{-/-}$ and $p53^{-/-}$ backgrounds are genetically unstable and may result in genetic mutations within lesions that confound gross lesion behavior and/or results from molecular analysis. Additionally, while this model has the advantage of allowing somatic hits to any cell type, it has the disadvantage of making it difficult to connect gross lesion behavior with lesion initiating cell type.

1.4 Summary and Project Goals

While RhoA inhibitors have proven promising in fCCM1 and fCCM2 patients in clinical trials, the molecular mechanisms contributing to fCCM3 pathology are still largely unknown, representing a major roadblock to providing pharmaceutical treatment options for patients in the clinic. A large body of literature has demonstrated that inadequate barrier integrity in the lesions of fCCM3 patients is the primary pathology that leads to secondary pathologies such as seizure and hemorrhage. Recent in vitro work suggests that disrupted junctional stability, particularly with TJ organization, is a contributing factor to BBB breakdown in fCCM3. However, contributions of GJ proteins to barrier integrity in homeostasis as well as in fCCM3 disease has not been evaluated. The overall goals of this project are to determine whether GJ proteins contribute to BBB breakdown in fCCM3 cell culture and evaluate GJ protein expression during lesion maturation in a second-hit mouse model of fCCM3.

1.5 References

1. Ehrlich P. (1885) Das Sauerstoff-Bedurfnis des Organismus: eine farbenanalytische Studie. Berlin: Hirschward.

2. Ribatti D, Nico B, Crivellato E, Artico M. (2006) THE ANATOMICAL RECORD (PART B: NEW ANAT.) 289B:3– 8,.

3. Bield A, Kraus R. (1898) U¨ ber eine bisher unbekannte toxische Wirkung der Gallensauren auf das Zentralnervensystem. Zhl Inn Med 19:1185–1200.

4. Lewandowsky M. (1900) Zur Lehre der Zerebrospinalflussigkeit. Z Klin Med 40: 480 –484.

5. Obermeier B, Daneman R, Ransohoff RM. (2013) Development, Maintenance and Disruption of the Blood Brain Barrier. *Nat Med* 19:1584–1596

6. Matter K, Balda MS. (2003) Holey barrier claudins and the regulation of brain endothelial permeability. *J. Cell Biol.* 161(3):459–460.

7. Van Itallie CM, Anderson JM. (2004) The role of claudins in determining paracellular charge selectivity. *Proc. Am. Thorac Soc*. 1(1):38–41.

8. Peppiatt, C. M., Howarth, C., Mobbs, P. & Attwell, D. (2006) Bidirectional control of CNS capillary diameter by pericytes. *Nature* 443: 700–704

9. Lindahl, P., Johansson, B.R., Leveen, P., Betsholtz, C. (1997) Pericyte loss and microaneurysm formation in PDGF-B–deficient mice. *Science* 277:242–245

10. Hellström, M. *et al*. (2001) Lack of pericytes leads to endothelial hyperplasia and abnormal vascular morphogenesis. *J. Cell Biol.* 153: 543–553.

11. Daneman, R., Zhou, L., Kebede, A.A. & Barres, B.A. (2010) Pericytes are required for blood-brain barrier integrity during embryogenesis. *Nature* 468: 562–566.

12. Hellström, M., Kalen, M., Lindahl, P., Abramsson, A. & Betsholtz, C. (1999) Role of PDGF-B and PDGFR-β in recruitment of vascular smooth muscle cells and pericytes during embryonic blood vessel formation in the mouse. *Development* 126: 3047–3055

13. Winkler, E.A., Bell, R.D. & Zlokovic, B.V. (2011) Central nervous system pericytes in health and disease. *Nat. Neurosci.* 14: 1398–1405.

14. Gerhardt, H., Wolburg, H. & Redies, C. (2000) N-cadherin mediates pericytic-endothelial interaction during brain angiogenesis in the chicken. *Dev. Dyn.* 218: 472–479

15. Li, F. *et al*. (2011) Endothelial Smad4 maintains cerebrovascular integrity by activating N-cadherin through cooperation with Notch. *Dev. Cell* 20:291–302

16. Paik, J.H. *et al*. (2004) Sphingosine 1-phosphate receptor regulation of N-cadherin mediates vascular stabilization. *Genes Dev.* 18:2392–2403.

17. Sobue, K. *et al*. (1999) Induction of blood-brain barrier properties in immortalized bovine brain endothelial cells by astrocytic factors. *Neurosci. Res.* 35:155–164

18. Sun, D., Lytle, C. & O'Donnell, M.E. (1997) IL-6 secreted by astroglial cells regulates Na-K-Cl cotransport in brain microvessel endothelial cells. *Am. J. Physiol.* 272:C1829–C1835

19. Hayashi, Y. *et al*. (1997) Induction of various blood-brain barrier properties in non-neural endothelial cells by close apposition to co-cultured astrocytes. *Glia* 19:13–26

20. Lee, S.W. *et al*. (2003) SSeCKS regulates angiogenesis and tight junction formation in blood-brain barrier. *Nat. Med.* 9:900–906.

21. Wosik, K. *et al*. (2007) Angiotensin II controls occludin function and is required for blood brain barrier maintenance: relevance to multiple sclerosis. *J. Neurosci.* 27:9032–9042

22. Carvey, P.M., Hendey, B. & Monahan, A.J. (2009) The blood-brain barrier in neurodegenerative disease: a rhetorical perspective. *J. Neurochem.* 111:291–314.

23. Osada, T. *et al*. (2011) Interendothelial claudin-5 expression depends on cerebral endothelial cell-matrix adhesion by β_1-integrins. *J. Cereb. Blood Flow Metab.* 31:1972–1985.

24. Cambier, S. *et al*. (2005) Integrin $\alpha_v\beta_8$-mediated activation of transforming growth factor-β by perivascular astrocytes: an angiogenic control switch. *Am. J. Pathol.* 166:1883–1894.

25. Willert, K. *et al*. (2003) Wnt proteins are lipid-modified and can act as stem cell growth factors. *Nature* 423:448–452.

26. Handel, T.M., Johnson, Z., Crown, S.E., Lau, E.K. & Proudfoot, A.E. (2005) Regulation of protein function by glycosaminoglycans—as exemplified by chemokines. *Annu. Rev. Biochem.* 74:385–410.

27. Shalaby, F. *et al*. (1995) Failure of blood-island formation and vasculogenesis in Flk-1–deficient mice. *Nature* 376:62–66.

28. Carmeliet, P. *et al*. (1996) Abnormal blood vessel development and lethality in embryos lacking a single VEGF allele. *Nature* 380:435–439.

29. Haigh, J.J. *et al*. (2003) Cortical and retinal defects caused by dosage-dependent reductions in VEGF-A paracrine signaling. *Dev. Biol.* 262:225–241.

30. Olsson, A.K., Dimberg, A., Kreuger, J. & Claesson-Welsh, L. (2006) VEGF receptor signalling—in control of vascular function. *Nat. Rev. Mol. Cell Biol.* 7:359–371.

31. Daneman, R. *et al*. (2009) Wnt/β-catenin signaling is required for CNS, but not non-CNS, angiogenesis. *Proc. Natl. Acad. Sci. USA* 106:641–646

32. Stenman, J.M. *et al*. (2008) Canonical Wnt signaling regulates organ-specific assembly and differentiation of CNS vasculature. *Science* 322:1247–1250.

33. Tam, S.J. *et al*. (2012) Death receptors DR6 and TROY regulate brain vascular development. *Dev. Cell* 22:403–417.

34. Alvarez, J.I. *et al*. (2011) The Hedgehog pathway promotes blood-brain barrier integrity and CNS immune quiescence. *Science* 334:1727–1731.

35. D.S. Miller. (2015) Regulation of ABC transporters blood-brain barrier: the good, the bad, and the ugly. *Adv. Cancer Res*. 125:43-70.

36. B.V. Zlokovic. (2011) Neurovascular pathways to neurodegeneration in Alzheimer's disease and other disorders. *Nat. Rev. Neurosci*. 12:723-738.

37. J.R. Cirrito, R. Deane, A.M. Fagan, M.L. Spinner, M. Parsadanian, M.B. Finn, H. Jiang, J.L. Prior, A. Sagare, K.R. Bales, et al. (2005) P-glycoprotein deficiency at the blood-brain barrier increases amyloid-beta deposition in an Alzheimer disease mouse model. *J. Clin. Invest*., 115:3285-3290

38. L. Lin, S.W. Yee, R.B. Kim, K.M. Giacomini. (2015) SLC transporters as therapeutic targets: emerging opportunities. *Nat. Rev. Drug Discov*. 14:543-560

39. E.E. Benarroch. (2014) Brain glucose transporters: implications for neurologic disease. *Neurology* 82:1374-1379.

40. W.M. Pardridge.(2015) Blood-brain barrier endogenous transporters as therapeutic targets: a new model for small molecule CNS drug discovery. *Expert Opin. Ther. Targets*. 19:1059-1072.

41. L.N. Nguyen, D. Ma, G. Shui, P. Wong, A. Cazenave-Gassiot, X. Zhang, M.R. Wenk, E.L.K. Goh, D.L. Silver. (2014) Mfsd2a is a transporter for the essential omega-3 fatty acid docosahexaenoic acid. *Nature*, 509:503-506.

42. Ohtsuki S, Yamaguchi H, Katsukura Y, Asashima T, Terasaki T. (2008) mRNA expression levels of tight junction protein genes in mouse brain capillary endothelial cells highly purified by magnetic cell sorting. *J Neurochem*; 104:147-54

43. Sadowska GB, Ahmedli N, Chen X, Stonestreet BS. (2015) Ontogeny of tight junction protein expression in the ovine cerebral cortex during development. *Neurosci* 310:422-9.

44. Liebner S, Corada M, Bangsow T, Babbage J, Taddei A, Czupalla CJ, Reis M, Felici A, Wolburg H, Fruttiger M, et al. (2008) Wnt/b-catenin signaling controls development of the blood-brain barrier. *J Cell Biol* 183:409-17.

45. Pfeiffer F, Schafer J, Lyck R, Makrides V, Brunner S, Schaeren-Wiemers N, Deutsch U, Engelhardt B. (2011) Claudin-1 induced sealing of blood-brain barrier tight junctions ameliorates chronic experimental autoimmune encephalomyelitis. *Acta Neuropathol* 122:601-14.

46. Nitta T, Hata M, Gotoh S, Seo Y, Sasaki H, Hashimoto N, Furuse M, Tsukita S. (2003) Size-selective loosening of the blood-brain barrier in claudin-5-deficient mice. *J Cell Biol* 161:653-60.

47. Saitou M, Furuse M, Sasaki H, Schulzke J, Fromm M, Takano H, Noda T, Tsukita S. (2000) Complex Phenotype of Mice Lacking Occludin, a Component of Tight Junction Strands. *Mol Biol Cell.* 11(12):4131–4142.

48. Bazzoni G, Martinez-Estrada OM, Mueller F, Nelboeck P, Schmid G, Bartfai T, Dejana E, Brockhaus M. (2000) Homophilic interaction of junctional adhesion molecule. *J Biol Chem* 275:30970-6

49. Severson EA, Jiang L, Ivanov AI, Mandell KJ, Nusrat A, Parkos CA. (2008) Cis-dimerization mediates function of junctional adhesion molecule A. *Mol Biol Cell* 19:1862-72.

50. Fanning AS, Little BP, Rahner C, Utepbergenov D, Walther Z, Anderson JM. (2007) The unique-5 and ¡6 motifs of ZO-1 regulate tight junction strand localization and scaffolding properties. *Mol Biol Cell* 18:721-31.

51. Giepmans BN, Moolenaar WH (1998) The gap junction protein connexin43 interacts with the second PDZ domain of the zona occludens-1 protein. *Curr Biol* 8:931-934.

52. Fanning AS, Jameson BJ, Jesaitis LA, Anderson JM. (1998) The Tight Junction Protein ZO-1 Establishes a Link between the Transmembrane Protein Occludin and the Actin Cytoskeleton. *J Biol Chem* 273:29745–29753.

53. Stamatovic SM, Sladojevic N, Keep RF, Andjelkovic AV. (2015) PDCD10 (CCM3) regulates brain endothelial barrier integrity in cerebral cavernous malformation type 3: role of CCM3-ERK1/2-cortactin cross-talk. *Acta Neuropathol* 130:731-50.

54. Hicks K, O'Neil RG, Dubinsky WS, Brown RC. (2010) TRPC-mediated actin-myosin contraction is critical for BBB disruption following hypoxic stress. *Am J Physiol Cell Physiol* 298:C1583-93

55. Harris TJ and Tepass U. (2010) Adherens junctions: from molecules to morphogenesis. *Nat Rev.* 11:502-14

56. Abbruscato TJ, Davis TP. (1999) Protein expression of brain endothelial cell E-cadherin after hypoxia/aglycemia: influence of astrocyte contact. *Brain Res* 842:277-86

57. Luo Y, Radice GL. (2005) N-cadherin acts upstream of VEcadherin in controlling vascular morphogenesis. *J Cell Biol* 169:29-34.

58. Chen YT, Stewart DB, Nelson WJ. (1999) Coupling assembly of the E-cadherin/beta-catenin complex to efficient endoplasmic reticulum exit and basal-lateral membrane targeting of E-cadherin in polarized MDCK cells*. J Cell Biol*. 144:687-99.

59. Nagafuchi A, Ishihara S, Tsukita S. (1994) The roles of catenins in the cadherin-mediated cell adhesion: functional analysis of E-cadherin-alpha catenin fusion molecules. *J Cell Biol*. 127:235-45.

60. Reynolds AB. (2007) p120-catenin: Past and present. *Biochim Biophys Acta.* 1773:2-7.

61. Nanes BA and Kowalczyk AP. (2012) Adherens junction turnover: regulating adhesion through cadherin endocytosis, degradation, and recycling. *Subcell Biochem*. 60:197–222.

62. G. Sohl, K. Willecke. (2003) An update on connexin genes and their nomenclature in mouse and man. *Cell Commun. Adhes*. 10:173–180

63. Solan JL and Lampe PD. (2009) Connexin43 phosphorylation: structural changes and biological effects. *Biochem. J.* 419:261–272.

64. Bruzzone, R., Haefliger, J.A., Gimlich, R.L. and Paul, D.L. (1993) Connexin40, a component of gap junctions in vascular endothelium, is restricted in its ability to interact with other connexins. *Mol Biol Cell* 4:7–20.

65. Gabriels JE, Paul DL (1998) Connexin43 is highly localized to sites of disturbed flow in rat aortic endothelium but connexin37 and connexin40 are more uniformly distributed. *Circ Res* 83:636–643.

66. Brink PR, Cronin K, Banach K, Peterson E, Westphale EM, Seul KH, Ramanan SV, Beyer EC. (1997) Evidence for heteromeric gap junction channels formed from rat connexin43 and human connexin37*. Am J Physiol* 273:C1386–C1396.

67. Martinez AD, Hayrapetyan V, Moreno AP, Beyer EC (2002) Connexin43 and Connexin45 Form Heteromeric Gap Junction Channels in Which Individual Components Determine Permeability and Regulation. *Circ Res* 90:1100–1107.

68. Oyamadaa M, Oyamadaa Y, Takamatsua T. (2009) Regulation of connexin expression. *Biochimica et Biophysica Acta (BBA) – Biomembranes*. 1719: 6–23

69. Lampe, P. D., Cooper, C. D., King, T. J. and Burt, J. M. (2006) Analysis of connexin43 phosphorylated at S325, S328 and S330 in normoxic and ischemic heart. *J. Cell Sci.* 119:3435–3442

70. G.E. Morley, J.F. Ek-Vitorin, S.M. Taffet, M. Delmar. (1997) Structure of connexin43 and its regulation by pHi *J. Cardiovasc. Electrophysiol.* 8:939–951.

71. Cottrell, G. T., Lin, R., Warn-Cramer, B. J., Lau, A. F. and Burt, J. M. (2003) Mechanism of v-Src- and mitogen-activated protein kinase-induced reduction of gap junction communication. *Am. J. Physiol. Cell Physiol.* 284:C511–C520

72. Maza J, Sarma JD, and Koval M. (2005) Defining a Minimal Motif Required to Prevent Connexin Oligomerization in the Endoplasmic Reticulum. *Biol Chem*. 280:21115–21121.

73. Musil, L. S. and Goodenough, D. A. (1993) Multisubunit assembly of an integral plasma membrane channel protein, gap junction connexin43, occurs after exit from the ER. *Cell* 74:1065–1077.

74. Das S, Smith TD, Sarma JD, Ritzenthaler JD, Maza J, Kaplan BE, Cunningham LA, Suaud L, Hubbard MJ, Rubenstein RC, and Koval M. (2009) ERp29 Restricts Connexin43 Oligomerization in the Endoplasmic Reticulum*. Mol Biol Cell* 20:2593–2604.

75. TenBroek, E. M., Lampe, P. D., Solan, J. L., Reynhout, J. K. and Johnson, R. G. (2001) Ser364 of connexin43 and the upregulation of gap junction assembly by cAMP. *J. Cell Biol*. 155:1307–1318.

76. Wu J, Taylor RN, Sidell N. (2013) Retinoic acid regulates gap junction intercellular communication in human endometrial stromal cells through modulation of the phosphorylation status of connexin 43. *J Cell Physiol*. 228:903-10.

77. Solan, J. L., Fry, M. D., TenBroek, E. M. and Lampe, P. D. (2003) Connexin43 phosphorylation at S368 is acute during S and G2/M and in response to protein kinase C activation*. J. Cell Sci*. 116:2203–2211

78. Lampe, P. D., TenBroek, E. M., Burt, J. M., Kurata, W. E., Johnson, R. G. and Lau, A. F. (2000) Phosphorylation of connexin43 on serine368 by protein kinase C regulates gap junctional communication. *J. Cell Biol*. 126:1503–1512

79. Leykauf K, Salek M, Bomke J, Frech M, Lehmann W, Dürst M and Alonso A. (2006) Ubiquitin protein ligase Nedd4 binds to connexin43 by a phosphorylation-modulated process. *J Cell Sci* 119:3634-3642

80. Liao CK, Jeng CJ, Wang HS, Wang SH, Wu JC (2013) Lipopolysaccharide Induces Degradation of Connexin43 in Rat Astrocytes via the Ubiquitin-Proteasome Proteolytic Pathway. *PLoS ONE* 8:e79350.

81. Girão H, Catarino S, Pereira P. (2009) Eps15 interacts with ubiquitinated Cx43 and mediates its internalization. *Exp Cell Res*. 315:3587-97.

82. Su V, Nakagawa R, Koval M and Lau AF. (2010) Ubiquitin-independent Proteasomal Degradation of Endoplasmic Reticulum-localized Connexin43 Mediated by CIP75. *J Biol Chem* 285:40979-40990.

83. Ye X, Wang L, Shang B, Wang Z, Wei W1. (2014) NEDD4: a promising target for cancer therapy. *Curr Cancer Drug Targets* 14:549-56.

84. Qin H1, Shao Q, Igdoura SA, Alaoui-Jamali MA, Laird DW. (2003) Lysosomal and proteasomal degradation play distinct roles in the life cycle of Cx43 in gap junctional intercellular communication-deficient and -competent breast tumor cells. *J Biol Chem*. 278:30005-14.

85. H.T. Xu, Q.C. Li, Y.X. Zhang, Y. Zhao, Y. Liu, Z.Q. Yang, E.H. Wang. (2008) Connexin 43 recruits E-cadherin expression and inhibits the malignant behaviour of lung cancer cells. *Folia Histochem Cytobiol*, 46:315–321

86. M. Ionta, R.A. Ferreira, S.C. Pfister, G.M. Machado-Santelli. (2009) Exogenous Cx43 expression decrease cell proliferation rate in rat hepatocarcinoma cells independently of functional gap junction. *Cancer Cell Int*. 9:22.

87. McLachlan E, Shao Q, Wang HL, Langlois S, Laird DW. (2006) Connexins act as tumor suppressors in three-dimensional mammary cell organoids by regulating differentiation and angiogenesis. *Cancer Res.* 66:9886-9894.

88. Kameritsch P, Pogoda K, Pohl U. (2012) Channel-independent influence of connexin 43 on cell migration*. Biochimica et Biophysica Acta (BBA) – Biomembranes*. 1818:1993–2001.

89. Leithea E, Mesnilb M, Aasen T. (2017) The connexin 43 C-terminus: A tail of many tales. *Biochimica et Biophysica Acta (BBA) – Biomembranes*.

90. De Bock M, Kerrebrouck M, Wang N, Leybaert L. (2013) Neurological manifestations of oculodentodigital dysplasia: a Cx43 channelopathy of the central nervous system? *Front Pharmacol*. 4:120.

91. Sun Y, Yang YQ, Gong XQ, Wang XH, Li RG, Tan HW, Liu X, Fang WY, Bai D. (2013) Novel germline GJA5/connexin40 mutations associated with lone atrial fibrillation impair gap junctional intercellular communication. *Hum Mutation* 34:603-9.

92. Dobrowolski R, Willecke K. (2009) Connexin-caused genetic diseases and corresponding mouse models. *Antioxidants Redox Signal* 11:283-95.

93. Meens MJ, Alonso F, Le Gal L, Kwak BR, Haefliger JA. (2015) Endothelial Connexin37 and Connexin40 participate in basal but not agonist-induced NO release. *Cell Comm Signal* 13:34.

94. O'Donnell JJ, Birukova AA, Beyer EC, Birukov KG (2014) Gap Junction Protein Connexin43 Exacerbates Lung Vascular Permeability. PLoS ONE 9:e100931.

95. Zhang J, O'Carroll SJ, Henare K, Ching LM, Ormonde S, Nicholson LF, Danesh-Meyer HV, Green CR. (2014) Connexin hemichannel induced vascular leak suggests a new paradigm for cancer therapy. *FEBS Letters* 588:1365–1371.

96. De Bock M, Wang N, Decrock E, Bol M, Gadicherla AK, Culot M, Cecchelli R, Bultynck G, Leybaert L. (2013) Endothelial calcium dynamics, connexin channels and blood–brain barrier function. *Prog Neurobiol* 108:1–20.

97. Lin JH, Weigel H, Cotrina ML, Liu S, Bueno E, Hansen AJ, Hansen TW, Goldman S and Nedergaard M. (1998) Gap-junction-mediated propagation and amplification of cell injury. *Nat Neurosci* 1(6).

98. Hunter AW, Barker RJ, Zhu C, Gourdie RG (2005) Zonula occludens-1 alters connexin43 gap junction size and organization by influencing channel accretion. *Mol Biol Cell* 16:5686-5698.

99. Bergametti F, Denier C, Labauge P, et al. (2005) Mutations within the programmed cell death 10 gene cause cerebral cavernous malformations. *Am J Hum Genet* 76:42–51

100. Liquori CL, Berg MJ, Siegel AM, et al. (2003) Mutations in a gene encoding a novel protein containing a phosphotyrosine-binding domain cause type 2 cerebral cavernous malformations. *Am J Hum Genet* 73:1459–1464.

101. Batra S, Lin D, Recinos PF, et al. (2009) Cavernous malformations: Natural history, diagnosis and treatment. *Nat Rev Neurol* 5: 659–670

102. Noto S, Fujii M, Akimura T, Imoto H, Nomura S, Kajiwara K, et al. (2005) Management of patients with cavernous angiomas presenting epileptic seizures. *Surg Neurol* 64:495–499.

103. Ojemann RG, Ogilvy CS. (1999) Microsurgical treatment of supratentorial cavernous malformations. *Neurosurg Clin N Am* 10:433–440.

104. S. H. Lee, H. J. Choi, H. S. Shin, S. K. Choi, I. H. Oh, and Y. J. Lim. (2014) Gamma knife radiosurgery for brainstem cavernous malformations: should a patient wait for the rebleed? *Acta Neurochir* 156:1937-46

105. Cooper AD, Campeau NG and Meissner I. (2008) Susceptibility-weighted imaging in familial cerebral cavernous malformations. *Neurology* 71;382.

106. Duffau, H. et al. (1997) Early radiologically proven rebleeding from intracranial cavernous angiomas: report of 6 cases and review of the literature. *Acta Neurochir*. 139: 914-922.

107. Gault J, Shenkar R, Recksiek P, Awad IA. (2005) Biallelic somatic and germ line CCM1 truncating mutations in a cerebral cavernous malformation lesion. *Stroke*. 36:872-4.

108. Pagenstecher A, Stahl S, Sure U, and Felbor U. (2009) A two-hit mechanism causes cerebral cavernous malformations: complete inactivation of CCM1, CCM2 or CCM3 in affected endothelial cells. *Hum Mol Genet*. 18: 911–918.

109. Davenport W.J., Siegel A.M., Dichgans J., Drigo P., Mammi I., Pereda P., Wood N.W., Rouleau G.A.. (2001) CCM1 gene mutations in families segregating cerebral cavernous malformations. *Neurology* 56:540-543.

110. Kehrer-Sawatzki H, Wilda M, Braun VM, Richter HP, Hameister H. (2002) Mutation and expression analysis of the KRIT1 gene associated with cerebral cavernous malformations (CCM1). *Acta Neuropathol*. 104:231-40.

111. McDonald DA, Shi C, Shenkar R, Stockton RA, Liu F, Ginsberg MH, Marchuk DA, Awad IA. (2012) Fasudil decreases lesion burden in a murine model of cerebral cavernous malformation disease. *Stroke* 43:571-4.

112. Li X, Zhang R, Zhang H, He Y, Ji W, Min W, Boggon TJ (2010) Crystal structure of CCM3, a cerebral cavernous malformation protein critical for vascular integrity. *J Biol Chem* 285:24099–24107

113. Serebriiskii I, Estojak J, Sonoda G, Testa JR, Golemis EA (1997) Association of Krev-1/rap1a with Krit1, a novel ankyrin repeat-containing protein encoded by a gene mapping to 7q21- 22. *Oncogene* 15:1043–1049

114. Zhang J, Clatterbuck RE, Rigamonti D, Chang DD, Dietz HC (2001) Interaction between krit1 and icap1alpha infers perturbation of integrin beta1-mediated angiogenesis in the pathogenesis of cerebral cavernous malformation. *Hum Mol Genet* 10:2953–2960

115. Zhang J, Clatterbuck RE, Rigamonti D, Dietz HC (2000) Cloning of the murine Krit1 cDNA reveals novel mammalian 5' coding exons. *Genomics* 70:392–395 40.

116. Zhang J, Rigamonti D, Dietz HC, Clatterbuck RE (2007) Interaction between krit1 and malcavernin: implications for the pathogenesis of cerebral cavernous malformations. *Neurosurgery* 60:353–359

117. Liquori CL, Berg MJ, Siegel AM, Huang E, Zawistowski JS, Stoffer T, Verlaan D, Balogun F, Hughes L, Leedom TP, Plummer NW, Cannella M, Maglione V, Squitieri F, Johnson EW, Rouleau GA, Ptacek L, Marchuk DA (2003) Mutations in a gene encoding a novel protein containing a phosphotyrosinebinding domain cause type 2 cerebral cavernous malformations. *Am J Hum Genet* 73:1459–1464.

118. Fisher OS, Zhang R, Li X, Murphy JW, Demeler B, Boggon TJ (2013) Structural studies of cerebral cavernous malformations 2 (CCM2) reveal a folded helical domain at its C-terminus. *FEBS Lett* 587:272–277

119. Voss K, Stahl S, Schleider E, Ullrich S, Nickel J, Mueller TD, Felbor U (2007) CCM3 interacts with CCM2 indicating common pathogenesis for cerebral cavernous malformations. *Neurogenetics* 8:249–256.

120. Stahl S, Gaetzner S, Voss K, Brackertz B, Schleider E, Surucu O, Kunze E, Netzer C, Korenke C, Finckh U, Habek M, Poljakovic Z, Elbracht M, Rudnik-Schoneborn S, Bertalanffy H, Sure U, Felbor U (2008) Novel CCM1, CCM2, and CCM3 mutations in patients with cerebral cavernous malformations: in-frame deletion in CCM2 prevents formation of a CCM1/CCM2/CCM3 protein complex. *Hum Mutat* 29:709–717.

121. Serebriiskii I, Estojak J, Sonoda G, Testa JR, Golemis EA (1997) Association of Krev-1/rap1a with Krit1, a novel ankyrin repeat-containing protein encoded by a gene mapping to 7q21- 22. *Oncogene* 15:1043–1049

122. Glading A, Han J, Stockton RA, Ginsberg MH (2007) KRIT- 1/CCM1 is a Rap1 effector that regulates endothelial cell cell junctions. *J Cell Biol* 179:247–254

123. Glading AJ, Ginsberg MH (2010) Rap1 and its effector KRIT1/CCM1 regulate beta-catenin signaling. *Dis Model Mech* 3:73–83

124. T Zhan, N Rindtorff and M Boutros. (2017) Wnt signaling in cancer. *Oncogene* 36:1461–1473

125. Faurobert E, Rome C, Lisowska J, Manet-Dupe S, Boulday G, Malbouyres M, Balland M, Bouin AP, Keramidas M, Bouvard D, Coll JL, Ruggiero F, Tournier-Lasserve E, Albiges-Rizo C (2013) CCM1-ICAP-1 complex controls beta1 integrin-dependent endothelial contractility and fibronectin remodeling. *J Cell Biol* 202:545–561.

126. Zhang XA, Hemler ME (1999) Interaction of the integrin beta1 cytoplasmic domain with ICAP-1 protein. *J Biol Chem* 274:11–19.

127. Calderwood DA, Tai V, Di Paolo G, De Camilli P, Ginsberg MH (2004) Competition for talin results in trans-dominant inhibition of integrin activation. *J Biol Chem* 279:28889–28895

128. Zawistowski JS, Serebriiskii IG, Lee MF, Golemis EA, Marchuk DA (2002) KRIT1 association with the integrin-binding protein ICAP-1: a new direction in the elucidation of cerebral cavernous malformations (CCM1) pathogenesis. *Hum Mol Genet* 11:389–396.

129. Crose LE, Hilder TL, Sciaky N, Johnson GL (2009) Cerebral cavernous malformation 2 protein promotes smad ubiquitin regulatory factor 1-mediated RhoA degradation in endothelial cells. *J Biol Chem* 284:13301–13305

130. Cao Y, Zhang L. (2013) A Smurf1 tale: function and regulation of an ubiquitin ligase in multiple cellular networks. *Cell Mol Life Sci*. 70:2305-17

131. Crose LE1, Hilder TL, Sciaky N, Johnson GL. (2009) Cerebral cavernous malformation 2 protein promotes smad ubiquitin regulatory factor 1-mediated RhoA degradation in endothelial cells. *J Biol Chem*. 284:13301-5.

132. Amano M, Nakayama M, and Kaibuchi K. (2010) Rho-Kinase/ROCK: A Key Regulator of the Cytoskeleton and Cell Polarity. *Cytoskeleton (Hoboken)*. 67:545–554.

133. Watanabe N, Kato T, Fujita A, Ishizaki T, Narumiya S. (1999) Cooperation between mDia1 and ROCK in Rho-induced actin reorganization. *Nat Cell Biol*. 1:136-43.

134. Amano M, Chihara K, Kimura K, Fukata Y, Nakamura N, Matsuura Y, Kaibuchi K. (1997) Formation of actin stress fibers and focal adhesions enhanced by Rho-kinase. *Science*. 275:1308-11.

135. Richardson BT, Dibble CF, Borikova AL, Johnson GL (2013) Cerebral cavernous malformation is a vascular disease associated with activated RhoA signaling. *Biol Chem* 394:35–42

136. Stockton RA, Shenkar R, Awad IA, Ginsberg MH (2010) Cerebral cavernous malformations proteins inhibit Rho kinase to stabilize vascular integrity. *J Exp Med* 207:881–896

137. Borikova AL, Dibble CF, Sciaky N, Welch CM, Abell AN, Bencharit S, Johnson GL (2010) Rho kinase inhibition rescues the endothelial cell cerebral cavernous malformation phenotype. *J Biol Chem* 285:11760–11764.

138. Maddaluno L et al., (2013) EndMT contributes to the onset and progression of cerebral cavernous malformations. *Nature* 498:492–496.

139. Goudreault M, D'Ambrosio LM, Kean MJ, Mullin MJ, Larsen BG, Sanchez A, Chaudhry S, Chen GI, Sicheri F, Nesvizhskii AI, Aebersold R, Raught B, Gingras AC (2009) A PP2A phosphatase high density interaction network identifies a novel striatin-interacting phosphatase and kinase complex linked to the cerebral cavernous malformation 3 (CCM3) protein. *Mol Cell Proteomics* 8:157–171 97.

140. Hwang J and Pallas DC (2014) STRIPAK complexes: Structure, biological function, and involvement in human diseases. *Int J Biochem Cell Biol* 47:118– 148.

141. Sugden PH, McGuffin LJ and Clerk A. (2013) SOcK, MiSTs, MASK and STicKs: the GCKIII (germinal centre kinase III) kinases and their heterologous protein–protein interactions. *Biochem. J*. 454:13–30.

142. Ceccarelli DF, Laister RC, Mulligan VK, Kean MJ, Goudreault M, Scott IC, Derry B, Chakrabartty A, Gingras A and Sicheri F. (2011) CCM3/PDCD10 Heterodimerizes with Germinal Center Kinase III (GCKIII) Proteins Using a Mechanism Analogous to CCM3 Homodimerization. *J Biol Chem* 286:25056 –25064.

143. Zhang Y, Tang W, Zhang H, Niu X, Xu Y, Zhang J, Gao K, Pan W, Boggon TJ, Toomre D, Min W and Wu D. (2013) A network of interactions enables CCM3 and STK24 to coordinate UNC13D-driven vesicle exocytosis in neutrophils. *Dev Cell.* 27:10.1016

144. Zhou HJ, Qin L, Zhang H, Tang W, Ji W, He Y, Liang X, Wang Z, Yuan Q, Vortmeyer A, Toomre D, Fuh G, Yan M, Kluger MS, Wu D & Min W. (2016) Endothelial exocytosis of angiopoietin-2 resulting from CCM3 deficiency contributes to cerebral cavernous malformation. *Nat Med* 22:1033–1042.

145. Zhou Z, Rawnsley D, Goddard L, Pan W, Cao XJ, Jakus Z, Zheng H, Yang J, Arthur S, Whitehead KJ, Li D, Zhou B, Garcia BA, Zheng X, and Kahn ML. (2016) The cerebral cavernous malformation pathway controls embryonic endocardial gene expression through regulation of MEKK3 signaling and KLF expression. *Dev Cell*. 32:168–180.

146. Zhou Z, Tang AT, Wong WY, Bamezai S, Goddard LM, Shenkar R, Zhou S, Yang J, Wright AC, Foley M, et al. (2016) Cerebral cavernous malformations arise from endothelial gain of MEKK3-KLF2/4 signalling. *Nature*. 532:122-6.

147. Tang AT et al., (2017) Endothelial TLR4 and the microbiome drive cerebral cavernous malformations. *Nature* 545:305–310.

148. Marchi S et al., (2015) Defective autophagy is a key feature of cerebral cavernous malformations. *EMBO Mol Med* 7:1403–1417

149. Whitehead KJ, Plummer NW, Adams JA, Marchuk DA, Li DY. (2004) Ccm1 is required for arterial morphogenesis: implications for the etiology of human cavernous malformations. *Development* 131:1437–1448.

150. Boulday G, et al. (2009) Tissue-specific conditional CCM2 knockout mice establish the essential role of endothelial CCM2 in angiogenesis: implications for human cerebral cavernous malformations. *Dis Model Mech*. 2:168–177

151. Chan AC, Drakos SG, Ruiz OE, Smith AC, Gibson CC, Ling J, Passi SF, Stratman AN, Sacharidou A, Revelo P, Grossmann AH, Diakos NA, Davis GE, Metzstein MM, Whitehead KJ and Li DY. (2011)

Mutations in 2 distinct genetic pathways result in cerebral cavernous malformations in mice. *J Clin Invest*. 121:1871–1881

152. He Y, Zhang H, Yu L, Gunel M, Boggon TJ, Chen H and Min W. (2010) Stabilization of VEGFR2 Signaling by Cerebral Cavernous Malformation 3 Is Critical for Vascular Development. *Science Signaling* 3**:**ra26.

153. Louvi A, Chen L, Two AM, Zhang H, Min W, Gunel M (2011) Loss of cerebral cavernous malformation 3 (Ccm3) in neuroglia leads to CCM and vascular pathology. *Proc. Natl. Acad. Sci*. 108:3737–3742.

154. Louvi A, Nishimura S and Günel M. (2014) Ccm3, a gene associated with cerebral cavernous malformations, is required for neuronal migration. *Development* 141:1404-1415.

155. Plummer NW, Gallione CJ, Srinivasan S, Zawistowski JS, Louis DN, and Marchuk DA. (2004) Loss of p53 Sensitizes Mice with a Mutation in Ccm1 (KRIT1) to Development of Cerebral Vascular Malformations. *Am J Path* 165:1509-18

156. McDonald DA, Shenkar R, Shi C, Stockton RA, Akers AL, Kucherlapati MH, Kucherlapati R, Brainer J, Ginsberg MH, Awad IA, Marchuk DA. (2011) A novel mouse model of cerebral cavernous malformations based on the two-hit mutation hypothesis recapitulates the human disease. *Hum Mol Gen* 20:211–222.

Chapter 2: Connexin 43 Gap Junctions Contribute to Brain Endothelial Barrier Hyperpermeability in Familial Cerebral Cavernous Malformations Type III by Modulating Tight Junction Structure

2.1 Introduction

Familial Cerebral Cavernous Malformation Type III disease (fCCM3) is a disease that affects cerebrovascular capillary beds. Patients carry a null-mutation in one allele of *ccm3* (*pdcd*10) and capillary lesions are initiated upon acquiring a mutation in the second *ccm3* allele that causes loss of functional CCM3 protein in the cell. Lesions are characterized by dilated vessels, blood-filled caverns, loss of contact between endothelial cells and insufficient blood-brain-barrier (BBB) integrity. The impaired BBB integrity is considered the primary cause of fCCM3 morbidities, including seizures, focal neurological deficits and cerebral hemorrhage (1, 2). Currently, no effective treatment is available to fCCM3 patients and therapeutic development is hindered by a lack of thorough understanding of pathways regulated by CCM3 protein. Proteomic analysis has revealed that 80% of CCM3 protein is bound to the Striatin-interacting phosphatase and kinase (STRIPAK) complex (3). This large complex contains many phosphatases and kinases that produce wide-ranging cellular effects, including Golgi apparatus development, calcium sensing, and most recently, a CCM3-dependent effect on actin cytoskeleton organization mediated by cortactin (4, 5).

BBB integrity is maintained by a unique junction complex at the endothelial-endothelial border that includes adherens junctions (AJ), tight junctions (TJ) and gap junctions (GJ). Under normal physiologic conditions, crosstalk mechanisms allow these complexes to form a stable barrier that prevents paracellular permeability. The TJ complex is composed of transmembrane proteins, claudins and occludin, that form *trans*-interactions with neighboring cell claudins and occludin. These proteins serve to occlude

the paracellular space. Claudins and occludin are stabilized by intracellular adaptor proteins, including ZO-1, that function to tether them to the actin cytoskeleton. Analysis of TJ proteins in fCCM3 patient lesions as well as *in vitro* work has demonstrated loss of TJ proteins from the junctional complex of fCCM3 but not fCCM type I or II lesions (5, 6). Meanwhile the presence of AJs, which are organized in a similar manner to TJs with transmembrane cadherins and adapter proteins including beta-catenin, is less clear and reported as affected and unaffected in fCCM3 lesions (5, 7).

The final member of the BBB junction complex, the GJ, has not traditionally been ascribed a regulatory role for paracellular permeability. Gap junctions are channel structures at adjacent cell borders. They are formed by members of the connexin family (Cx) and allow direct passage of ions and small molecules <1kDa between the cytosols of adjacent cells. Channels are formed by the aggregation of homo- or hetero-hexameric connexin proteins (8, 9). Many Cx family members exist and display tissue-specific expression, with Cx37, Cx40 and Cx43 being expressed in brain endothelia (10, 11). How or if GJs can regulate paracellular permeability has not been established. Aberrant elevation of Cx43 protein has recently been shown to be detrimental to barrier integrity but whether this effect is dependent on Cx43 GJs or other functions of Cx43, including hemichannels (HC) that do not directly oppose another Cx43 channel, has not been thoroughly described (12, 13).

We have identified that $ccm3^{+/-}p53^{-/-}$ mice, a murine model of fCCM3, have elevated Cx43 protein expression in lesions. Analysis of Cx43 in CCM3 knock down (CCM3KD) brain endothelial cells *in vitro* also reveals increased GJ activity and that reducing Cx43 expression and GJ activity rescues the permeability defect in CCM3KD cells. The focus of this study is to define the mechanism by which Cx43 GJs can regulate permeability as well as to establish whether increased Cx43 protein is a primary defect in the maturation of CCM3 lesions in a mouse model of fCCM3.

2.2 Results

2.2.1 Connexin 43 is elevated in brain endothelial cells and pericytes lacking CCM3.

To determine if the expression or activity of connexin (Cx) family members was altered by CCM3 deficiency, we established an *in vitro* fCCM3 model using siRNA-mediated CCM3 knockdown (CCM3KD) in a murine brain pericyte and brain endothelial cell line (mBECs). The endothelial cell line was selected for use in this study due to its unaltered expression of junction proteins and unaffected barrier properties. We achieved greater than 80% efficiency of CCM3KD (Fig 2.2.1A) and identified that Cx43 protein is elevated in CCM3KD mBECs (Fig. 2.2.1A). Cx43 transcript, however, is not affected (Fig. 2.2.1B), indicating post-translational regulation of Cx43 by CCM3. This observation is consistent with the regulation of TJ proteins by CCM3 (5). No difference in protein expression was observed for the two additional Cx family members expressed by mBECs, Cx37 and Cx40, though a compensatory upregulation of Cx40 transcript is apparent. This observation is significant given that it suggests loss of CCM3 regulates Cx43 specifically instead of having broad effects on Cx protein expression as a whole.

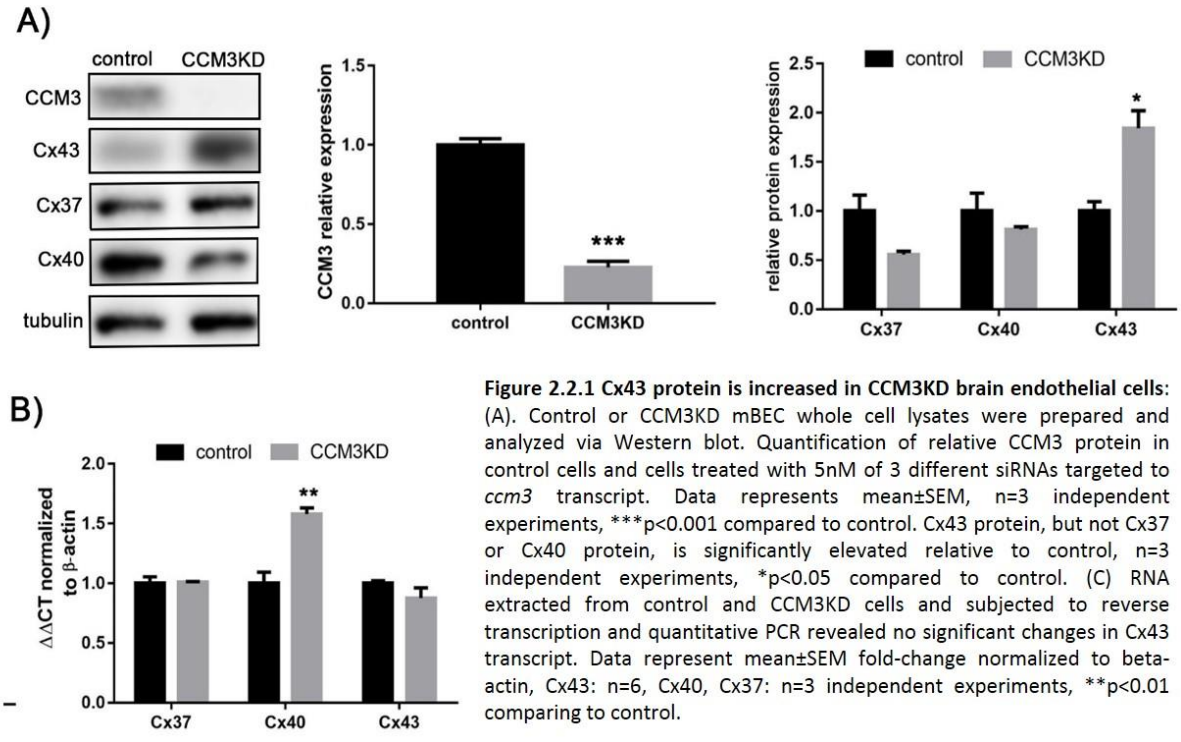

Figure 2.2.1 Cx43 protein is increased in CCM3KD brain endothelial cells: (A). Control or CCM3KD mBEC whole cell lysates were prepared and analyzed via Western blot. Quantification of relative CCM3 protein in control cells and cells treated with 5nM of 3 different siRNAs targeted to *ccm3* transcript. Data represents mean±SEM, n=3 independent experiments, ***p<0.001 compared to control. Cx43 protein, but not Cx37 or Cx40 protein, is significantly elevated relative to control, n=3 independent experiments, *p<0.05 compared to control. (C) RNA extracted from control and CCM3KD cells and subjected to reverse transcription and quantitative PCR revealed no significant changes in Cx43 transcript. Data represent mean±SEM fold-change normalized to beta-actin, Cx43: n=6, Cx40, Cx37: n=3 independent experiments, **p<0.01 comparing to control.

Pericytes also express Cx43 and this represents a central mechanism enabling crosstalk between pericytes and endothelial cells in homeostasis (14). In addition to its elevation in mBECs, we also observed that Cx43 protein is elevated in CCM3KD pericytes (Figure 2.2.2).

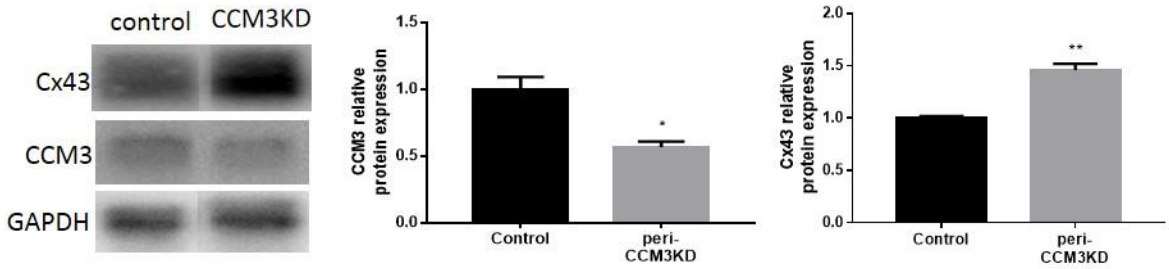

Figure 2.2.2 Cx43 is evelated in CCM3KD pericytes. Control and CCM3KD pericyte whole cell lysates were prepared and analyzed via western blot. CCM3KD efficiency was approximately 50% and resulted in a significant increase in Cx43 protein expression compared to control pericytes. n=3 independent experiments, *p<0.05, **p<0.01 compared to control.

Cx43 has many functions that are dependent on its cellular localization (15, 16). We performed cell fractionation of control and CCM3KD mBECs to determine whether CCM3KD affected the localization of Cx43 (Fig. 2.2.3A). This analysis revealed that in both control and CCM3KD mBECs, Cx43 is incorporated into the insoluble fraction of the cell, but was absent from the soluble, cytosolic compartment. Immunofluorescence of Cx43 confirmed that in both control and CCM3KD mBECs, Cx43 was localized to the membrane region and formed plaque-like structures consistent with GJ plaques (Fig. 2.2.3C). Cx43 GJ plaques in CCM3KD mBECs appeared much larger than in controls and quantitation of plaque size revealed a significant increase in the size of Cx43 GJ plaques in CCM3KD mBECs compared to controls (Fig. 2.2.3D). Cx43 GJ plaques showed no difference in mobility between control and CCM3KD mBECs, as assessed by FRAP, indicating that, while more Cx43 accumulates in GJ plaques of CCM3KD mBECs, no difference in Cx43 protein stability within the GJ plaque exists between control and CCM3KD mBECs (Fig. 2.2.3B).

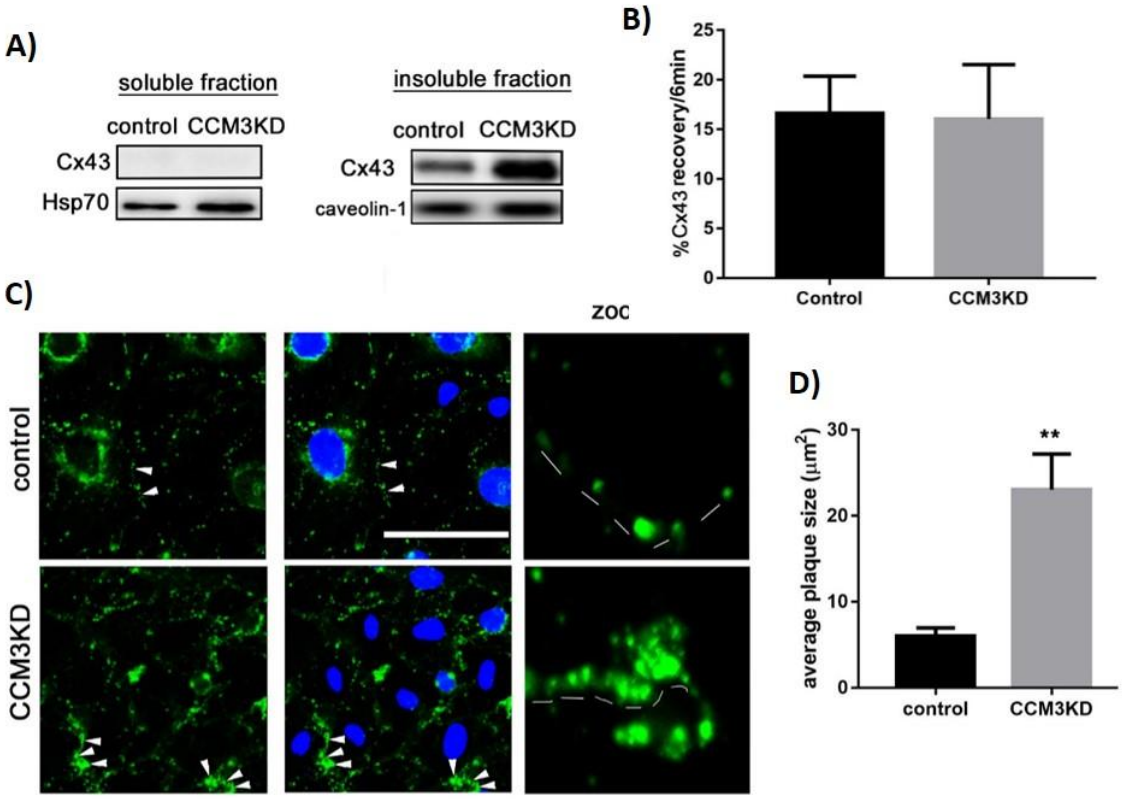

Figure 2.2.3 CCM3KD mBECs express large Cx43 GJ plaques on cell borders. (A) mBEC whole cell lysates were subjected to cell fractionation. Cx43 was only present in the insoluble fraction (Caveolin-1) and not in the cytosol (Hsp70). Representative Western blot, n=3 independent experiments. (B) FRAP analysis of control and CCM3KD cells expressing Cx43-AcGFP. FRAP was performed on membrane regions of interest (ROIs), n=6 ROIs from 6 cells. (C) Immunofluorescence staining of Cx43 (column 1), merged Cx43 and DAPI staining (column 2), and zoom images of Cx43 GJs along the cell membrane (column 3, dashed lines) in control and CCM3KD cells (GJ plaques indicated with white arrows). Scale bar = 100μm. (D) Cx43 GJ plaque size was measured in ImageJ. For 3 image fields with approximately 8 cells/field, the entire membrane region of every cell was selected to analyze particle (GJ plaque) size in Cx43 labeled samples. The average plaque size is reported as the mean±SEM of all GJ plaques measured (~50 plaques/field). This analysis revealed significantly larger GJ plaques in CCM3KD cells compared to controls, **p<0.01.

To determine whether Cx43 is elevated in other fCCM subtypes, Cx43 protein expression was analyzed in CCM1KD and CCM2KD mBECs (Fig 2.2.4). Cx43 protein expression was significantly, but not robustly elevated following siRNA-mediated KD of CCM1 or CCM2. Overall, our initial analysis of Cx43 expression indicates that 1) Cx43 is the only endothelial Cx family member regulated at the level of protein by CCM3 and 2) while CCM1 and CCM2 have some contribution to Cx43 protein regulation, CCM3 demonstrates the most robust effect on Cx43 protein expression.

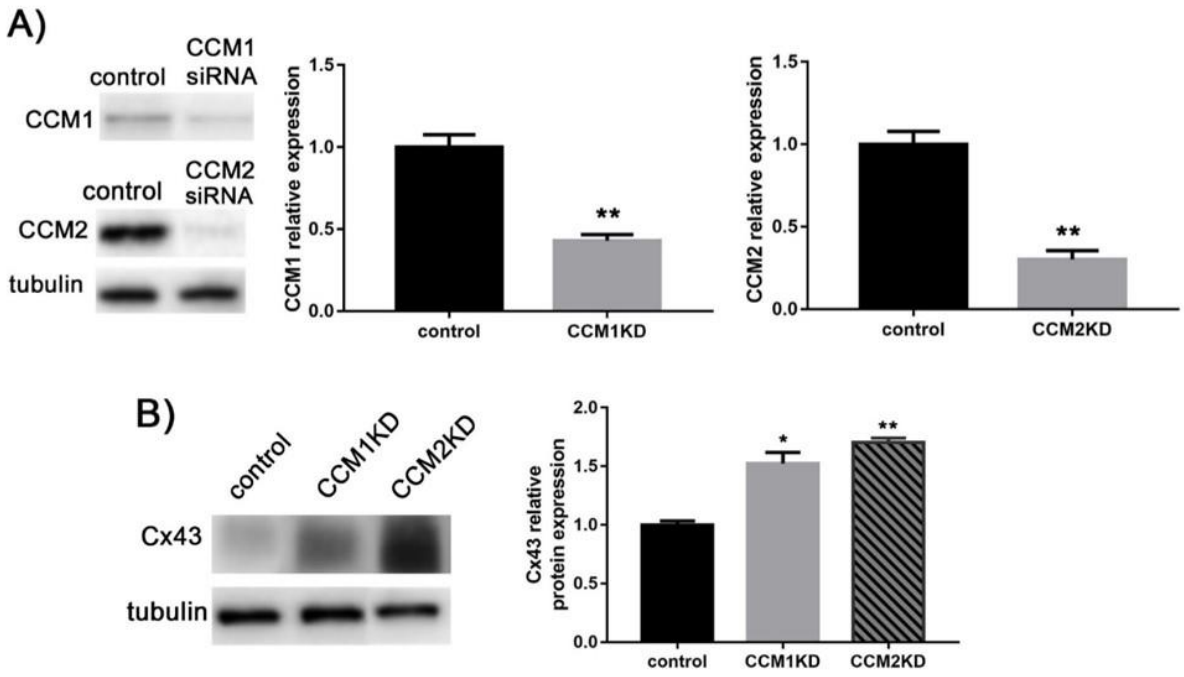

Figure 2.2.4 Cx43 is moderately elevated in CCM1KD and CCM2KD mBECs (A) Representative western blot of CCM1 and CCM2 protein in whole cell lysates prepared from cells treated with 10nM siRNA targeted to *ccm1* or *ccm2* transcript. Quantification of relative CCM1 or CCM2 protein expression in control and CCM1KD or CCM2KD cells reveals significant 60% and 70% decrease of CCM1 or CCM2 protein relative to control, respectively, n=3 independent experiments, **p<0.01 compared to control. (B) Cx43 expression evaluated by western blot in control, CCM1KD and CCM2KD cells in whole cell lysates. Quantification of Cx43 protein reveals a significant increase in both CCM1KD and CCM2KD cells, n=3 independent experiments, *p<0.05, **p<0.01 compared to control.

2.2.2 Loss of CCM3 results in elevated Cx43 Gap Junction and Hemichannel activity

Whether or not the larger Cx43 GJ plaques in CCM3KD mBECs have a functional effect on GJ intracellular communication (GJIC) – a canonical function of Cx43 – was evaluated using two assays to assess the ability of control or CCM3KD mBECs to transfer a non-cell permeable dye, Lucifer Yellow (LY), from one cell to another. Both assays work on the basis that more LY transfers indicates higher GJIC. First, single-cell microinjection of LY into control or CCM3KD mBEC monolayers showed significantly higher capacity for CCM3KD mBECs to transfer dye to adjacent cells than in controls (Fig. 2.2.5A). Second, scratch assay analysis of LY dye transfer in control or CCM3KD mBEC monolayers confirmed the microinjection results, demonstrating significantly greater ability of CCM3KD mBECs to transfer dye than control cells. To

validate that LY dye transfer was occurring specifically through Cx43 GJs, and not Cx37 or Cx40 GJs, scratch assays were performed in the presence of a Cx43 GJ-specific inhibitor, GAP27. GAP27 is a peptide that binds to the 2nd extra-cellular loop of Cx43 and prevents physical contact between neighboring cell GJ plaques (17). GAP27 completely inhibited CCM3KD GJIC, ruling out the possibility that Cx37 and Cx40 were directly contributing to increased GJIC in CCM3KD mBECs.

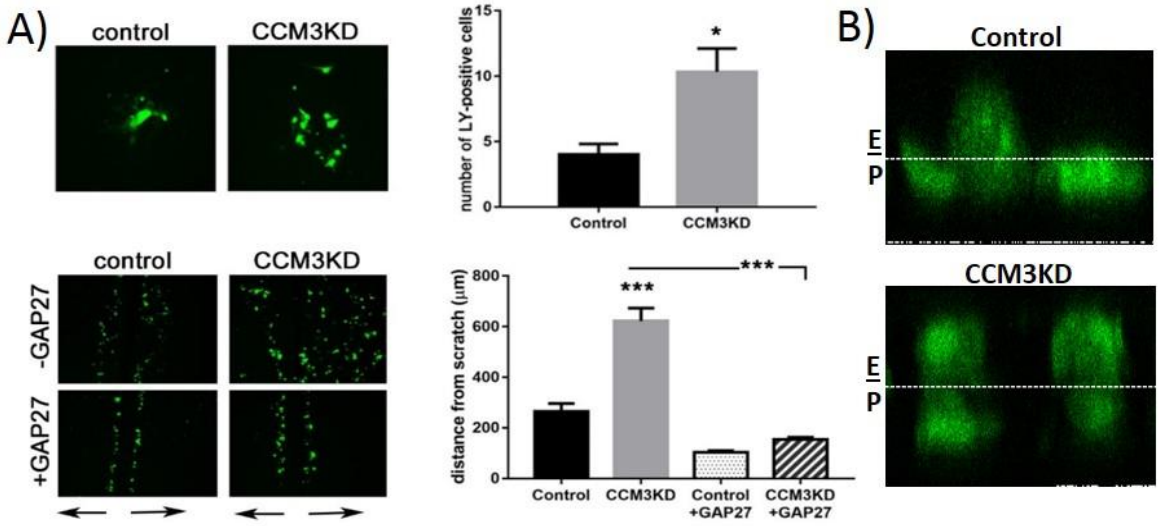

Figure 2.2.5 CCM3KD cells have elevated GJIC (A) GJIC measured by microinjection (top) and scratch assay (bottom). Single-cell injections were performed in control and CCM3KD samples. The number of neighboring LY+ cells was counted in ImageJ, n=3 independent injections over 3 plates, *p<0.05. Scratch assays also reveal a significant increase in GJIC function, measured by distance of LY spreading perpendicular to scratch (black arrows below image) in CCM3KD cells compared to controls. GJIC could be rescued by treatment with 100μM GAP27 for 24hrs. Data represent mean±SEM; n=3 independent experiments, 10 measurements/experiment, ***p<0.0001 compared to control or CCM3KD. 4X magnification. (B) GJIC between mBECs and pericytes in control mBECs and control pericytes (control) or CCM3KD mBECs and CCM3KD pericytes (CCM3KD). mBECs and pericytes were cultured at a 1:5 ratio in a transwell with mBECs on top of insert membrane and pericytes on the underside of insert membrane. mBECs were microinjected with LY and allowed to transfer dye for 30sec prior to wash, fixation and imaging. Images are z-sections of insert membrane (dashed line). LY above insert represent mBECs microinjected or with transferred dye from injected mBEC, LY below insert represent LY transferred from injected mBECs to pericytes.

Given that fCCM3 lesions display disrupted architecture and are often lacking pericytes, we tested the hypothesis that GJIC between CCM3KD mBECs and CCM3KD pericytes was inhibited. Using microinjections of LY in a transwell system, with physiologically relevant mBEC:pericyte ratios, we determined that GJIC remained intact between mBECs and pericytes, as determined by z-section imaging

of microinjected mBEC and pericyte monolayers (Fig. 2.2.5B). While this experiment was not quantitative, it does rule out the possibility that GJIC is inhibited between these cell types and inhibited communication between these cell types does not explain the absence of pericytes from fCCM3 lesions.

The HC activity of CCM3KD mBECs was also assessed. Using similar principles as GJIC assays, control or CCM3KD mBECs were overlayed with LY without previous injury to the plate, unlike GJIC assays. In this scenario, only cells with open HCs can uptake LY. We observed that CCM3KD mBEC monolayers had significantly more LY^+ cells compared to control cell monolayers (Fig. 2.2.6). When the volume of LY uptaken by each cell was measured using ImageJ, we determined that while more CCM3KD mBECs uptook LY compared to control cells, no significant difference in the LY volume/cell was observed. HC activity could be significantly decreased in CCM3KD mBECs by treatment of GAP19, a Cx43-specific HC inhibitor,

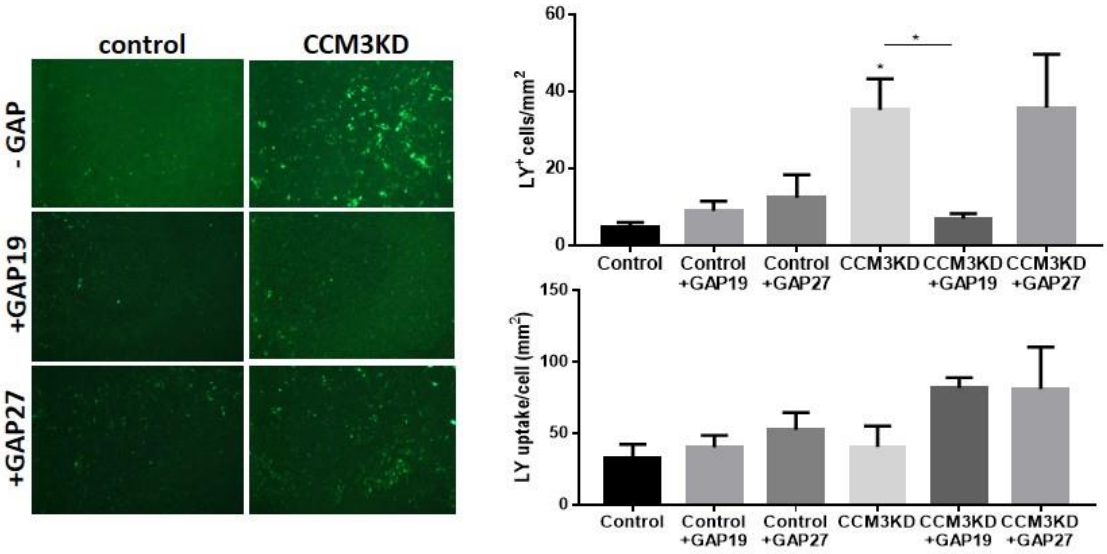

Figure 2.2.6 Hemichannel activity is elevated in CCM3KD cells. Control or CCM3KD mBEC monolayers were overlayed with LY and allowed to uptake dye for 30sec prior to wash, fixation and imaging. Cells were untreated or treated with 100μM GAP19 or 100μm GAP27 for 1hr prior to LY overlay. The number of LY^+ cells/mm2 were counted using ImageJ. Untreated CCM3KD had significantly more LY^+ cells compared to control cells, with significant reduction of LY^+ cell count with GAP19 treatment. Data represents average ± SEM, *$p<0.05$ compared to control or CCM3KD. The amount of LY uptake by individual cells was calculated using ImageJ by measuring the area of LY^+ present in individual LY^+ cells. Compared to control cells, untreated CCM3KD mBECs did not uptake significantly more LY/cell. 1hr treatment with 100μM GAP19 or 100μm GAP27 did not affect amount of LY uptake in control or CCM3KD cells. Data represent average ± SEM.

indicating that LY uptake is due to increased Cx43 HCs and not due to HCs formed by other Cx family members.

Finally, the morphology of GJ plaques in CCM3KD mBECs treated with GAP27 visualized by immunofluorescence staining of Cx43 suggests that prolonged GAP27 treatment inhibits GJIC by disbanding GJ plaques (Fig. 2.2.7A). Quantitation of Cx43 plaque size confirmed that GAP27 treatment reduces plaque size. Super resolution imaging highlights the reduction in GJ plaque size, such that GJ plaque size in CCM3KD cells treated with GAP27 is comparable to control cell (Fig. 2.2.7B).

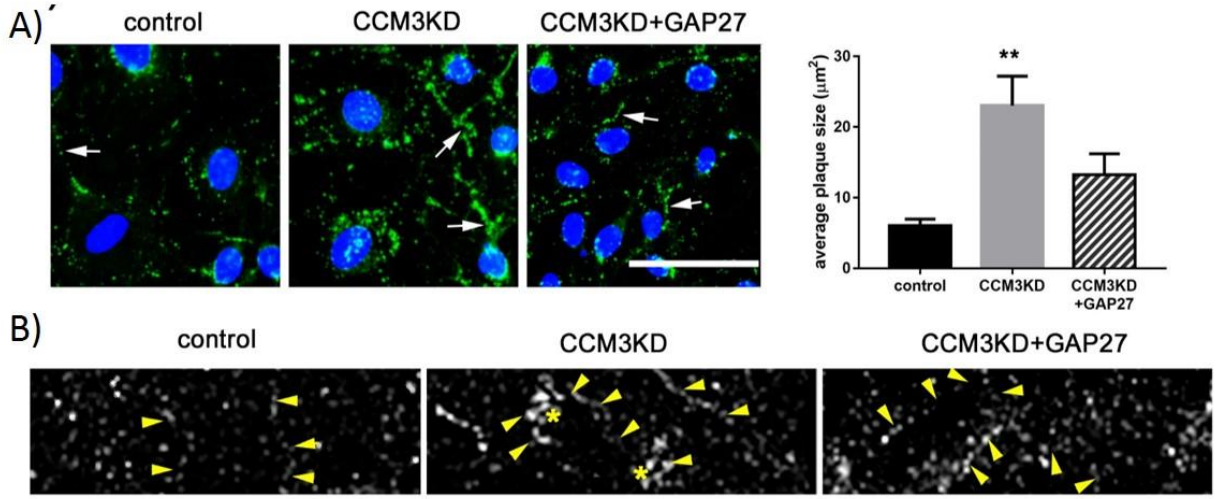

Figure 2.2.7 CCM3KD cells have larger GJ plaques. (A) Immunofluorescence staining of Cx43 GJ plaques (white arrows) in control, CCM3KD and CCM3KD+GAP27 reveals rescue of plaque size by 100μM GAP27 treatment for 24hrs. Scale bar = 100μm. Plaque size was quantified in ImageJ as described in Fig 2.2.3 legend, n=3 image fields, ~50 plaques/field. **p<0.01 compared to control. (B) Super resolution imaging of control, CCM3KD and CCM3KD cells treated with 100μM GAP27 for 24 hrs. Arrows indicate cell border, stars indicate GJ plaques.

2.2.3 Blockage of Gap Junction Intercellular Communications rescues hyperpermeability of brain endothelial cells lacking CCM3.

To evaluate whether elevated Cx43 protein expression in CCM3KD cells contributes to the hyperpermeability characteristic of fCCM3, we measured the transendothelial electrical resistance (TEER) in CCM3KD cells in which Cx43 protein expression was reduced through siRNA-mediated knockdown (Fig 2.2.8). As expected, CCM3KD cells alone displayed reduced monolayer electrical resistance, indicative of

increased monolayer permeability. Importantly, reducing Cx43 expression in CCM3KD cells partially but significantly restored CCM3KD monolayer TEER. As an additional control, TEER of brain endothelial cell monolayers over-expressing Cx43 ($Cx43^{over}$) was evaluated and revealed that Cx43 overexpression alone resulted in cell monolayers as permeable as CCM3KD.

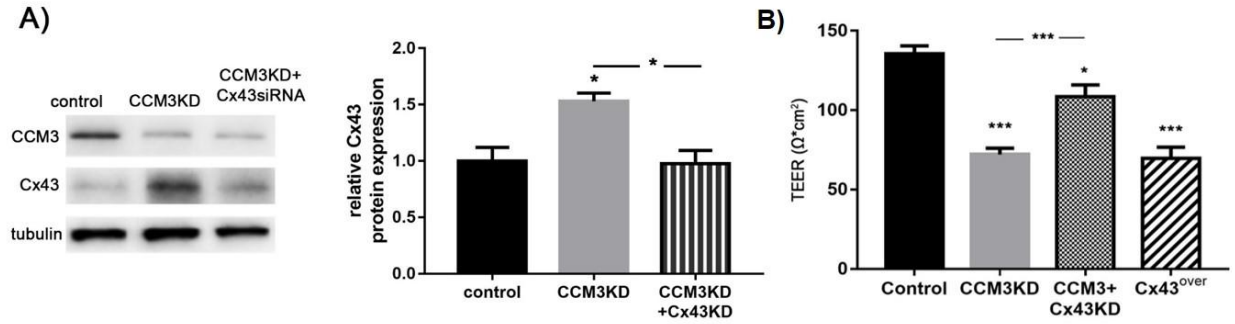

Figure 2.2.8: Depletion of Cx43 protein rescues CCM3KD monolayer permeability. (A) Double KD of Cx43 and CCM3KD was achieved by treating cells with 10nM siRNA targeting Cx43 transcript in addition to ccm3 targeted siRNA. Quantification of Cx43 protein reveals a significant decrease of Cx43 in Cx43+CCM3KD cells compared to CCM3KD cells, n=3 independent experiments, *p<0.05 compared to control, *p<0.05 compared to CCM3KD. (B) Transwell TEER assays revealed a significant increase in CCM3KD permeability and partial, significant rescue following reduction of Cx43 expression in CCM3KD cells via Cx43 siRNA-mediated KD. Data represent means±SEM, n=3-10 independent experiments, *p<0.05, ***p<0.0001 compared to control; ***p<0.001 compared to CCM3KD. Cx43+CCM3KD efficiency was determined by western blot analysis of whole cell lysates from control, CCM3KD or Cx43+CCM3KD cells.

The expression of TJ proteins ZO-1 and Claudin-5 was evaluated to determine whether elevated Cx43 protein expression in CCM3KD cells or $Cx43^{over}$ cells may regulate permeability in a TJ-dependent manner (Fig 2.2.9). CCM3KD cells exhibited reduced expression of both Claudin-5 and ZO-1, consistent with the observed decrease in monolayer permeability. Overexpression of Cx43 replicates the pattern of TJ protein expression in CCM3KD cells, particularly with ZO-1 expression, overall suggesting that elevated Cx43 protein expression may be pathologic to CCM3KD cells by regulating permeability by a TJ protein expression-dependent mechanism.

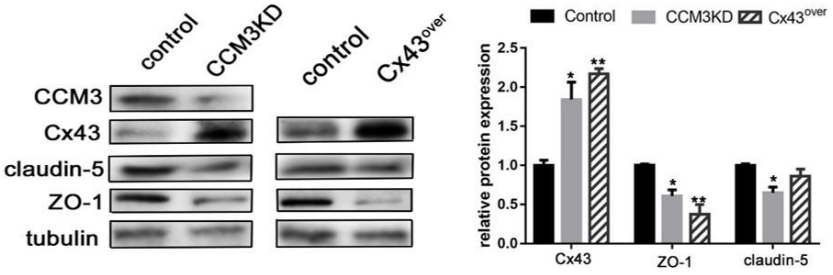

Figure 2.2.9: CCM3 depleted and Cx43 overexpressing mBECs exhibit decreased TJ protein expression. Representative western blot and quantification of Cx43, Claudin-5 and ZO-1 in whole cell lysates of control, CCM3KD and Cx43 over-expressing ($Cx43^{over}$) cells, n=3 independent experiments, Cx43: *p<0.05, **p<0.01 compared to control; ZO1: *p<0.05, **p<0.01 compared to control; Claudin-5: *p<0.05 compared to control.

Given that rescue of Cx43 protein expression in CCM3KD cells partially restores CCM3KD cell permeability, and that elevated Cx43 expression functionally translates to increased GJIC, we examined whether inhibition of Cx43 GJIC

specifically would rescue CCM3KD monolayer permeability (Fig 2.2.10). TEER analysis of control and CCM3KD cells in the presence of GAP27 revealed that GAP27 completely rescued CCM3KD monolayer electrical resistance, with no adverse effect on control cells. GAP19, a Cx43 hemichannel (HC)-specific inhibitor (18), had no effect on CCM3KD TEER, suggesting that it is the GJ-specific functions of Cx43 that are pathologic to CCM3KD permeability. This finding is the first demonstration that inhibition of GJs can prevent the increased permeability characteristic of CCM3KD cells.

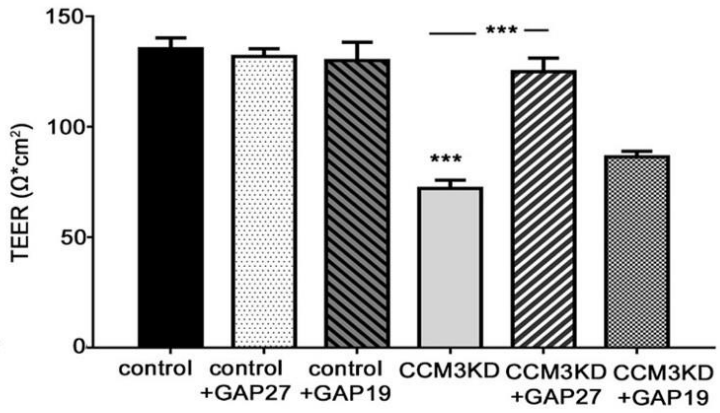

Figure 2.2.10 GAP27-mediated inhibition of Cx43 GJIC rescues CCM3KD monolayer permeability. Transwell TEER assays performed with control and CCM3KD cells treated with 100μM GAP19 or 100μM GAP27 for 24 hrs. Treatment with GAP27 completely rescues CCM3KD permeability. GAP19 treatment has no effect, n=3-10 independent experiments, ***p<0.0001 compared to control or CCM3KD.

2.2.4 Cx43 Gap Junctions disrupt Tight Junction organization in brain endothelial cells lacking CCM3.

Having determined that Cx43 GJIC is pathologic to CCM3KD permeability, we next examined how Cx43 GJs regulate permeability in CCM3KD cells. In addition to the observation that CCM3KD and Cx43^{over} cells have reduced ZO-1 protein expression, and that ZO-1 is absent from fCCM3 lesions (5, 7), ZO-1 has emerged as a candidate protein linking Cx43 to permeability because of a well-described Cx43-ZO-1 interaction (19-21). The Cx43/ZO-1 interaction restricts Cx43 GJ size (22, 23). However, whether Cx43 GJs can regulate ZO-1, particularly its function in TJs, is not known. We tested the hypothesis that Cx43 GJs affect the organization of TJs through regulating ZO-1 localization. We first analyzed Cx43 and ZO-1 co-localization in control, CCM3KD and GAP27-treated CCM3KD cells by immunofluorescence staining (2.2.11A). In control cells, ZO-1 is localized at TJs along the cell border, identified by its continuous staining along the cell border. Small protrusions of ZO-1 are visible in control cells when co-localized with Cx43 GJs, however, ZO-1 continuity along the border in TJs is not broken by its co-localization with GJ plaques. CCM3KD cells show striking differences in ZO-1 localization. ZO-1 is mostly absent from the TJ structures,

exhibiting only fragmented, non-continuous staining along the cell border. Also in contrast to controls, ZO-1 forms large plaque-like structures when co-localized with Cx43 GJs in CCM3KD cells. Measurement of Cx43 GJ-associated ZO-1 plaques revealed that CCM3KD cells had significantly larger ZO-1 plaques (Fig 2.2.11B). When we measured the length of TJ-associated, continuous cell-border ZO-1 staining, CCM3KD cells had significantly smaller TJ-associated fragments compared to controls (Fig 2.2.11C). Comb-like ZO-1 structures extending into the cytosol from the cell border, characteristic of disorganized ZO-1, were

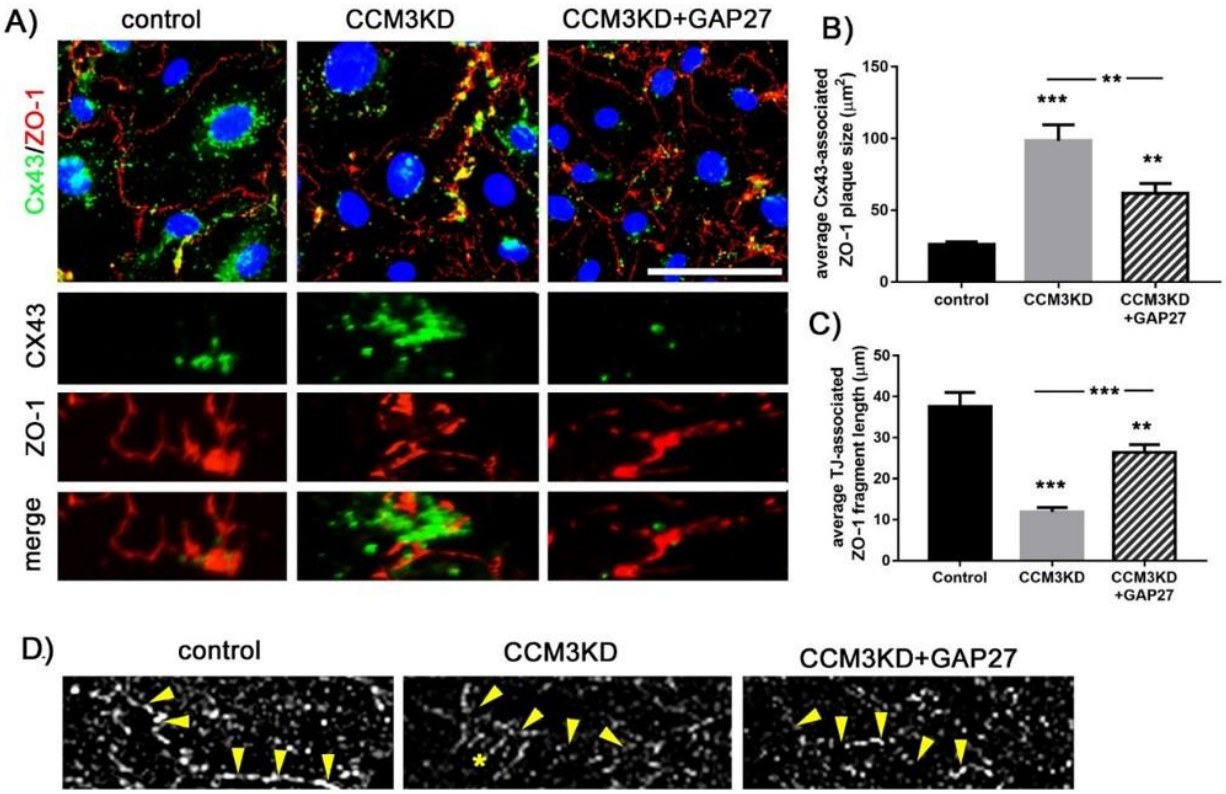

Figure 2.2.11 Inhibition of Cx43 GJIC rescues TJ disorganization in CCM3KD cells. (A) Immunofluorescence staining of Cx43 and ZO-1 in control, CCM3KD and CCM3KD+GAP27 (100μM) cells. Zoom images demonstrate 1) Cx43 GJ-plaque associated ZO-1 and 2) TJ-associated ZO-1, represented by continuous staining along the cell border. Scale bar = 100μm. (B) Quantitation of Cx43 GJ-associated ZO-1 plaque size was performed in ImageJ by measuring individual ZO-1 plaques associated with Cx43 as determined by corresponding Cx43/ZO-1 merge images. Three image fields with ~8 cells/field, 15 plaques/field were analyzed. CCM3KD cells display significantly larger Cx43-associated ZO-1 plaques compared to control. GAP27 treatment of CCM3KD cells significantly reduced CCM3KD ZO-1 plaques, ***p<0.0001, **p<0.01 compared to control; **p<0.01 compared to CCM3KD. (C) Quantitation of TJ-associated ZO-1 fragments along the cell border. The length of ZO-1 fragments along the cell border was measured for 3 image fields with 8 cells/field in ImageJ, ***p<0.0001, **p<0.01 compared to control; ***p<0.0001 compared to CCM3KD. (D) Super-resolution images of TJ-associated ZO-1 fragments on the cell border (arrows) and comb-like organization in CCM3KD cells (star)

observed in super-resolution imaging of ZO-1 in CCM3KD cells (Fig 2.2.11D). Together, these observations suggest that in control cells, ZO-1 preferentially localizes to TJs and does not accumulate at Cx43 GJs. However, in CCM3KD cells, ZO-1 preferentially localizes to and accumulates at Cx43 GJs and does not form continuous, organized TJ structures at the cell border. Intriguingly, treatment of CCM3KD cells with GAP27 partially restores the localization of ZO-1 to TJs and away from GJs. The observed ZO-1 localization is consistent with our permeability results – loss of ZO-1 from TJs increases permeability and restoration of ZO-1 to TJs by GAP27 restores permeability. Quantification of Cx43 GJ- or TJ-associated ZO-1 and super resolution imaging demonstrate the restoration of ZO-1 organization and distribution to TJ fragments in CCM3KD cells following inhibition of Cx43 GJs by GAP27 treatment.

The mobility of TJ-associated ZO-1 was analyzed by FRAP (Fig 2.2.12A). Given its size and function as a scaffolding protein, ZO-1 is a relatively immobile protein in healthy cells. We determined that ZO-1 is significantly more mobile in CCM3KD cells compared to controls. This supports our data the ZO-1 is not localized and anchored in highly immobile TJ structures. GAP27 treatment restores ZO-1 mobility to control levels, also consistent with redistribution of ZO-1 to TJ structures in GAP27-treated CCM3KD cells.

To further delineate the nature of Cx43/ZO-1 co-localization observed in CCM3KD cells, we used acceptor-photobleaching FRET analysis in cells co-expressing Cx43-mCherry and ZO-1-AcGFP. Given that the ZO-1 binding site on Cx43 is located at its very C-terminus, Cx43 was tagged on its N-terminus to facilitate interaction between these two proteins. CCM3KD cells had significantly lower FRET efficiency between Cx43 and ZO-1 compared to controls (Fig. 2.2.12B). These data indicate that while Cx43 and ZO-1 strongly co-localize in CCM3KD cells, they do not physically interact to the same extent as in control cells. This is consistent with our data indicating higher GJ activity and the literature showing Cx43/ZO-1 interaction is inhibitory to GJIC. Finally, GAP27 treatment of CCM3KD cells restores the Cx43/ZO-1

interaction, consistent with inhibition of GJIC, and further supporting the notion that theCx43/ZO-1 interaction is important for Cx43-mediated effects on permeability.

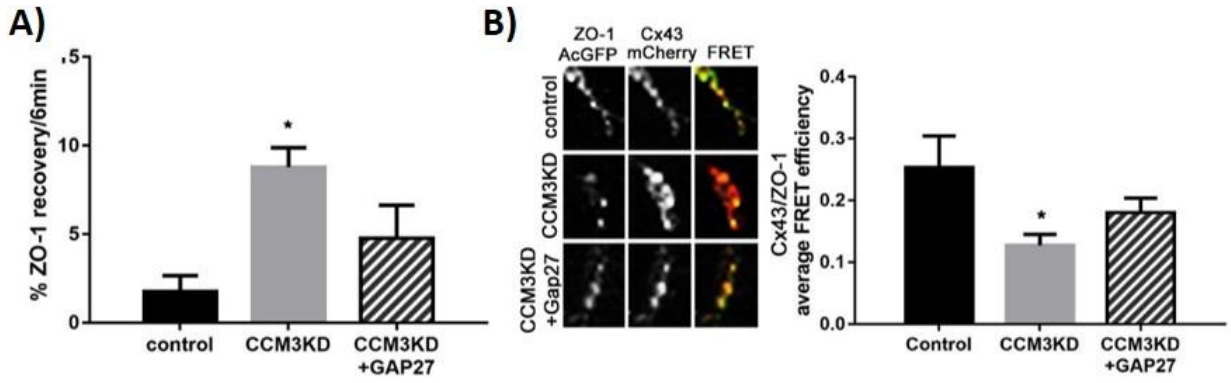

Figure 2.2.12 CCM3KD alters ZO-1 mobility and interaction at the membrane. (A) FRAP analysis of TJ-associated ZO-1 in control, CCM3KD and CCM3KD+GAP27 cells expressing ZO-1-AcGFP, *p<0.05 compared to control. (B) Acceptor photo-bleaching FRET of Cx43 GJ-associated ZO-1 in cells co-expressing Cx43-mCherry and ZO-1-AcGFP in control, CCM3KD or CCM3KD+GAP27 cells, n=30 ROIs/group, *p<0.05 compared to control.

We extended our analysis of Cx43 GJ apparent regulation of TJs to include the TJ transmembrane protein, Claudin-5. Similar to ZO-1, we observed that Claudin-5 is more mobile in CCM3KD cells compared to controls and that this trend is rescued by GAP27 treatment (Fig. 2.2.13A). Super resolution imaging of Claudin-5 demonstrated continuous staining of Claudin-5 along the cell border in control cells, indicative of TJ-incorporation (Fig. 2.2.13B). As with ZO-1, TJ incorporated Claudin-5 appears fragmented in CCM3KD cells but GAP27-mediated inhibition of Cx43 restores localization of Claudin-5 to the TJs. Examination of ZO-1/Claudin-5 co-localization, a necessary step for the formation of functional TJs (24), indicated expected co-localization at TJ structures along the cell border in control cells but fragmented TJ-associated Claudin-5 in CCM3KD cells (Fig. 2.2.13C). Quantitation of TJ-associated Claudin-5 fragment length revealed highly fragmented TJ-associated Claudin-5 in CCM3KD cells but rescue of TJ-associated fragment length by inhibition of Cx43 GJs with GAP27 (Fig. 2.2.13D).

Finally, the frequency of Claudin-5/ZO-1 and Claudin-5/Claudin-5 *trans*-interactions was analyzed by FRET. TJ-associated Claudin-5 and ZO-1 interacted less frequently in CCM3KD cells but this interaction was restored by Cx43 GJ inhibition. Similarly, the ability of Claudin-5 to form *trans*-interactions with neighboring cell Claudin-5 was compromised in CCM3KD cells and restored by GAP27-mediated inhibition of Cx43 GJs.

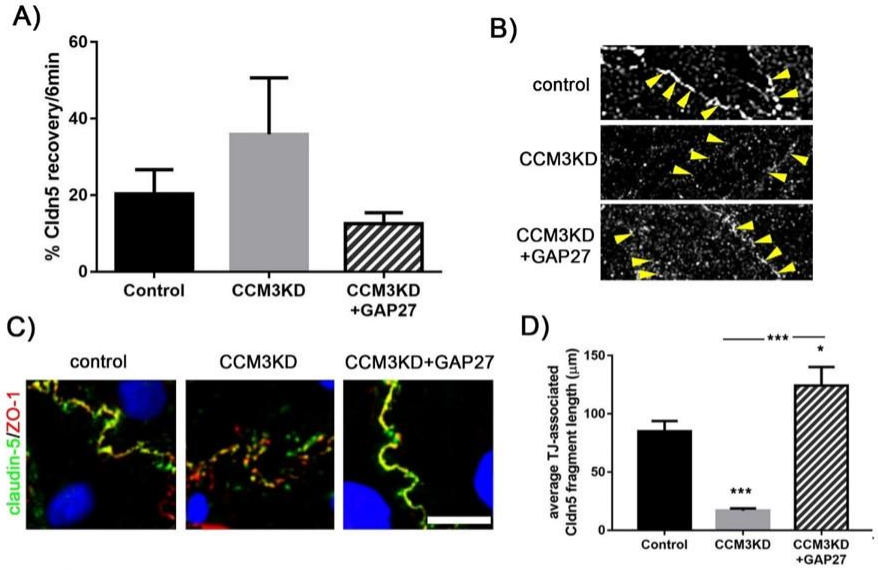

Figure 2.2.13 Claudin-5 incorporation into TJs is rescued by Cx43 GJ inhibition. (A) FRAP analysis of Claudin-5 (Cldn5) in control, CCM3KD and CCM3KD+GAP27 (100μM) cells expressing Claudin-5-AcGFP. (B) Super-resolution imaging of TJ-associated Claudin-5 (arrows). (C) Immunofluorescence staining of Claudin-5 and ZO-1 in control, CCM3KD and CCM3KD+GAP27 (100μM) cells. Scale bar = 25μm. (D) Quantitation of the average TJ-associated Claudin-5 fragment length in Claudin-5/ZO-1 co-stained immunofluorescent images. Fragment length was measured in ImageJ as described for ZO-1 fragment length in Fig 5C legend; *p<0.05, ***p<0.0001 compared to control; ***p<0.0001 compared to CCM3KD.

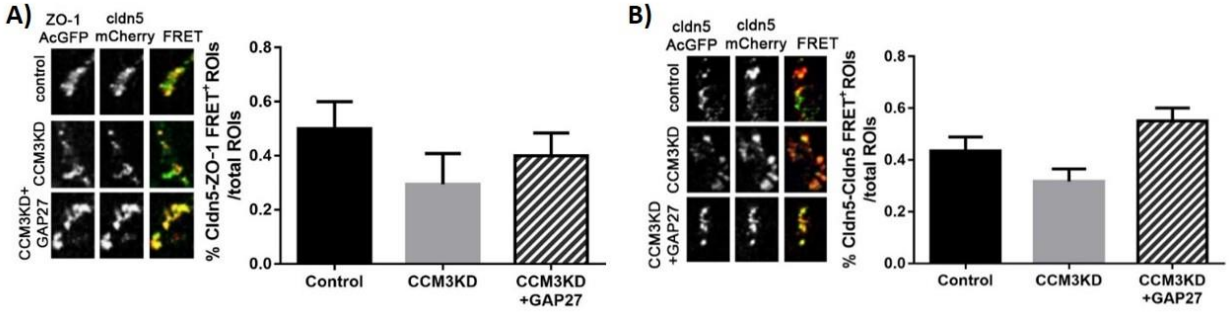

Figure 2.2.14 Claudin-5 interactions at the membrane are affected by CCM3KD. (A) FRET analysis of TJ-associated Claudin-5 and ZO-1 in cells co-expressing Claudin-5-mCherry and ZO-1-AcGFP. The number of cell-border ROIs giving a FRET signal ($FRET^+$ ROI) was measured as a percent of the total number of cell-border ROIs analyzed. N=20 total ROIs (4 ROIs/cell), 2 independent experiments. (B) FRET analysis of Claudin-5 *trans*-interaction. Cells were separately transfected with either Claudin-5-AcGFP or Claudin-5-mCherry at 1:1 concentration then seeded together. ROIs in which neighboring cells exhibited incorporation of Claudin-5-AcGFP and Claudin-5-mCherry into a shared TJ were selected for FRET analysis. FRET was performed and analyzed as described in 6E for 15 ROIs (3 ROIs/cell), 2 independent experiments.

2.3 Discussion

fCCM3 is believed to be a disease of progression – where the primary defect in fCCM3 lesions is their hyperpermeability and this produces many secondary pathologies over time, including hemorrhage, if left untreated (1, 2). However, the mechanism of lesion maturation and TJ disorganization contributing to hyperpermeability is not well defined. The present study observed: 1) Increased Cx43 protein expression in lesions of *ccm3*$^{+/-}$*p53*$^{-/-}$ mice. 2) Cx43 forms large GJ plaques and displays increased GJIC in CCM3KD cells. 3) Inhibition of Cx43 GJIC completely rescued CCM3KD hyperpermeability. 4) Cx43 GJs regulate permeability in brain endothelial cells through modulation of TJ protein localization at the membrane.

Permeability of the brain microvascular system is regulated in part by the TJ complex. The formation of TJ structures on the membrane is a highly regulated, multistep process. ZO-1 is recruited and distributed along the cell border, which signals recruitment and insertion of claudins and occludin into the membrane, in turn allowing trans-interactions between claudins and occludin on neighboring cells (24). claudin-5 is a particularly crucial claudin for BBB occlusion. Claudin-5 knock out mice die hours after birth from brain edema due to inhibited BBB occlusion (25). Other claudin KO mice suggest that claudin-5 is uniquely important for barrier occlusion (26). Previous work has demonstrated that fCCM3 lesions have highly disorganized TJ structures, including absent or incomplete incorporation of ZO-1 and claudin-5 into TJs, and suggest that this is a principal mechanism by which fCCM3 lesions are hyperpermeable (5, 27). However, the underlying mechanism that contributes to TJ organization has not been defined.

Elevated Cx43 has recently been suggested to be detrimental to barrier permeability in GJ- and HC-dependent mechanisms. Multiple studies in lung endothelia demonstrate rescue of barrier properties following suppression of inflammation-induced Cx43 expression (13, 28). In brain endothelia, elevated GJIC is suggested to be pathogenic to barrier function due to the effects of Ca^{2+} propagation on cytoskeletal integrity or localized endothelial cell death (29, 30). Cx43 has not previously been evaluated

in fCCM. Brain endothelial cells subjected to CCM3KD also show high protein expression of Cx43 and form abnormally large GJ plaques that result in elevated GJIC. We found that reducing Cx43 expression and specific blockage of GJIC but not HC function, rescues their hyperpermeability.

Understanding how elevated GJIC in fCCM3 causes hyperpermeability is of great importance. Here, we propose a mechanism separate from aforementioned studies examining Cx43-dependent hyperpermeability by which increased Cx43 GJs inhibit the distribution of ZO-1, and consequently claudin-5, to the TJ. A large body of literature has described the interaction between Cx43 and ZO-1 in the context of GJ size and activity, where direct interaction of Cx43 and ZO-1 at the GJ plaque perimeter decreases GJ plaque size and activity (31-33). We observed an intriguing phenomenon not yet described by which ZO-1 accumulates at the GJ plaque perimeter in CCM3KD cells but does not physically interact, as determined by FRET analysis. It is unclear what mechanism in CCM3KD cells signals the preferential localization and accumulation of ZO-1 at Cx43 GJs over TJ localization. When GJ plaques are disbanded by GAP27 treatment, the preferential conditions switch such that ZO-1 localizes to TJs and does not accumulate at Cx43 GJs. Consequently, claudin-5 is also re-localized at the TJ and form trans-interactions with neighboring cell claudin-5, sealing the barrier.

Additional consequences outside of GJIC-induced hyperpermeability should be considered in the pathology of fCCM3. In particular, elevated GJIC may represent a mechanism by which injury can be propagated to otherwise healthy cells, including other cell types of the neurovascular unit – pericytes and astrocytes. Several fCCM studies have demonstrated disrupted neurovascular unit architecture where pericytes and astrocytes lose contact with endothelial cells or are completely absent (34-36). Developmental venous anomalies, common in fCCM3, could be explained by the propagation of injury from capillaries to venules or arterioles (37). It is also important to highlight that fCCM3 lesions are believed to be initiated by a second hit to the functional *ccm3* allele (38, 39). However, it is not clear when in development this second hit is acquired or how many $ccm3^{-/-}$ cells are required to initiate a lesion. While

endothelial cell-specific ccm3KO mice develop fCCM3, and astrocyte- and neuron-specific ccm3KO mice show low or no fCCM disease penetrance, respectively, it is not yet understood whether multiple cell types are involved in the initiation and maturation of lesions (7, 40). Elevated GJIC in *ccm3*$^{-/-}$ cells may represent a mechanism by which *ccm3*$^{+/-}$ cells become damaged despite being genetically healthy.

It is interesting to note that Cx43 is the only Cx family member expressed in brain endothelial cells that is affected at the level of protein by CCM3KD. Several subtle, but functionally significant differences exist between the Cx family members, particularly with the existence of phosphorylation sites in the C-terminal tail directing the connexin life cycle, interactome and downstream signaling events in response to stimuli (41, 42). Given the accumulation of Cx43 protein without upregulation of Cx43 transcript, it is possible that sites in the C-terminal tail directing Cx43 degradation are affected by CCM3KD and result in accumulation at the membrane. Future work will focus on delineating the mechanism by which CCM3 regulates Cx43 specifically and additionally whether Cx43 is unique among the connexins in its ability to regulate the establishment of TJs.

We have demonstrated that Cx43 is most robustly affected by CCM3KD and less so by CCM1 or CCM2KD. Proteomic analysis of the CCM3 interactome has revealed that 80% of total CCM3 protein is bound to the STRIPAK complex and 20% bound to a CCM1-CCM2-CCM3 complex (3, 43), thus the STRIPAK complex is likely responsible for downstream events unique to CCM3. Given that the most robust effect of CCMKD on Cx43 protein occurs via loss of CCM3, it is possible that CCM1 and CCM2 effects on Cx43 are propagated through CCM3 via the CCM1-CCM2-CCM3 complex. The STRIPAK complex has many functions in the cell, regulating several phosphatases and kinases, and CCM3 is capable of regulating the activation of GCKIII kinases within STRIPAK (4, 5, 44). Elucidation of a CCM3-STRIPAK-Cx43 regulatory axis is needed. Several resident STRIPAK proteins are likely candidates, including calmodulin and PP2A. The former acts as a calcium sensor and is reported to regulate Cx43 channel opening, while the latter directly dephosphorylates residues Ser279/Ser282 of Cx43, phosphorylation events which inhibit Cx43 GJ plaque

formation (45-47). Elevated ERK1/2 activation is a consequence of CCM3 loss from the STRIPAK complex and causes dysregulation of TJ structure through modulation cortactin protein expression, a cytoskeletal and ZO-1-interacting protein (5). Cortactin and Cx43 can be co-immunoprecipitated but whether this occurs through a ZO-1 linker or a direct interaction between cortactin and ZO-1 is not clear and how cortactin expression or organization may affect Cx43 is not known (48). In addition to potential modulation of Cx43 through in a STRIPAK-ERK1/2-cortactin signaling axis, Ser279/Ser282 of Cx43 are also direct targets of ERK1/2, however, phosphorylation at these sites are typically inhibitory, and thus may not represent a primary mechanism by which CCM3 regulates Cx43 through the STRIPAK complex (49, 50).

In conclusion, our study demonstrates that Cx43 protein is aberrantly upregulated in developing CCM3 lesions prior to hemorrhage. *In vitro* data suggest that Cx43 GJs are instigators of BBB breakdown by regulating ZO-1 localization and, subsequently, limiting TJ formation and TJ trans-interactions. The Cx43 GJ inhibitor, GAP27, blocked these changes. How loss of CCM3 regulates the Cx43 GJ plaque formation and signaling events regulating Cx43/ZO-1 plaque formation is the focus of future studies. Additionally, whether *in vivo* treatment of fCCM3 mice with GAP27 can ameliorate Gd-DTPA leakage and subsequent hemorrhage is of paramount importance to determine if GAP27 or similar peptides may be candidate pharmaceutical options for fCCM3 patients. Importantly, this is the first study to definitively show that GJs can regulate BBB permeability through a TJ-dependent manner. Whether other mechanisms exist by which GJs can regulate permeability (i.e. through GJIC itself) will need to be further elucidated.

2.4 Materials and Methods

2.4.1 Cell culture

A transformed murine brain microvascular endothelial cell line (mBECs, Angioproteomie) or transformed murine brain microvascular pericyte cell line were cultured in growth media (DMEM, 4.5g/L glucose, 1X

L-glutamine, 1X antibiotic-antimycotic, 20% fetal bovine serum) at 37°C and 5% CO2. All experiments were conducted following 24 hrs serum deprivation (DMEM, 4.5g/L glucose, 1X L-glutamine).

2.4.2 Cell transfection

CCM1, CCM2, CCM3, and Cx43 knock downs were achieved through transfection with Lipofectin (Invitrogen) and the following siRNAs: Ccm3 - silencer select s80540, s80539, s80538 (Fisher), Ccm1 - siGENOME, D-056854-02-0002 (GE Dharmacon), Ccm2 - siGENOME, D-057315-02-0002 (GE-Dharmacon), Cx43 - SASI-Mm01-00135298 (PDSIRNA2D, Sigma).

2.4.3 Fusion proteins

Expression constructs: complete ORFs of Cx43, zonula occludens 1 (ZO-1) and claudin 5 (claudin-5) were cloned out of commercially available untagged cDNA constructs. ORFs were cloned into the following vectors to create N-terminally fused fluorescent proteins: pmCherry-C1 vector and pAcGFP-C1 infusion ready vector (Clontech). Plasmid DNA was isolated from individual, transformed Stellar Competent (Takara) colonies using Qiagen plasmid midiprep kits. DNA sequences were validated with Sanger sequencing. mBECs were transfected using Torpedo^{DNA} (Ibidi).

2.4.4 Inhibition studies

Inhibition of Cx43 GJs and HCs was achieved by cell treatment with 100μM GAP27 or 100μM GAP19 (Tocris Biosciences) for 24 hrs. No change in cell viability was observed following treatment, tested by Live Dead assay, Invitrogen).

2.4.5 Histology and Immunofluorescence

For immunofluorescence staining, brain slices or cells were incubated for 30 minutes in blocking solution (0.05% Triton X-100, 5% Goat Serum) at room temperature followed by incubation with primary antibody in blocking solution at room temperature for 2hr. The following primary antibodies were used: Cx43 (Cell

Signaling), ZO-1-AlexaFluor 594 (Fisher), claudin-5 unconjugated or claudin-5-AlexaFluor 488 (Fisher), CD31/PECAM-1 (Novus). Reactions were visualized following addition of secondary antibodies in blocking solution at 1:200 dilution for 1hr at room temperature following wash of primary antibodies. The following secondary antibodies were used: FITC anti-rabbit (Vector Laboratories) and Texas Red anti-mouse (Vector Laboratories). Images were acquired on the Nikon A-1 confocal microscope.

Quantitation of plaque size and TJ-associated fragments for Cx43, ZO-1 and claudin-5 were performed using ImageJ software. Three images with equal cell number were used per group.

2.4.6 Super Resolution imaging

Super Resolution imaging was conducted in conjunction with the Single Molecule Analysis in Real-Time (SMART) Center at the University of Michigan. Cells were plated at confluency in LabTek II Coverglass slides, #1.5 thickness (Fisher). The following primary and secondary antibodies were used: ZO-1-AlexaFluor647, claudin-5 (unconjugated, Fisher), Cx43 (unconjugated, Cell Signaling), Goat anti-Rabbit IgG AlexaFluor Plus 647 (Invitrogen), Goat anti-Mouse IgG AlexaFluor Plus 647 (Invitrogen). Immediately before imaging, sample buffer was exchanged with STORM imaging buffer: 100 mM Tris-Cl, 25 uM NaCl, 1% v/v BME (beta-mercaptoethanol), pH 9.0, and freshly added 2.5 mM PCA (3,4-dihydroxybenzoic acid (Sigma, P5630)) and 25 nM PCD (protocatechuate dioxygenase (Sigma, P8279)). Images were collected in HILO (highly inclined laminated optical sheet microscopy) illumination with 641 nm laser excitation on an Olympus IX81 microscope with a cell^TIRF module. Images were collected on an Andor iXon Ultra EMCCD camera. Images were processed using ThunderSTORM plugin of ImageJ.

2.4.7 Quantitative PCR

qPCR was performed following RNA extraction with Trizol/Chloroform (Fisher) and reverse transcription (SuperScript II RT, Fisher). 100ng of cDNA was used for each reaction. Reactions were performed using SYBR Green PCR Master Mix (Applied BioSystems) and performed using the 7500 Real-Time PCR System

(Applied BioSystems). The following primers were used: Cx37 F: CTGGACCATGGAGCCGGTGT, R: GGTTGAGCACCAGGGAGATGACTC; Cx40 F: TCCAGGGCACCCTACTCAACACCT, R: GGACTCCTGCGGCAGACATGC; Cx43 F: TACCACGCCACCACCGGCCCA, R: GGCATTTTGGCTGTCGTCAGGGAA; beta-actin F: GCCCTGAGGCTCTTTTCCAG, R: TGCCACAGGATTCCATACCC. A minimum n=3 was used for each group, with each group normalized to beta-actin. $\Delta\Delta$CT values were calculated and reported.

2.4.8 Western blotting

Western blotting was performed using the following primary antibodies: Cx37 (Abcam), Cx40 (GeneTex), Cx43 (Cell Signaling), CCM1 (Boster Bio), CCM2 (Sigma), CCM3 (Proteintech), ZO-1 (Cell Signaling), claudin-5 (Invitrogen), beta-tubulin (2128, Cell Signaling), beta-actin (A5316, Sigma). Reactions were visualized by addition of the following secondary antibodies: Goat Anti-Rabbit IgG-HRP conjugate (Biorad) or Goat Anti-Mouse IgG-HRP conjugate (Biorad). Blots were developed with SuperSignal West Femto Maximum Sensitivity Substrate (ThermoFisher) and imaged using the Molecular Imager ChemiDoc XRS+ Imaging System (Biorad). Band intensities were analyzed using Image Lab software (Biorad).

2.4.9 Gap junction activity assays

For scratch assays, cells were grown to confluency prior to siRNA treatment to ensure a proper monolayer. Cells were washed 3 times in PBS, PBS was removed, and a scratch was made in the center of the dish using a glass-etching tool. 0.05% Lucifer Yellow (LY, Sigma) was immediately applied to the scratch. Dye uptake was allowed to occur for 30s. Cells were subsequently washed 4 times with PBS then fixed with 4% paraformaldehyde for 10min. Scratch assays were immediately imaged using 488nm laser line. Cell confluency surrounding the scratch was confirmed under transmitted light. Dye transfer distance was measured using ImageJ and taken from scratch center, perpendicularly to the furthest LY-positive cell. Three plates with one scratch each were analyzed per group, with approximately 10 distance measurements collected per scratch.

Microinjections were performed using the PicoSpritzer 3 (Parker Instruments). Cells were grown on ibidi 35mm low, grid500, ibiTreat plates to facilitate knowing location of injected cell. Eppendorf Femptotips Microinjection capillary tips 0.5μm (Fisher) were loaded with 0.05% LY. Healthy, confluent cells were selected for injection. Injection was done at 40kPa for 500ms. The injection of LY was visualized real-time to ensure LY was injected into cell of origin. Three injections were made at distant spots on each plate. Following injection, cells were washed 4 times in PBS and fixed using 4% paraformaldehyde. Plates were imaged immediately. The number of LY positive cells surrounding the cell-of-origin were counted using ImageJ.

2.4.10 Hemichannel Activity Assay

Hemichannel activity assays were performed as described for scratch assays, however, no scratch was made to cell monolayers. Instead, control or CCM3KD mBECs were overlaid with LY without prior injury (scratch). Dye uptake was allowed to occur for 30s. Cells were subsequently washed 4 times with PBS then fixed with 4% paraformaldehyde for 10min. HC assays were immediately imaged using 488nm laser line. Cell confluency surrounding the scratch was confirmed under transmitted light. The number of LY^+ cells and LY volume/cell was measured using ImageJ. Six images per experiment with 3 independent experiments performed were analyzed.

2.4.11 Fluorescence Resonance Energy Transfer (FRET) and Fluorescence Recovery After Photobleaching (FRAP) Analysis

FRET and FRAP experiments were performed using a Leica SP5X Inverted 2-Photon FLIM Confocal microscope at the University of Michigan Microscopy Imaging Laboratories core. LAS X software was used to perform experiments. The following laser power and line intensities were used: FRET – white light laser at 70%, red laser line at 587nm, 40% intensity, green laser line at 488nm, 30% intensity. Acceptor photo-bleaching performed with laser lines 579nm, 587nm, 595nm each at 100% for 80 seconds; FRAP - Argon

laser at 25%, green laser line at 488, 30% intensity, photobleaching performed with laser line 488 at 100%. Laser power and laser line intensities were kept constant across all sample groups. Experimental values were calculated as follows: FRET – following acceptor bleaching, FRET efficiencies were calculated as $((donor^{post}-donor^{pre})/donor^{post})$. FRAP - % recovery = [(6 min post bleach fluorescence – 0 min post bleach fluorescence)/pre-bleach fluorescence]*100.

The following controls were used for FRET and FRAP experiments: FRET - efficiencies of control samples co-expressing empty GFP and empty mCherry vectors were collected and subtracted from experimental FRET efficiencies during analysis; FRAP – a background region of interest (ROI) was selected in non-GFP positive region to assess non-specific changes to fluorescence intensity and this background %recovery was subtracted from all ROIs analyzed.

2.4.12 Transendothelial Electrical Resistance (TEER) assay

Cells were grown to confluency in 12mm transwells with 0.4μm pores (Corning) prior to manipulation to ensure a complete monolayer had formed. Following control or siRNA treatment, cells were allowed to recover for 24hrs, then serum-deprived for 24 hrs. TEER values were measured using the EVOM^2 Epithelial Voltohmmeter (World Precision Instruments). Blank measurements were obtained in wells with serum deprivation media only, no cells. Blank measurements were subtracted from experimental values during analysis.

2.4.13 Statistical Analyses

All statistical analyses were performed using GraphPad Prism 6.0 software. Data in bar graphs are presented as averages ± standard deviation of the mean (SEM). In experiments comparing two groups, significant differences were determined by unpaired, two-tailed Student's t-test. In experiments comparing more than two groups, significant differences were determined by a One-way ANOVA with

Tukey *post-hoc* test. A probability value of $p<0.05$ was considered statistically significant. Degrees of freedom for ANOVA (F statistic) and Student's t-test are presented for each analysis in the figure legend.

2.5 References

1. Yadla S, Jabbour PM, Shenkar R, Shi C, Campbell PG, Awad IA (2010) Cerebral cavernous malformations as a disease of vascular permeability: from bench to bedside with caution. Neurosurgical Focus 29:E4.

2. Mikati AG, Khanna O, Zhang L, Girard R, Shenkar R, Guo X, Shah A, Larsson HB, Tan H, Li L, Wishnoff MS, Shi C, Christoforidis GA Awad IA (2015) Vascular permeability in cerebral cavernous malformations. Journal of Cerebral Blood Flow & Metabolism 35:1632-9.

3. Goudreault M, D'Ambrosio LM, Kean MJ, Mullin MJ, Larsen BG, Sanchez A, Chaudhry S, Chen GI, Sicheri F, Nesvizhskii AI, Aebersold R, Raught B, Gingras AC (2009) A PP2A Phosphatase High Density Interaction Network Identifies a Novel Striatin-interacting Phosphatase and Kinase Complex Linked to the Cerebral Cavernous Malformation 3 (CCM3) Protein. Molecular and Cellular Proteomics. 8:157–171.

4. Hwang J and Pallas DC (2014) STRIPAK complexes: Structure, biological function, and involvement in human diseases. The International Journal of Biochemistry & Cell Biology 47:118– 148.

5. Stamatovic SM, Sladojevic N, Keep R, Andjelkovic AV (2015) PDCD10 (CCM3) regulates brain endothelial barrier integrity in cerebral cavernous malformation type 3: role of CCM3-ERK1/2-cortactin cross-talk. Acta Neuropathologica 130:731–750.

6. McDonald DA, Shenkar R, Shi C, Stockton RA, Akers AL, Kucherlapati MH, Kucherlapati R, Brainer J, Ginsberg MH, Awad IA, Marchuk DA. (2011) A novel mouse model of cerebral cavernous malformations based on the two-hit mutation hypothesis recapitulates the human disease. Human Molecular Genetics 20:211–222.

7. He Y, Zhang H, Yu L, Gunel M, Boggon TJ, Chen H, Min W (2010) Stabilization of VEGFR2 Signaling by Cerebral Cavernous Malformation 3 Is Critical for Vascular Development. Science Signaling 3:ra26.

8. Brink PR, Cronin K, Banach K, Peterson E, Westphale EM, Seul KH, Ramanan SV, Beyer EC. (1997) Evidence for heteromeric gap junction channels formed from rat connexin43 and human connexin37. American Journal of Physiology 273:C1386–C1396.

9. Martinez AD, Hayrapetyan V, Moreno AP, Beyer EC (2002) Connexin43 and Connexin45 Form Heteromeric Gap Junction Channels in Which Individual Components Determine Permeability and Regulation. Circulation Research 90:1100–1107.

10. Bruzzone, R., Haefliger, J.A., Gimlich, R.L. and Paul, D.L. (1993) Connexin40, a component of gap junctions in vascular endothelium, is restricted in its ability to interact with other connexins. Molecular Biology of the Cell 4:7–20.

11. Gabriels JE, Paul DL (1998) Connexin43 is highly localized to sites of disturbed flow in rat aortic endothelium but connexin37 and connexin40 are more uniformly distributed. Circulation Research 83:636–643.

12. Zhang J, Yang G-M, Zhu Y, Peng X-Y, Li T, Liu L-M (2015) Role of connexin 43 in vascular hyperpermeability and the relationship to the Rock 1-MLC20 pathway in septic rats. American Journal of Physiology - Lung Cellular and Molecular Physiology 309: L1323–L1332

13. Kandasamy K, Escue R, Manna J, Adebiyi A, Parthasarathi K (2015) Changes in endothelial connexin 43 expression inversely correlate with microvessel permeability and VE-cadherin expression in endotoxin-challenged lungs. American Journal of Physiology - Lung Cellular and Molecular Physiology 309: L584–L592.

14. Winkler, E.A., Bell, R.D. & Zlokovic, B.V. Central nervous system pericytes in health and disease. Nat. Neurosci. 14, 1398–1405 (2011).

15. Aasen T (2015) Connexins: junctional and non-junctional modulators of proliferation. Cell and Tissue Research 360:685–699.

16. Olk S, Zoidl G, and Dermietzel R (2009) Connexins, Cell Motility, and the Cytoskeleton. Cell Motility and the Cytoskeleton 66: 1000–1016.

17. Chaytor AT, Evans WH, Griffith TM (1998) Central role of heterocellular gap junctional communication in endothelium-dependent relaxations of rabbit arteries. Journal of Physiology 508:561-573.

18. Wang et al., (2013) Selective inhibition of Cx43 hemichannels by Gap19 and its impact on myocardial ischemia/reperfusion injury. Basic Research in Cardiology 108: 309-325

19. Toyofuku T, Yabuki M, Otsu K, Kuzuya T, Hori M, Tada M (1998) Direct Association of the Gap Junction Protein Connexin-43 with ZO-1 in Cardiac Myocytes. Journal of Biological Chemistry 273:12725–12731.

20. Giepmans BN, Moolenaar WH (1998) The gap junction protein connexin43 interacts with the second PDZ domain of the zona occludens-1 protein. Current Biology, 8:931-934.

21. Sorgen PL, Duffy HS, Sahoo P, Coombs W, Delmar M, Spray DC (2004) Structural Changes in the Carboxyl Terminus of the Gap Junction Protein Connexin43 Indicates Signaling between Binding Domains for c-Src and Zonula Occludens-1. Journal of Biological Chemistry 279:54695–54701.

22. Segretain D, Fiorini C, Decrouy X, Defamie N, Prat J, Pointis G (2004) A proposed role for ZO-1 in targeting connexin 43 gap junctions to the endocytic pathway. Biochimie 86:241–244.

23. Jin C, Martyn KD, Kurata WE, Warn-Cramer BJ, Lau AF (2004) Connexin43 PDZ2 Binding Domain Mutants Create Functional Gap Junctions and Exhibit Altered Phosphorylation. Cell Communication & Adhesion 11:67–87.

24. Fanning AS, Anderson JM (2009) Zonula occludens-1 and -2 are cytosolic scaffolds that regulate the assembly of cellular junctions. Annals of the New York Academy of Science 1165:113–120.

25. Nitta T, Hata M, Gotoh S, Seo Y, Sasaki H, Hashimoto N, Furuse M, Tsukita S (2003) Size-selective loosening of the blood-brain barrier in claudin-5–deficient mice. The Journal of Cell Biology 161:653–660.

26. Krause G, Winkler L, Mueller SL, Haseloff RF, Piontek J, Blasig IE (2008) Structure and function of claudins. Biochimica et Biophysica Acta 1778:631–645.

27. Schneider H, Errede M, Ulrich NH, Virgintino D, Frei K, Bertalanffy H (2011) Impairment of Tight Junctions and Glucose Transport in Endothelial Cells of Human Cerebral Cavernous Malformations. Journal of Neuropathology and Experimental Neurololgy 70:417-429.

28. O'Donnell JJ, Birukova AA, Beyer EC, Birukov KG (2014) Gap Junction Protein Connexin43 Exacerbates Lung Vascular Permeability. PLoS ONE 9:e100931.

29. Lin JH, Weigel H, Cotrina ML, Liu S, Bueno E, Hansen AJ, Hansen TW, Goldman S, Nedergaard M (1998) Gap-junction-mediated propagation and amplification of cell injury. Nature Neuroscience 1:494-500.

30. de Bock MD, Culot M, Wang N, Bol M, Decrock E, Vuyst ED, Costa AD, Dauwe I, Vinken M, Simon AM, Rogiers V, Ley GD, Evans WH, Bultynck G, Dupont G, Cecchelli R, Leybaert L (2011) Connexin Channels Provide a Target to Manipulate Brain Endothelial Calcium Dynamics and Blood—Brain Barrier Permeability. Journal of Cerebral Blood Flow & Metabolism 31:1942–1957.

31. Hunter AW, Gourdie RG (2008) The second PDZ domain of zonula occludens-1 is dispensable for targeting to connexin 43 gap junctions. Cell Communication & Adhesion 15:55-63.

32. Hunter AW, Barker RJ, Zhu C, Gourdie RG (2005) Zonula occludens-1 alters connexin43 gap junction size and organization by influencing channel accretion. Molecular Biology of the Cell 16:5686-5698.

33. Rhett JM, Jourdan J, Gourdie RG. (2011). Connexin 43 connexon to gap junction transition is regulated by zonula occludens-1. Molecular Biology of the Cell 22:1516-1528.

34. Clatterbuck RE, Eberhart CG, Crain BJ, Rigamonti D (2001) Ultrastructural and immunocytochemical evidence that an incompetent blood-brain barrier is related to the pathophysiology of cavernous malformations. Journal of Neurology, Neurosurgery and Psychiatry 71:188–192.

35. Tu J, Stoodley MA, Morgan MK, Storer KP (2005) Ultrastructural characteristics of hemorrhagic, nonhemorrhagic, and recurrent cavernous malformations. Journal of Neurosurgery 103:903–909.

36. Tanriover G, Sozen B, Seker A, Kilic T, Gunel M, Demir N (2013) Ultrastructural analysis of vascular features in cerebral cavernous malformations. Clinical Neurology and Neurosurgery 115:438–444.

37. Meng G, Bai C, Yu T, Wu Z, Liu X, Zhang J, Zhao J (2014) The association between cerebral developmental venous anomaly and concomitant cavernous malformation: an observational study using magnetic resonance imaging. BMC Neurology 14:50-55.

38. Akers AL, Johnson E, Steinberg GK, Zabramski JM, Marchuk DA (2009) Biallelic somatic and germline mutations in cerebral cavernous malformations (CCMs): evidence for a two-hit mechanism of CCM pathogenesis. Human Molecular Genetics 18:919–930.

39. Pagenstecher A, Stahl S, Sure U, Felbor U (2009) A two-hit mechanism causes cerebral cavernous malformations: complete inactivation of CCM1, CCM2 or CCM3 in affected endothelial cells. Human Molecular Genetics 18:911–918.

40. Louvi A, Chen L, Two AM, Zhang H, Min W, Gunel M (2011) Loss of cerebral cavernous malformation 3 (Ccm3) in neuroglia leads to CCM and vascular pathology. Proceedings of the National Academy of Sciences 108:3737–3742.

41. Su V, Lau AF (2014) Connexins: Mechanisms regulating protein levels and intercellular communication. FEBS Letters 588:1212–1220.

42. Leithe E, Mesnilb M, Aasen T (2017) The connexin 43 C-terminus: A tail of many tales. Biochimica et Biophysica Acta (BBA) – Biomembranes. 2017 May 16. [Epub ahead of print]

43. Hilder TL, Malone MH, Bencharit S, Colicelli J, Haystead TA, Johnson GL, Wu CC (2007) Proteomic identification of the cerebral cavernous malformation signaling complex. Journal of Proteome Research 6:4343–4355.

44. Yoruk B, Gillers BS, Chi NC, Scott IC (2012) Ccm3 functions in a manner distinct from Ccm1 and Ccm2 in a zebrafish model of CCM vascular disease. Developmental Biology 362:121–131.

45. Zhou Y, Yang W, Lurtz MM, Ye Y, Huang Y, Lee HW, Chen Y, Louis CF, Yang JJ (2007) Identification of the calmodulin binding domain of connexin 43. Journal of Biological Chemistry 282:35005-17

46. Zou J, Salarian M, Chen Y, Veenstra R, Louis CF, Yang J (2014) Gap Junction Regulation by Calmodulin. FEBS Letters 588:1430–1438.

47. Wu J, Taylor RN, Sidell N (2013) Retinoic Acid Regulates Gap Junction Intercellular Communication in Human Endometrial Stromal Cells Through Modulation of the Phosphorylation Status of Connexin 43. Journal of Cellular Physiology 228: 903–910.

48. Vitale ML, Akpovi CD, Pelletier RM (2009) Cortactin/Tyrosine-Phosphorylated Cortactin Interaction With Connexin 43 in Mouse Seminiferous Tubules. Microscopy Research and Technique 72:856–867.

49. Riquelme MA, Burra S, Kar R, Lampe PD, Jiang JX (2015) Mitogen-activated Protein Kinase (MAPK) Activated by Prostaglandin E2 Phosphorylates Connexin 43 and Closes Osteocytic Hemichannels in Response to Continuous Flow Shear Stress. The Journal of Biological Chemistry 290:28321–2832.

50. Ruch RJ, Trosko JE, Madhukar BV (2001). Inhibition of connexin43 gap junctional intercellular communication by TPA requires ERK activation. Journal of Cellular Biochemistry 83:163-169.

Chapter 3: Characterization of Lesions and Connexin 43 Expression in Lesions of a Murine Model of fCCM3

3.1 Introduction

In Chapter 2, we observed a significant increase in Cx43 expression in CCM3KD endothelial cells and pericytes and intriguingly, that inhibition of increase Cx43 GJIC in endothelial cells could rescue the increased monolayer permeability of CCM3KD cells. To further establish whether Cx43 is a potential therapeutic target in fCCM3, we extended our evaluation of Cx43 to fCCM3 mice.

As discussed in Chapter 1, multiple mouse models of fCCM have been described (1-8). Global and endothelial-specific CCM3KO mice are embryonic lethal due to cardiovascular defects, thus studies including fCCM3 models commonly use an inducible, endothelial-specific Cre system (iEcKO) (3, 4). Two separate *ccm3* mutant alleles have been created that result in the deletion of different regions of CCM3 upon induction of Cre expression (3, 4). Both alleles render CCM3 non-functional by removal of entire exons, mirroring fCCM3 patient mutations in a broad sense. However, germline and somatic mutations in patients are most commonly point mutations that result in non-functional CCM3 by different mechanisms that are not entirely understood or described (9, 10). Additionally, Cre-induced KO animals are very likely not representative of human disease, given that in these mice, CCM3 mutation and lesion initiation occurs at one time point – Cre administration – versus somatic mutations and subsequent lesion initiation that occur over the lifetime of a patient. For reasons not understood, fCCM models of all CCM subtypes develop lesions exclusively in the cerebellum and eyes, unlike patients that develop lesions indiscriminately throughout the cerebrovascular system.

The second type mouse model employed in fCCM studies is based exclusively on the second-hit hypothesis, whereby lesions are initiated when patients who inherit one null CCM allele acquire a second,

somatic hit to the functional allele (7, 8). To model this hypothesis, global *ccm*$^{+/-}$ mice are bred with either *Msh2*$^{-/-}$ or *p53*$^{-/-}$ mice, with global deletion of tumor suppressors Msh2 or p53. This model has overcome many problems of the iEcKO CCM model in terms of patient disease representation. All *ccm1*, *-2*, and *-3*$^{+/-}$ mice bred to an *Msh2*$^{-/-}$ or *p53*$^{-/-}$ background develop lesions indiscriminately in the cerebrovascular system, unlike iEcKO CCM mice. Additionally, two-hit mice develop lesions at different time points instead of a single time point following Cre administration, as with iEcKO mice. While it has not been carefully examined, second-hit mouse models also represent a model in which the lesion-initiating cell type may be variable, a question that tissue-specific CCMKO models have attempted to address. Inherent, however, to *Msh2*$^{-/-}$ and *p53*$^{-/-}$ mice are potentially confounding genetic mutations that arise independently of *ccm* heterozygosity and instead from tumor suppressor KO.

A central question to address is not only whether Cx43 is elevated in fCCM3 lesions, but also whether Cx43 expression is associated with lesion permeability. To address these questions, the two-hit model of fCCM3 (*ccm3*$^{+/-}$*p53*$^{-/-}$) was chosen for use in this study for multiple reasons, but particularly because this model produces lesions at different maturation states in a single time point and would thus allow us to describe Cx43 expression throughout lesion maturation. Using *ccm3*$^{+/-}$*p53*$^{-/-}$ mice, we establish the existence of multiple lesion stages, lesion permeability to contrast agent gadolinium diethylenetriaminepentacetate (Gd-DTPA), and elevated expression of Cx43 in all lesion stages but particularly newly formed lesions.

3.2 Results

3.2.1 – Development of lesions in fCCM3 mice replicate human disease progression

We identified three *ccm3*$^{+/-}$*p53*$^{-/-}$ mice – one female and two males. All three mice were evaluated for the presence of hemorrhagic cerebrovascular lesions consistent with human disease using T2*-weighted MRI imaging. Several hemorrhagic lesions were present in the female in multiple regions of the brain at 5 weeks of age (Fig 3.2.1A), while lesions in male mice were identified by 8 and 9 weeks of age.

New hemorrhagic lesions appeared at a rate of 3 to 4.5 lesions/week (Fig 3.2.1B). Lesion volume at first appearance varied considerably between 0.005-3.9mm^3 (Fig 3.2.1C). The average lesion size trended downward with age, however, this appeared to be due to a slowed growth rate of existing lesions and appearance of numerous smaller lesions with age (Fig 3.2.1E-F). Appearance of disease in young mice, variable lesion size, location and positive rate of development are all consistent with human fCCM3 (11).

A)

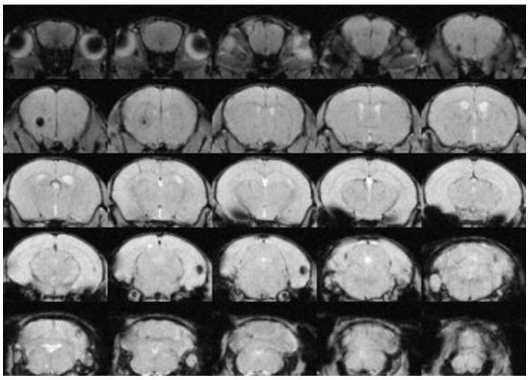

C)

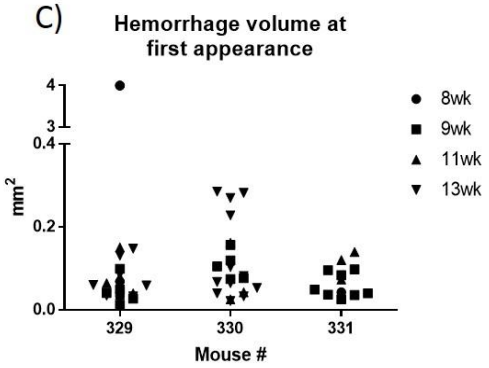

B)

age	5 wk	8 wk	9 wk	11 wk	13 wk	total #	avg rate of development
329	0	4	9	14	21	21	3.08
330	0	0	7	8	20	20	4.50
331	4	4	11	16	N/A	16	3.17

D)

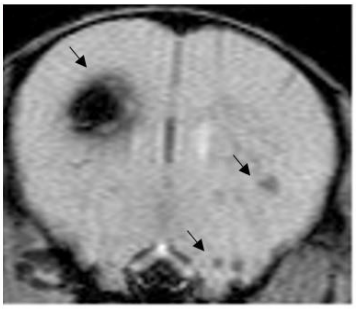

E)

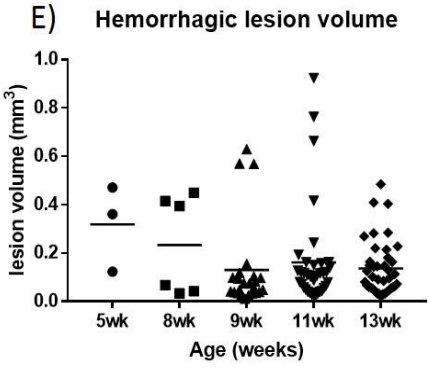

F)

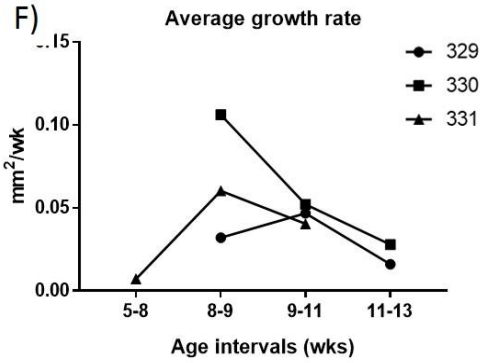

Figure 3.2.1 Hemorrhagic lesion volume in fCCM3 mice. (A) Representative T2*-weighted MRI of a ccm3+/-p53-/- mouse. (B) Table showing lesion burden in all ccm3+/-p53-/- mice evaluated. Mouse #331 already had 4 lesions when first evaluated at 5wks of age, with mice #329 and #330 developing lesions by 8 and 9wks of age, respectively. The average rate of lesion development is between 3 and 4.5 lesions/wk. (C) The lesion volume at first appearance was measured using ImageJ to determine if any correlation could be seen between individual lesion volume and age at lesion initiation. No trend in lesion size at first hemorrhage was observed. (D) T2*-weighted MRI slice showing hemorrhagic lesions (arrows) of variable size. (E) The average lesion volume per age was analyzed to determine if a trend in lesion volume and age exists. Average lesion volume becomes smaller with age. Data points represent individual lesion volumes compiled from all three mice assessed. Horizontal bars represent average values. (F) The average growth rate for lesions was calculated to determine if growth rate varies with age. Data points represent the average growth rate of lesions, calculated by difference in individual lesion size between 5-8, 8-9, 9-11, or 11-13 weeks of age. Each line represents an individual mouse. Growth rates of lesions had a downward trend with age.

3.2.2 – Lesions of fCCM3 mice are hyperpermeable

Given that improper BBB permeability is the central pathologic feature of fCCM3, analysis of the *ccm3*$^{+/-}$*p53*$^{-/-}$ model was extended to evaluate lesion permeability during lesion maturation. We observed that Gd-DTPA tracer leakage occurred in all three *ccm3*$^{+/-}$*p53*$^{-/-}$ mice at distinct, focal points, similar to the appearance of hemorrhagic lesions (Fig 3.2.2A). Gd-DTPA leakage could frequently be observed in conjunction with hemorrhage on companion T2*-weighted MRI images. Lesions were categorized into 3 types: Gd-DTPA leakage only, hemorrhage only, and hemorrhagic with Gd-DTPA leakage (Fig 3.2.2A). When first assessed at 8 weeks, the majority of *ccm3*$^{+/-}$*p53*$^{-/-}$ mouse lesions could be categorized as having Gd-DTPA leakage only. By 13 weeks of age, the majority of lesions visualized had hemorrhaged (Figure 3.2.2B). When individual lesions that only had Gd-DTPA leakage at 8 weeks of age were followed to 13

A)

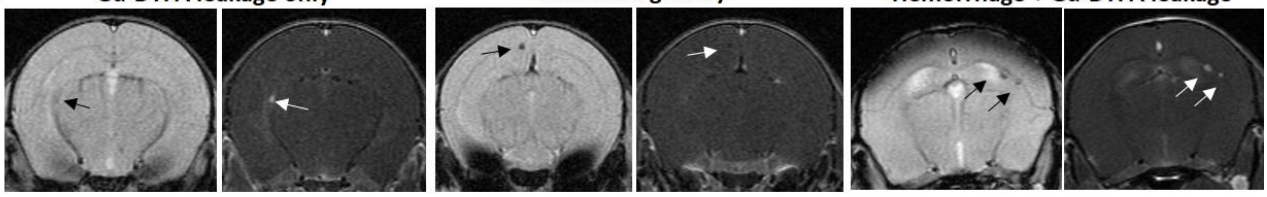

B)

Age (wk)	Gd leakage only	Hemorrhage only	Hemorrhage + Gd leakage
8 (n=3)	71.9	9.4	18.8
11 (n=3)	34.6	23.1	42.3
13 (n=2)	16.7	26.2	57.1

C)

Transition	% of total transitions
hem^{neg}/Gd^{pos} to hem^{pos}/Gd^{pos}	90.9
Hem^{neg}/Gd^{pos} to hem^{pos}/Gd^{neg}	9.1
Hem^{neg}/Gd^{pos} to hem^{neg}/Gd^{neg}	0

Figure 3.2.2. Gd-DTPA leakage predicts lesion hemorrhage. (A) ccm3+/-p53-/- mice were IP injected with Gd-DTPA and allowed to roam for 10min. T2*-weighted (left) and T1-weighted (right) MRI images were obtained sequentially. Black spots on T2*-weighted images indicate hemorrhage (black arrows), while white spots on T1-weighted images indicate Gd-DTPA leakage (white arrows). Three subtypes of lesions appeared: Gd-DTPA leakage with no hemorrhage (left pair), hemorrhage with no Gd-DTPA leakage (center pair), and lesions with both hemorrhage and Gd-DTPA leakage (right pair). (B) Data represents the number of each lesion subtype as a percent of total lesion burden at 8, 11, or 13 weeks of age using lesions from all 3 mice (8 and 11wks) or 2 mice (13wks). Gd-DTPA leakage only lesions went down as a percent of total lesions over time, while hemorrhagic lesions rose over time. (C) The transitions of individual lesions with Gd-DTPA leakage only (hem^{neg}/Gd^{pos}) at 8 weeks were followed until 13 weeks of age. The number of hem^{neg}/Gd^{pos} transitions to either hem^{neg}/Gd^{pos}, hemorrhage only (hem^{pos}/Gd^{neg}) or Gd-DTPA leakage with hemorrhage (hem^{pos}/Gd^{pos}) was calculated as a percent of total number of lesion transitions that occurred, n=22 transitions.

weeks of age, the probability of the lesion hemorrhaging was 100% (Fig 3.2.2C). These findings demonstrate that developing lesions already have compromised BBB function prior to hemorrhage, and that Gd-DTPA leakage predicts the maturation of lesions from leaky to hemorrhagic.

3.2.3 – Connexin 43 is elevated in fCCM3 lesions

Following sacrifice, all three *ccm3*$^{+/-}$*p53*$^{-/-}$ mouse brains were examined histologically. H&E staining of lesion sections revealed multiple lesion stages present in all mice (Figure 3.2.3A panel 1). As classified by MacDonald et al., stage 1 and 2 lesions were visible, characterized by single, spherical, enlarged caverns with hemorrhage (stage 1) or enlarged caverns with intervening endothelial layers and robust hemorrhage (stage 2) (8). We also observed a previously undefined lesion stage, which we termed 'stage 0', in which brain capillaries were elongated and dilated with occasional small hemorrhage, but had not yet formed cystic-like caverns. Prussian blue staining was performed so as to demonstrate iron accumulation in the surrounding tissue, indicative of prolonged hemorrhage (Figure 3.2.3A panel 2). As expected, dark blue staining could be observed in an ascending manner from stage 0 through stage 2, with stage 0 lesions exhibiting little to no accumulation and stage 2 exhibiting the most robust iron accumulation. From the initial histological examination, we demonstrated that lesion maturation progresses from a dilated vessel (stage 0), to re-organized, cystic-like caverns with complete loss of barrier properties, allowing for hemorrhage (stage 1 and 2), consistent with published literature of second-hit fCCM mouse models (7, 8).

Lesion sections were evaluated for Cx43 protein expression using immunofluorescence. Quantification of Cx43 staining in lesions of all three mice showed elevated Cx43 expression in the endothelial cells (CD31) of lesions of all stages compared to control vessels of *ccm3*$^{+/-}$*p53*$^{-/-}$ mice (Figure 3.2.3A panels 3-5). Only two stage 2 lesions were identified out of all brain sections examine, thus while they are included in the quantification, a higher sample size is needed to make conclusions regarding Cx43

expression in stage 2 lesions. Cx43 expression was much higher in stage 0 lesions compared to stage 1, though both stages exhibited significantly higher Cx43 expression compared to controls (Fig 3.2.3B).

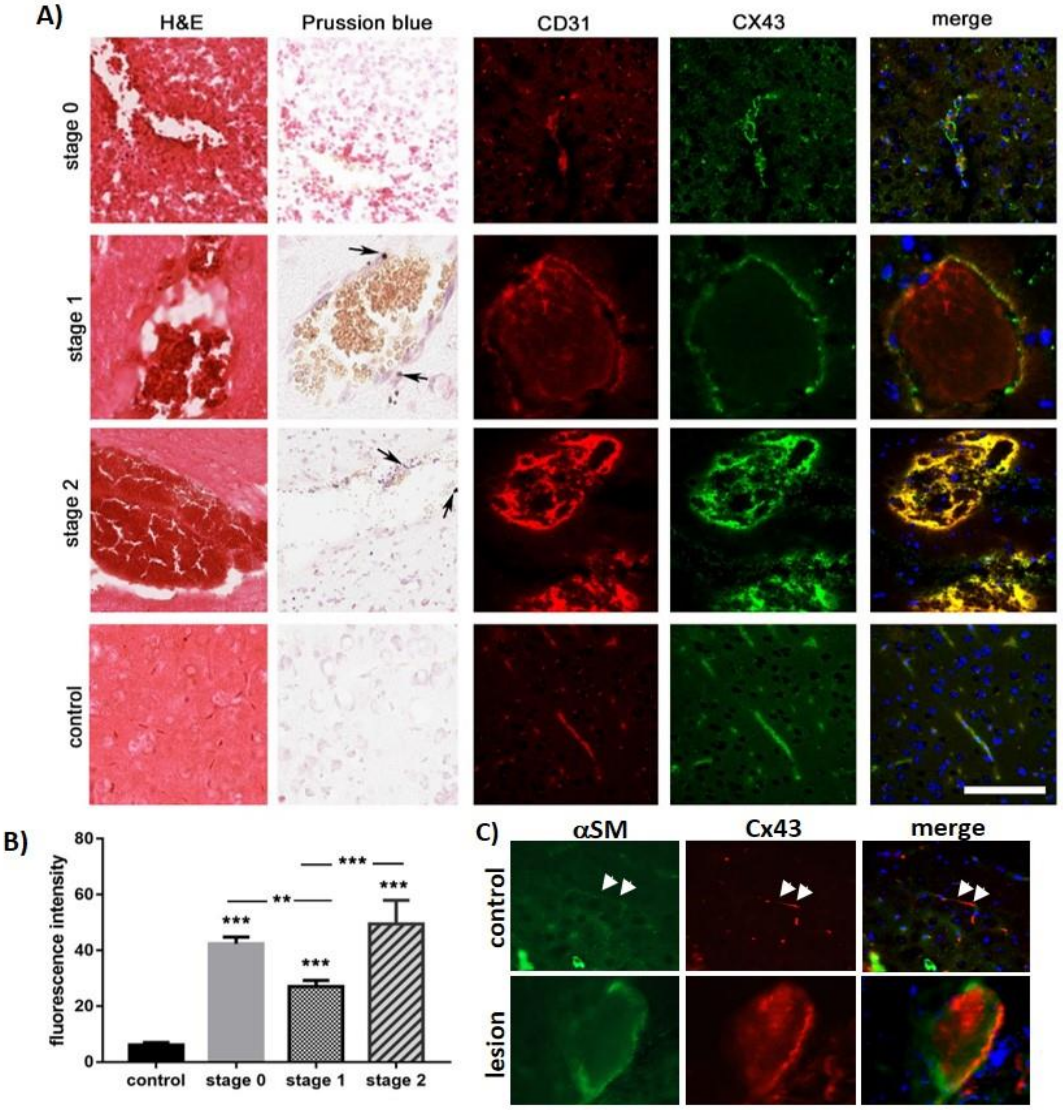

Figure 3.2.3. Developing lesions expressing Cx43 are susceptible to hemorrhage. (A) H&E (panel 1), Prussian Blue (panel 2, black arrows indicate spots of iron accumulation), immunofluorescence staining of CD31 (panel 3), Cx43 (panel 4) and merge images (panel 5) of stage 0, 1 and 2 lesions and control vessels in ccm3$^{+/-}$p53$^{-/-}$ mice. Scale bar = 100μm (B) Quantitation of Cx43 expression in control and lesion stages, n=10. n=10 individual lesions for stage 0, 1; n=2 individual lesions for stage 2. Cx43 was quantified using ImageJ by selecting the entire endothelial layer surrounding each lesion and measuring the fluorescent signal. Cx43 expression is quantified relative to control vessel fluorescence, ***p<0.0001 compared to control, **p<0.01 compared to stage 0; ***p<0.0001 compared to stage 1. (C) Immunofluorescence staining of a control vessel (white arrows) and stage 1 lesion with a pericyte cell marker (alpha smooth muscle, αSM) and Cx43. Merge image demonstrates that pericytes surrounding fCCM3 lesion express Cx43.

3.2.4 Cx43 is elevated in multiple cell types of CCM3 lesions

Finally, we examined whether Cx43 was present in other cell types surrounding the lesion. While tissue-specific CCM3KO mice have shown varying levels of disease penetrance, with the most robust being the endothelial cell-specific CCM3KO mice, it has not been definitely established which originating or supporting cell types are required for the initiation and maturation of lesions (5, 6). The *ccm3*$^{+/-}$*p53*$^{-/-}$ second-hit model allows for a second hit in any cell type. Using double-labeling of Cx43 and the pericyte marker, alpha smooth muscle (αSM), we demonstrate that Cx43 expression is low in control vessel pericytes, but robust co-staining is observed in lesion pericytes (Fig 3.2.3C). A larger sample size is required for statistical comparison of Cx43 between control vessels and lesions, however, our initial observations of Cx43 in lesion pericytes as well as CCM3KD pericytes (Chapter 2) suggests that Cx43 is also elevated in lesion pericytes.

3.3 Discussion

fCCM3 is believed to be a disease of progression – where the primary defect in fCCM3 lesions is their hyperpermeability and this produces many secondary pathologies over time, including hemorrhage, if left untreated (12, 13). However, the mechanism of lesion maturation contributing to hyperpermeability is not well defined. This study observed 1) lesions mature from enlarged vessels to organized, cystic caverns with hemorrhage, 2) Gd-DTPA leakage occurs prior to hemorrhage and 3) increased Cx43 protein expression in lesions of *ccm3*$^{+/-}$*p53*$^{-/-}$ mice.

Our initial evaluation of *ccm3*$^{+/-}$*p53*$^{-/-}$ mice suggest that this model recapitulates human disease well and overcomes many problems with conditional CCM3KO mice. In particular, lesions in *ccm3*$^{+/-}$*p53*$^{-/-}$ mice were observed in multiple regions of the brain with the appearance of new lesions over time. When first observed at 5 weeks old, the female mouse already had significant lesion burden, with male mice developing lesions by 9 weeks of age. Consistent with this mouse model, onset of clinical disease in fCCM3

patients typically occurs prior to 10 years of age. Interestingly, it has been suggested but not definitely shown that human fCCM3 disease is particularly aggressive in females (14, 15).

Understanding lesion maturation is critical to the development of therapeutic targets. The current study demonstrates that lesions of *ccm3*$^{+/-}$*p53*$^{-/-}$ mice exhibit a progression from permeable vessels to hemorrhagic vessels, a finding consistent with previous murine fCCM1 and fCCM2 studies (16). Gd-DTPA leakage occurs prior to hemorrhage and permeable vessels have a 100% probability of hemorrhaging in the future. Taken together with histological analysis that demonstrates hemorrhage (H&E) and iron accumulation (Prussian Blue) with stage 1 and 2, but not stage 0 vessels, lesions demonstrate a progression from permeable, non-hemorrhagic stage 0 and hemorrhagic stage 1 and 2 lesions in *ccm3*$^{+/-}$ *p53*$^{-/-}$ mice. To further establish the progression of hyperpermeability during lesion maturation, future studies will include *in vivo* injection of labelled tracers into *ccm3*$^{+/-}$*p53*$^{-/-}$mice, sacrifice and brain sectioning to analyze the extent of tracer leakage in all lesion stages. Based on our Gd-DTPA study, we expect to observe tracer leakage in stage 0 lesions. Such results will strengthen our current study suggesting that identifying a mechanism by which the permeability and maturation of stage 0 lesions can be blocked represents an opportunity to prevent additional pathologies.

We demonstrate that Cx43 expression is significantly elevated in *ccm3*$^{+/-}$*p53*$^{-/-}$ lesions, and particularly elevated in pre-hemorrhagic stage 0 lesions, compared to control vessels. This suggests that elevated Cx43 may contribute to early events in lesion maturation, including hyperpermeability of vessels prior to hemorrhage. In Chapter 2, it was determined that increased Cx43 expression and GJIC contributed to CCM3KD monolayer hyperpermeability *in vitro*. Taken together, our *in vivo* and *in vitro* data support a role for Cx43 is the pathology of lesion maturation and breakdown of the BBB. The next step in pursuing Cx43 as a therapeutic target will be the treatment of *ccm3*$^{+/-}$*p53*$^{-/-}$ with GAP27 and subsequent observation of changes in new lesion development, existing lesion permeability and hemorrhage frequency.

Another finding of our initial mouse studies has been the confirmation of elevated Cx43 expression in endothelial cells as well as pericytes in *ccm3*$^{+/-}$*p53*$^{-/-}$ mouse lesions. The *ccm3*$^{+/-}$*p53*$^{-/-}$ mouse model leaves the possibility of multiple initiating cells types, given that global p53 deletion renders all cell types susceptible to acquisition of a somatic mutation to ccm3 at any time point. It is possible, though unlikely, that the lesions examined for tissue-specific expression of Cx43 had multiple cell types with ccm3 second-hits. Another explanation is the induction of Cx43 expression in otherwise healthy cells from signaling or even direct passage of material from a *ccm3*$^{-/-}$ cell to healthy cells. It has not been examined whether the existence of GJs on one cell can directly influence the presence of GJs on a neighboring cell, however, docking signals likely influence this process.

Future directions of this project include treatment of *ccm3*$^{+/-}$*p53*$^{-/-}$ with GAP27. Specifically, prior to sacrifice, GAP27-treated *ccm3*$^{+/-}$*p53*$^{-/-}$ mice will be evaluated for multiple endpoints including lesion burden, rate of lesion development, presence of Gd-DTPA-permeable lesions and the progression of Gd-DTPA permeable lesions to hemorrhagic lesions. Given that in vitro treatment of CCM3KD mBEC monolayers rescued their hyperpermeability (Chapter 2.3.3) and that Cx43 is more highly expressed in stage 0 lesions, we hypothesize that *in vivo* GAP27 treatment will inhibit or slow 1) the permeability of developing lesions and/or 2) the progress of lesions from leaky to hemorrhagic. Additional experiments with and without GAP27 treatment will include *in vivo* injection of tracers capable of traversing permeable lesions. Immediate sacrifice, brain sectioning and immunofluorescence analysis will allow us to measure such outcomes as the correlation between tracer leakage and Cx43 expression, as well as quantitative comparison of total tracer leakage between mice treated with and without GAP27. To further our goal of identifying lesion-initiating and maturation-supporting cell types will include post-mortem immunofluorescence analysis including double labeling of CCM3 with cell-type specific markers and CCM3 with Cx43, the latter of which will determine whether CCM3 deficiency is a requirement for the upregulation of Cx43 in otherwise healthy, lesion surrounding cells.

3.4 Materials and Methods

3.4.1 Mouse model of fCCM3

C57BL/6J mice heterozygous for *ccm3* ($ccm3^{+/-}$) were obtained from Yale University (He et al., 2010). B6.129S2-*Trp53*^{tm1Tyj}/J mice, carrying a null mutation of p53 ($p53^{-/-}$), were obtained from The Jackson Laboratory. $Ccm3^{+/-}$ and $p53^{-/-}$ mice were bred together for two generations to produce $ccm3^{+/-}$ $p53^{-/-}$ mice to enable acquisition of a somatic second hit to *ccm3*. This model is based on the two hit hypothesis of fCCM development (17, 18). One female and two male $ccm3^{+/-}p53^{-/-}$ mice were used in lesion burden, Cx43 expression and Gd-DTPA leakage studies described below. For Cx43 expression and Gd-DTPA leakage studies, age-matched female and male $ccm3^{+/-}p53^{+/-}$ mice were used as controls.

3.4.2 Mouse MRIs

All mice were anesthetized with 2% isoflurane/air mixture throughout MRI examination. Mice lay prone, head first in a 7.0T or 9.4T Agilent MR scanner (horizontal bore, Agilent, Palo Alto, CA) with the body temperature maintained at 37°C, using forced heated air. A quadrature volume radiofrequency coil was used to scan the head region of the mice. Axial T2-weighted images were acquired using a fast spin-echo sequence with the following parameters: repetition time (TR)/effective echo time (TE), 4000/60 ms; echo spacing, 15 ms; number of echoes, 8; field of view (FOV), 20x20 mm; matrix, 256x128; slice thickness, 0.5 mm; number of slices, 25; and number of scans, 1 (tscan time 4.5 min). Additionally T1-weighted spin echo images were acquired pre- and post-gadolinium contrast injection using the same slice package as above and with a TR/TE of 600/17 ms and an acquisition time of approximately 2.5 minutes. Finally T2*-weighted gradient echo images were acquired using the same slice package as above and with a TR/TE of 300/6 ms and an acquisition time of approximately 2.5 min. Tracer leakage studies were performed by intra-peritoneal injection of 0.5mL Gadolinium-DTPA (Gd-DTPA, 0.5 mmol gadopentetate dimeglumine/ml, BioPAL). Mice were active for 10 min prior to post-injection imaging.

3.4.3 Histology and Immunofluorescence

H&E staining was performed with frozen brain sections using standard procedures. Prussian Blue staining was performed by placing brain slices in working solution (2% potassium ferrocyanide, 2% hydrochloric acid) for 1hr at room temperature. Counterstaining was performed in 0.2% Safranin O for 2 min then washed in 1% acetic acid. Samples were dehydrated in 95% then 100% alcohol, cleared in xylene and mounted with Permount (Fisher). Classification of lesion stage was performed according to criteria described by MacDonald et al., 2011. Briefly, stage 1 lesions are singular, dilated caverns exhibiting hemorrhage, while stage 2 lesions have segmented caverns with robust, prolonged hemorrhage. We introduce stage 0 lesions as vessels exhibiting dilation but with little or no hemorrhage.

For immunofluorescence staining, brain slices or cells were incubated for 30 minutes in blocking solution (0.05% Triton X-100, 5% Goat Serum) at room temperature followed by incubation with primary antibody in blocking solution at room temperature for 2hr. The following primary antibodies were used: Cx43 (Cell Signaling), ZO-1-AlexaFluor 594 (Fisher), claudin-5 unconjugated or claudin-5-AlexaFluor 488 (Fisher), CD31/PECAM-1 (Novus). Reactions were visualized following addition of secondary antibodies in blocking solution at 1:200 dilution for 1hr at room temperature following wash of primary antibodies. The following secondary antibodies were used: FITC anti-rabbit (Vector Laboratories) and Texas Red anti-mouse (Vector Laboratories). Images were acquired on the Nikon A-1 confocal microscope.

Cx43 immunofluorescence intensity in healthy capillaries of control (*ccm3*$^{+/-}$*p53*$^{+/-}$) mice or lesions of fCCM3 mice was quantified in ImageJ by selecting the entire endothelial region surrounding the control vessel or lesion and measuring signal intensity. 10 individual lesions for stage 0 and 1, 2 individual stage 2 lesions and 10 control vessels were analyzed from 3 control and 3 fCCM3 mice. Fluorescence intensity of Cx43 in mouse lesions was quantified using ImageJ. Background fluorescence was subtracted from both control vessel and lesion fluorescence readings.

3.5 References

1. Whitehead KJ, Plummer NW, Adams JA, Marchuk DA, Li DY. (2004) Ccm1 is required for arterial morphogenesis: implications for the etiology of human cavernous malformations. *Development*. 131:1437–1448.

2. Boulday G, et al. (2009) Tissue-specific conditional CCM2 knockout mice establish the essential role of endothelial CCM2 in angiogenesis: implications for human cerebral cavernous malformations. *Dis Model Mech* 2:168–177

3. Chan AC, Drakos SG, Ruiz OE, Smith AC, Gibson CC, Ling J, Passi SF, Stratman AN, Sacharidou A, Revelo P, Grossmann AH, Diakos NA, Davis GE, Metzstein MM, Whitehead KJ and Li DY. (2011) Mutations in 2 distinct genetic pathways result in cerebral cavernous malformations in mice. *J Clin Invest*. 121:1871–1881

4. He Y, Zhang H, Yu L, Gunel M, Boggon TJ, Chen H and Min W. (2010) Stabilization of VEGFR2 Signaling by Cerebral Cavernous Malformation 3 Is Critical for Vascular Development. *Science Signaling* 3**:**ra26.

5. Louvi A, Chen L, Two AM, Zhang H, Min W, Gunel M (2011) Loss of cerebral cavernous malformation 3 (Ccm3) in neuroglia leads to CCM and vascular pathology. Proceedings of the National Academy of Sciences 108:3737–3742.

6. Louvi A, Nishimura S and Günel M. (2014) Ccm3, a gene associated with cerebral cavernous malformations, is required for neuronal migration. *Development* 141:1404-1415.

7. Plummer NW, Gallione CJ, Srinivasan S, Zawistowski JS, Louis DN, and Marchuk DA. (2004) Loss of p53 Sensitizes Mice with a Mutation in Ccm1 (KRIT1) to Development of Cerebral Vascular Malformations. *Am J Path* 165:1509-18

8. McDonald DA, Shenkar R, Shi C, Stockton RA, Akers AL, Kucherlapati MH, Kucherlapati R, Brainer J, Ginsberg MH, Awad IA, Marchuk DA. (2011) A novel mouse model of cerebral cavernous malformations based on the two-hit mutation hypothesis recapitulates the human disease. *Hum Mol Gen* 20:211–222.

9. Davenport W.J., Siegel A.M., Dichgans J., Drigo P., Mammi I., Pereda P., Wood N.W., Rouleau G.A.. (2001) CCM1 gene mutations in families segregating cerebral cavernous malformations, *Neurology* 56:540-543

10. Kehrer-Sawatzki H, Wilda M, Braun VM, Richter HP, Hameister H. (2002) Mutation and expression analysis of the KRIT1 gene associated with cerebral cavernous malformations (CCM1). *Acta Neuropathol.* 104:231-40.

11. Shenkar R, Shi C, Rebeiz T, Stockton RA, Mcdonald DA, Mikati AG, Zhang L, Austin C, Akers AL, Gallione CJ, Rorrer A, Gunel M, Min W, Souza JMD, Lee C, Marchuk DA, Awad IA (2014) Exceptional aggressiveness of cerebral cavernous malformation disease associated with PDCD10 mutations. *Gen Med* 17:188–196.

12. Yadla S, Jabbour PM, Shenkar R, Shi C, Campbell PG, Awad IA (2010) Cerebral cavernous malformations as a disease of vascular permeability: from bench to bedside with caution. *Neurosurgical Focus* 29:E4.

13. Mikati AG, Khanna O, Zhang L, Girard R, Shenkar R, Guo X, Shah A, Larsson HB, Tan H, Li L, Wishnoff MS, Shi C, Christoforidis GA Awad IA (2015) Vascular permeability in cerebral cavernous malformations*. J Cereb Blood Flow Metab* 35:1632-9.

14. Porter RW, Detwiler PW, Spetzler RF et al. (1999) Cavernous malformations of the brainstem: experience with 100 patients. *J Neurosurgery* 90:50–58.

15. Aiba T, Tanaka R, Koike T, Kameyama S, Takeda N and Komata T. (1995) Natural history of intracranial cavernous malformations*. J Neurosurgery* 83:56–59.

16. Stockton RA, Shenkar R, Awad IA, Ginsberg MH (2010) Cerebral cavernous malformations proteins inhibit Rho kinase to stabilize vascular integrity*. J Exp Med* 207:881-896.

17. Akers AL, Johnson E, Steinberg GK, Zabramski JM, Marchuk DA (2009) Biallelic somatic and germline mutations in cerebral cavernous malformations (CCMs): evidence for a two-hit mechanism of CCM pathogenesis. *Hum Mol Gen* 18:919–930.

18. Pagenstecher A, Stahl S, Sure U, Felbor U (2009) A two-hit mechanism causes cerebral cavernous malformations: complete inactivation of CCM1, CCM2 or CCM3 in affected endothelial cells. *Hum Mol Gen* 18:911–918.

Chapter 4: Over-expression of the C-terminal Tail of Connexin 43 Regulates Brain Endothelial Cell Permeability

4.1 Introduction

The cytoplasmic, C-terminal tail of Cx43 serves as the main regulator of Cx43 channel functions. It spans from AA243-382 and contains several phosphorylatable residues that can result in conformation changes to regulate canonical channel functions of Cx43 hexamers (1, 2). In particular, phosphorylation of C-terminal residues create a negatively charged C-terminal tail (CT) that allows for interaction with the positively charged cytoplasmic loop (CL) of Cx43, termed the CT-CL interaction (2). The CT-CL interaction functions to close GJs but open HCs (3-5). Truncated Cx43 lacking the CT results in permanently open GJs and permanently closed HCs (6).

In addition to channel opening and closing, the Cx43 CT has many channel-independent functions, including Cx43 trafficking, turnover and signal transduction. In recent years, several Cx43 CT isoforms have been described that have emerging functional roles in Cx43 regulation. Smyth and Shaw report that several methionines contained in the C-terminus of Cx43 serve as internal translation start sites, resulting in the expression of multiple Cx43 isoforms incorporating the C-terminal tail (Fig. 4.1.1A) (7). The most abundant of these isoforms is the 20 kilo-Daltons (kD) isoform initiated at Methionine 213 (M213, 20-Cx43). They have described a trafficking role for 20-Cx43, such that introduction of point mutation M213A results in inhibited Cx43 trafficking to the membrane and greatly reduced Cx43 GJ appearance and GJIC. Another study has proposed the origin of lower molecular weight Cx43 isoforms arise from MMP cleavage events at the cell membrane that regulate channel-dependent signal transduction (Fig. 4.1.1B) (8). Yet more numerous studies not evaluating specific Cx43 CT isoforms, have simply overexpressed the entire

Cx43 CT or portions of the CT and observed various cellular effects, all indicating that the Cx43 CT, as an independent entity, is capable of wide-ranging cellular functions that have significant implications for disease (9-12).

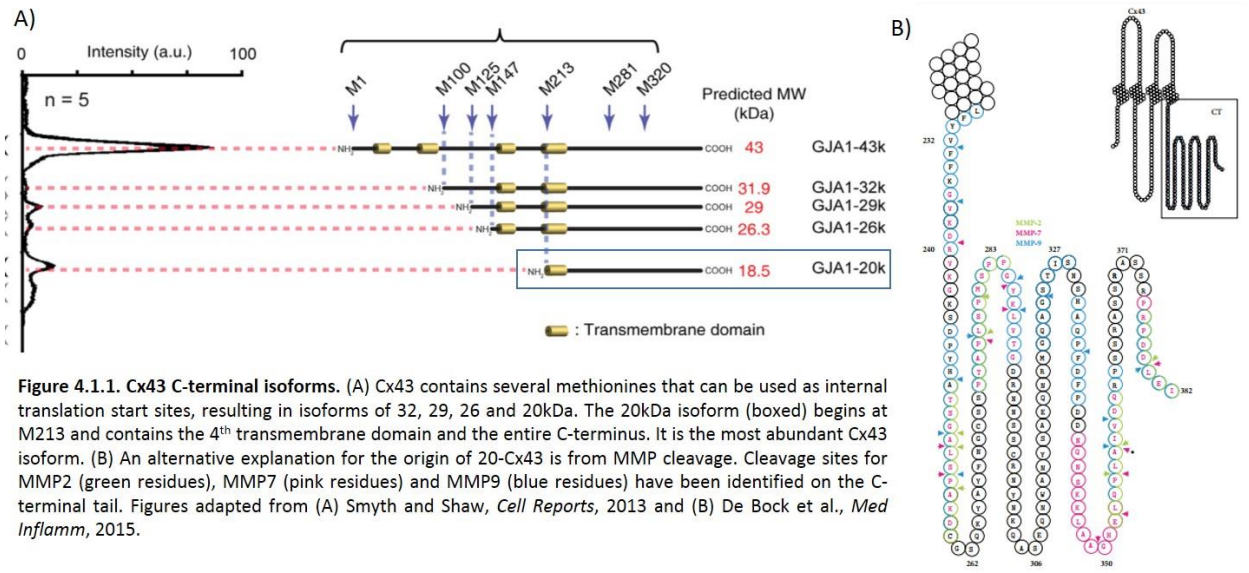

Figure 4.1.1. Cx43 C-terminal isoforms. (A) Cx43 contains several methionines that can be used as internal translation start sites, resulting in isoforms of 32, 29, 26 and 20kDa. The 20kDa isoform (boxed) begins at M213 and contains the 4th transmembrane domain and the entire C-terminus. It is the most abundant Cx43 isoform. (B) An alternative explanation for the origin of 20-Cx43 is from MMP cleavage. Cleavage sites for MMP2 (green residues), MMP7 (pink residues) and MMP9 (blue residues) have been identified on the C-terminal tail. Figures adapted from (A) Smyth and Shaw, *Cell Reports*, 2013 and (B) De Bock et al., *Med Inflamm*, 2015.

We sought to determine whether Cx43 CT isoforms are overexpressed in CCM3KD cells, and whether overexpression of 20-Cx43 in mBECs alone may recapitulate phenotypes observed in CCM3KD cells, particularly with respect to permeability and TJ protein organization. Additionally, given the novelty of the 20-Cx43 isoform, we sought to characterize the biological functions of 20-Cx43 in mBECs independent of CCM3 disease.

4.2 Results

4.2.1 Validation of 20kD expression in mBECs

We first sought to identify whether CCM3KD cells display increased expression of reported Cx43 isoforms. Using an antibody directed to the C-terminal tail of Cx43, made against residues C-terminal to M213, we observed a detectable band at approximately 20kDa whose expression was significantly elevated in CCM3KD cells compared to controls (20-Cx43, Fig 4.2.1A). The increase in 20kDa isoform was roughly proportionate to the increase in full length Cx43 (43-Cx43). To validate that the band at 20kDa was indeed the C-terminus tail, lysates of control and CCM3KD cells were blotted and tested against an

N-terminal Cx43 antibody, made against Cx43 AA107-138 that are not included in any lower molecular weight Cx43 C-terminal isoform. No bands were observed at 20kDa, while 43kDa bands were detected as expected (Fig. 4.2.1B). This supports that the 20kDa band is the C-terminal tail of Cx43.

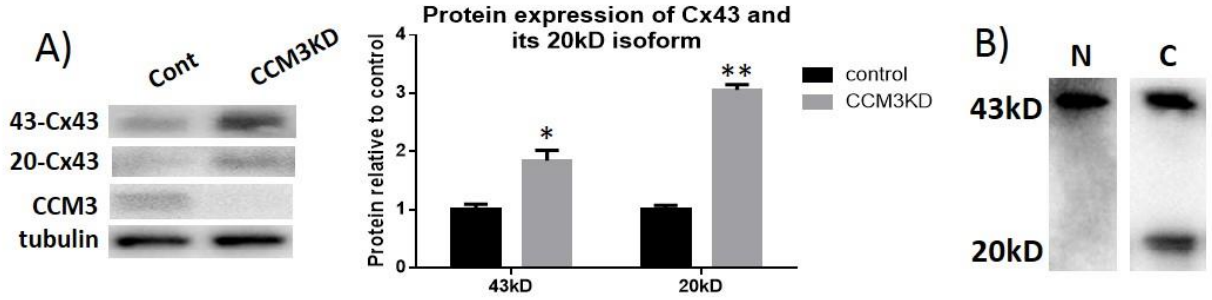

Figure 4.2.1. Cx43 C-terminal isoform is elevated in CCM3KD cells. (A) Western blot analysis of whole cell lysates of control and CCM3KD mBECs demonstrated significantly elevated expression of both full length Cx43 (43-Cx43) and a reported isoform of 20kD (20-Cx43) in CCM3KD cells compared to controls. n=3 independent experiments, *p<0.05, **p<0.01 compared to control. (B) Western blotting of CCM3KD whole cell lysates was performed with a Cx43 antibody directed towards the N-terminus ("N") or C-terminus ("C"). While the expected 43kD Cx43 band appeared using the N-terminal antibody, no 20kD band was visible.

Two hypotheses exist to describe the origin of 20-Cx43 isoform: 1) MMP cleavage events that occur at multiple sites, but produce several C-terminal cleavage products of approximately 15-20kDa and 2) internal translation utilizing the M213 start codon (7, 8). Each hypothesis was tested. MMP2, 7 and 9 have all showed activity against Cx43, therefore, we employed the MMP inhibitor, Batimastat, with inhibition of MMP1 (IC50, 3nM), MMP 2 (4nM), MMP3 (20nM), MMP7 (6nM), and MMP9 (4nM) in control and CCM3KD cells. No change in 20- or 43-Cx43 expression was observed following western blot analysis of lysates from treated cells. No additional molecular weight bands were observed following treatment (Fig 4.2.2).

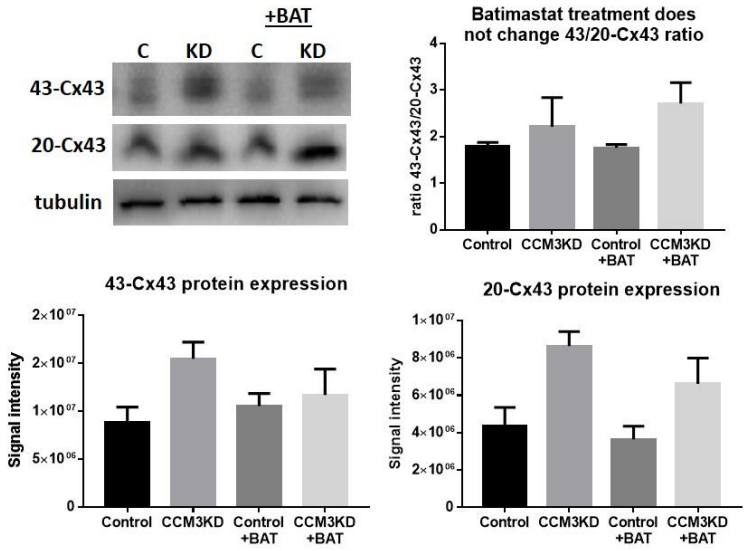

Figure 4.2.2. The 20kD Cx43 isoform does not arise from MMP cleavage events. Control or CCM3KD mBECs were treated with or without 100nM Batimastat (+BAT) for 1hr prior to harvest. Western blot analysis for Cx43 using a C-terminal antibody was performed. Quantitation revealed that batimastat treatment does not alter the ratio of 43kD/20kD Cx43 expression, nor does batimastat treatment significantly alter the expression of 43kD or 20kD Cx43.

To examine whether the observed 20kDa isoform arises from internal translation, we made an expression construct according to (7), containing the entire C-terminal Cx43 tail, beginning with the reported endogenous M213 start codon. Transfection of mBECs with this construct and subsequent western blot analysis revealed robust expression of 20-Cx43 (Fig. 4.2.3A). Intriguingly, lysates from cells overexpressing full-length Cx43 (FL^{over}) or 20-Cx43 (213^{over}) exhibited the same expression pattern of both 43- and 20-Cx43. In FL^{over} mBECs, this suggests that internal translation of either exogenous or endogenous 20-Cx43 is increased. In 213^{over} mBECs, the expression of endogenous 43-Cx43 is significantly upregulated.

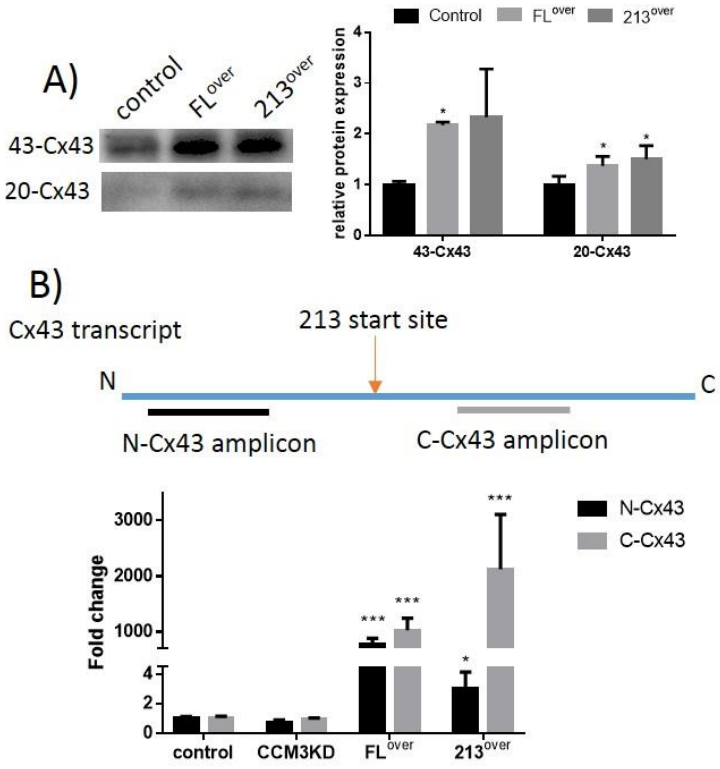

Figure 4.2.3. The 20kD Cx43 isoform arises from internal translation. (A) Western blot analysis of whole cell lysates of mBECs transfected with vechicle, full length Cx43 expression construct (FL^{over}) or a construct encoding the C-terminal tail of Cx43 with a methionine 213 start codon (213^{over}). Quantitation confirmed overexpression of full length (43-Cx43) and 20kD Cx43 (20-Cx43). n=3 independent experiments, *p<0.05. (B) qPCR was performed with control, CCM3KD, FL^{over} and 213^{over} mBECs using primer sets designed to amplify the N-terminal or C-terminal Cx43 transcript (diagram). This analysis revealed expected unchanged Cx43 transcript in CCM3KD cells, upregulation of both N- and C-terminal regions in FL^{over} cells, and upregulation of C-terminal Cx43 transcript in 213^{over} cells. Surprisingly, a significant upregulation of N-terminal Cx43 transcript, indicative of endogenous Cx43 transcription was also observed in 213^{over} cells. n=3 independent experiments, *p<0.05, ***p<0.001.

To confirm that exogenous 20-Cx43 induces expression of endogenous 43-Cx43, qPCR was performed using primer sets for either N-terminal or C-terminal Cx43 transcript (Fig 4.2.3B). In FL^{over} mBECs, it was expected to observe N- and C-terminal primer sets to amplify Cx43 to approximately the same extent, given that the exogenous and endogenous Cx43 transcripts will contain both the N- and C-terminal regions. This is what we observed. Intriguingly, while we observed the expected increase in C-terminal Cx43 transcript (exogenous construct), we observed a significant 3-fold increase in N-terminal

Cx43 transcript (endogenous transcript), consistent with the observed 2-fold increase in 43-Cx43 protein in 213^{over} cells. This finding suggests that 20-Cx43 is capable of regulating Cx43 transcription. Overall, our initial analysis suggest that 20-Cx43 arises from translation of Cx43 transcript at M213 and is capable of regulating 43-Cx43 protein expression.

4.2.2 Overexpression of 20-Cx43 increases GJIC, HC activity and monolayer permeability of mBECs

To determine whether increased 20- or 43-Cx43 protein expression is responsible for the permeability defect of CCM3KD cells, FL^{over} and 213^{over} mBECs were examined for canonical Cx43 functional effects observed in CCM3KD cells. First, scratch assays revealed that GJIC is significantly elevated in FL^{over} mBECs, confirming that exogenously expressed Cx43 is functional (Fig. 4.2.4). Interestingly, 213^{over} mBECs also demonstrated significantly elevated GJIC. Whether this is due to 20-Cx43 itself or the ability of 20-Cx43 to upregulate the expression of 43-Cx43 is not known.

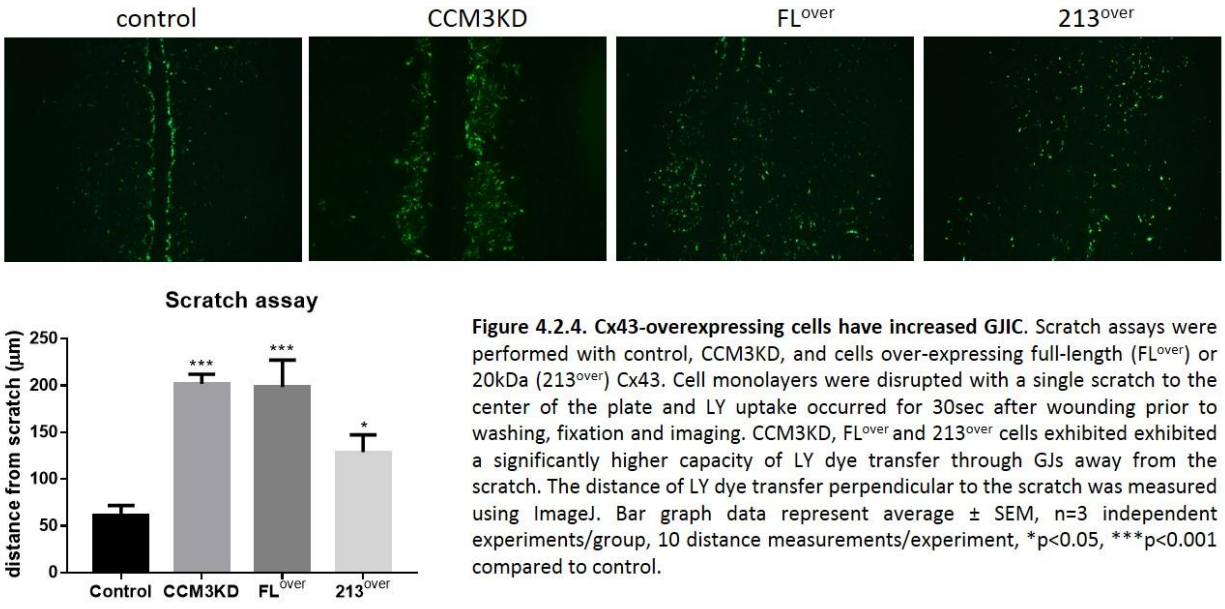

Figure 4.2.4. Cx43-overexpressing cells have increased GJIC. Scratch assays were performed with control, CCM3KD, and cells over-expressing full-length (FL^{over}) or 20kDa (213^{over}) Cx43. Cell monolayers were disrupted with a single scratch to the center of the plate and LY uptake occurred for 30sec after wounding prior to washing, fixation and imaging. CCM3KD, FL^{over} and 213^{over} cells exhibited exhibited a significantly higher capacity of LY dye transfer through GJs away from the scratch. The distance of LY dye transfer perpendicular to the scratch was measured using ImageJ. Bar graph data represent average ± SEM, n=3 independent experiments/group, 10 distance measurements/experiment, *p<0.05, ***p<0.001 compared to control.

Hemichannel activation was also evaluated in FL^{over} and 213^{over} mBECs, as examined by the overlay of LY onto mBEC monolayers. As with CCM3KD cells, the number of LY-positive cells was significantly greater in FL^{over} and 20^{over} mBECs compared to control cells (Fig. 4.2.5). 213^{over} mBECs demonstrated the greatest capacity of mBECs to uptake LY. When the amount of LY uptake per cell was analyzed, FL^{over}

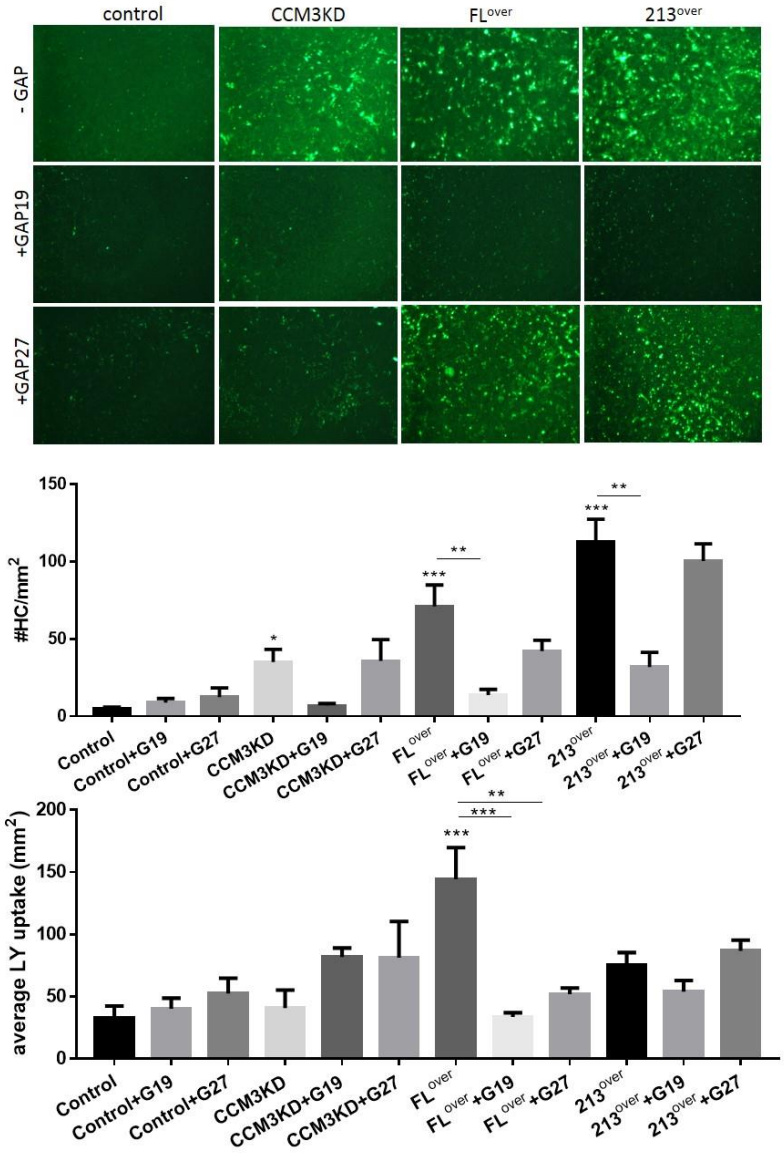

Figure 4.2.5. Hemichannel activity is increased in Cx43-overexpressing mBECs. (A) mBECs were transfected with appropriate siRNA or constructs and grown to confluency. Cell monolayers were overlayed with LY and allowed to uptake dye for 30sec prior to wash, fixation and imaging. Cells were untreated or treated with 100μM GAP19 or 100μm GAP27 for 1hr prior to LY overlay. (B) The number of LY^+ cells/mm2 were counted using ImageJ. Untreated CCM3KD, FL^{over} and 213^{over} mBECs had significantly more LY^+ cells compared to control cells, with significant reduction of LY^+ cell count with GAP19 treatment of FL^{over} and 213^{over} cells. Data represents average ± SEM, *p<0.05, **p<0.01, ***p<0.001 compared to control or as indicated with bars. (C) LY uptake by individual cells was calculated using ImageJ by measuring the area of LY^+ present in individual LY^+ cells. Compared to control cells, untreated CCM3KD and 213^{over} mBECs did not uptake significantly more LY/cell, however, FL^{over} cells did. The amount of LY uptaken by FL^{over} mBECs was significantly reduced following 1hr treatment with 100μM GAP19 or 100μm GAP27. Data represent average ± SEM, **p<0.01, ***p<0.001 compared to control or untreated FL^{over} cells.

mBECs demonstrated a higher capacity for LY uptake volume. These differences are important, given that it is important to distinguish differences between the number of HCs as well as the function of HCs. When comparing all groups, it appears that while CCM3KD, FL^{over} and 213^{over} mBECs all have more numerous HCs, LY volume uptake data suggests that FL^{over} mBECs may have altered HC function, such that FL^{over} mBECs HCs may have defects in open/close mechanisms. Elevated GJIC may also be contributing to the ability of LY dye to be transferred in a non-HC dependent manner, thus making it difficult to distinguish between HC and GJIC capacity. HC activity could be inhibited in all groups by treatment with GAP19, a

Cx43 HC-specific peptide inhibitor. GAP27, reported to inhibit Cx43 HCs in addition to Cx43 GJs, had surprisingly little effect on HC activity.

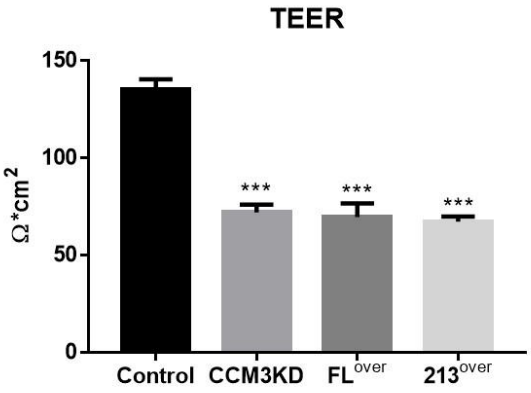

Figure 4.2.6. Cx43 overexpression increases mBEC monolayer permeability. TEER values were measured in confluent CCM3KD, full-length or 20kD Cx43-overexpressing (FL^{over}, 213^{over}) mBEC monolayers. This analysis revealed a significant, equivalent decrease in monolayer permeability in CCM3KD, FL^{over} and 213^{over} mBECs compared to controls, n≥3 independent experiments, ***p<0.001 compared to control.

Given that GAP27 treatment of CCM3KD cells reduced Cx43 GJIC and most importantly, rescued elevated CCM3KD monolayer permeability, we examined whether Cx43 overexpression alone could cause an increase in monolayer permeability. Indeed, the monolayer permeability of FL^{over} and 213^{over} mBEC monolayers was significantly elevated compared to controls and comparable to CCM3KD cells (Fig. 4.2.6).

4.2.3 TJ protein expression and organization is altered by Cx43-20kD overexpression

CCM3KD cells exhibit reduced expression of TJ proteins ZO-1 and claudin-5. Given that FL^{over} and 213^{over} mBECs exhibit increased monolayer permeability, we examined whether Cx43 overexpression alone affects TJ protein expression. ZO-1 was significantly reduced compared to controls in FL^{over} and 213^{over} mBECs, comparable to CCM3KD cells, while claudin-5 was less affected by Cx43 overexpression and CCM3KD (Fig. 4.2.7).

Larger Cx43 GJ plaques of CCM3KD cells disrupted ZO-1 localization, such that ZO-1 preferentially localized to GJ plaques instead of TJ structures along the cell border. We examined whether ZO-1 distribution to TJ structures was disrupted in FL^{over} and 213^{over} mBECs. Indeed, a similar pattern of ZO-1 fragmentation along the border was observed in FL^{over} and 213^{over} mBECs compared to controls and comparable to CCM3KD cells (Fig. 4.2.8). Almost no regions of continuous ZO-1 cell border staining could be observed.

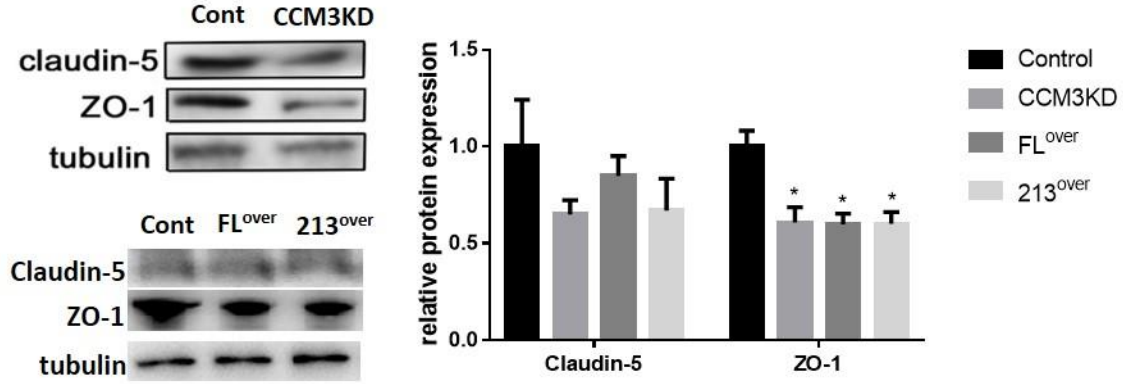

Figure 4.2.7. ZO-1 protein expression and localization is affected by Cx43-overexpression. Representative western blot and quantitation of ZO-1 and Claudin-5 protein expression in whole cell lysates of CCM3KD, full-length or 20kD Cx43 overexpressing (FL^{over}, 213^{over}) mBECs. Significant reduction in ZO-1 expression in CCM3KD, FL^{over} and 213^{over} cells compared to controls was observed. No significant changes to Cldn5 protein expression was observed, though a downtrend could be observed for CCM3KD and 213^{over} cells. n=3 independent experiments, *p<0.05.

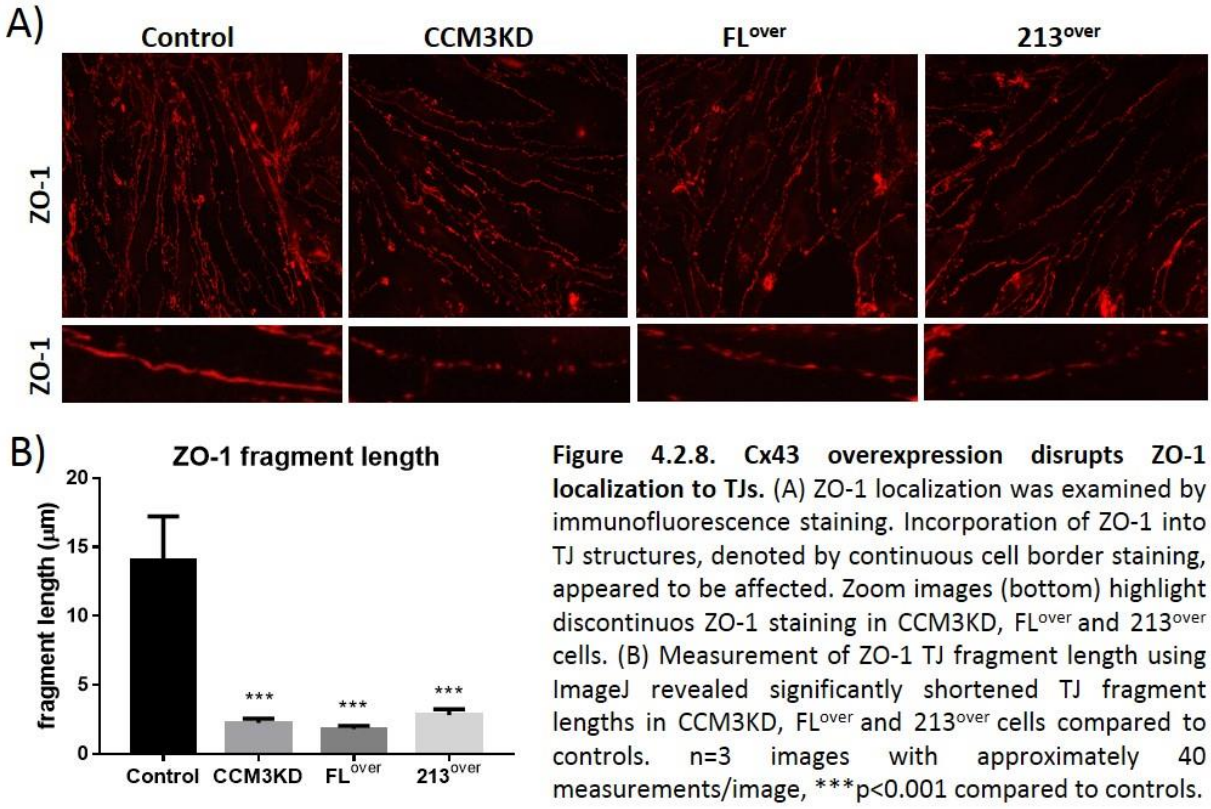

Figure 4.2.8. Cx43 overexpression disrupts ZO-1 localization to TJs. (A) ZO-1 localization was examined by immunofluorescence staining. Incorporation of ZO-1 into TJ structures, denoted by continuous cell border staining, appeared to be affected. Zoom images (bottom) highlight discontinuos ZO-1 staining in CCM3KD, FL^{over} and 213^{over} cells. (B) Measurement of ZO-1 TJ fragment length using ImageJ revealed significantly shortened TJ fragment lengths in CCM3KD, FL^{over} and 213^{over} cells compared to controls. n=3 images with approximately 40 measurements/image, ***p<0.001 compared to controls.

We demonstrated that full-length Cx43 and ZO-1 exhibited reduced interaction in CCM3KD cells compared to control cells. Given that ZO-1 binds Cx43 at I382, it is possible that 20-Cx43 and ZO-1 can interact, though no study has examined this. Based on our initial results that 43-Cx43 and ZO-1 exhibit reduced interaction, we hypothesized that a competition for ZO-1 binding may exist between 20-Cx43 and 43-Cx43. To address this hypothesis, we performed FRET using an N-terminal mCherry-tagged 20-Cx43 and N-terminal AcGFP-tagged ZO-1. As with 43-Cx43, 20-Cx43 demonstrated reduced interaction instances with ZO-1 in cell border regions of CCM3KD cells compared to control cells (Fig. 4.2.9). Overall, this suggests that 20-Cx43 does not outcompete 43-Cx43 for ZO-1 binding and in fact, shows reduced interaction as well.

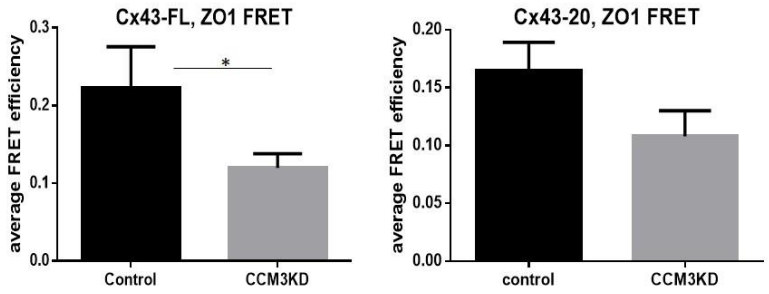

Figure 4.2.9. 20-Cx43/ZO-1 interaction is reduced in CCM3KD cells. The physical interaction between full length Cx43 (Cx43-FL) and ZO-1 (C) or 20kD Cx43 (Cx43-20) and ZO-1 (D) was evaluated using N-terminal tagged FL or 20kD Cx43 mCherry-tagged constructs and AcGFP-tagged ZO-1. FRET efficiencies were measured for membrane-localized Cx43 and ZO-1 regions of interest. The average FRET efficiency for 15 ROIs was calculated and demonstrated decreased instances of interaction between both Cx43-FL and Cx43-20 with ZO-1 in CCM3KD cells compared to controls. n=3 independent experiments, 2 ROIs/cell, *p<0.05 compared to control.

4.2.4 Cx43-20kD is localized to the chromatin-bound fraction and is associated with transcriptional changes.

Overexpression of 20-Cx43 alone upregulated endogenous Cx43 transcript. Signaling roles for 20-Cx43 have been described but transcription regulation has not. We next sought to test the hypothesis that Cx43 may act as a transcriptional regulator. First, we performed cell fractionation experiments to determine the cellular localization of Cx43 in control, CCM3KD, FL^{over}, or 213^{over} cells. Of the fractions examined – cytosol, plasma membrane, chromatin-bound and cytoskeleton – Cx43 was localized principally to the plasma membrane, chromatin-bound and cytoskeletal fractions (Fig. 4.2.10A). Both 20-Cx43 and 43-Cx43 appeared in these three fractions and while some difference in expression level was observed between all groups in particular compartments, CCM3KD or Cx43 overexpression did not cause

complete disappearance or appearance of 20- or 43-Cx43 into a cellular compartment. FRAP analysis of 20- and 43-Cx43 in control and CCM3KD cells revealed that 20-Cx43 is significantly more mobile in CCM3KD cells compared to controls, supporting the notion of 20-Cx43 as a signaling molecule that may be more capable of traveling between cellular compartments in CCM3KD cells (Fig. 4.2.10B).

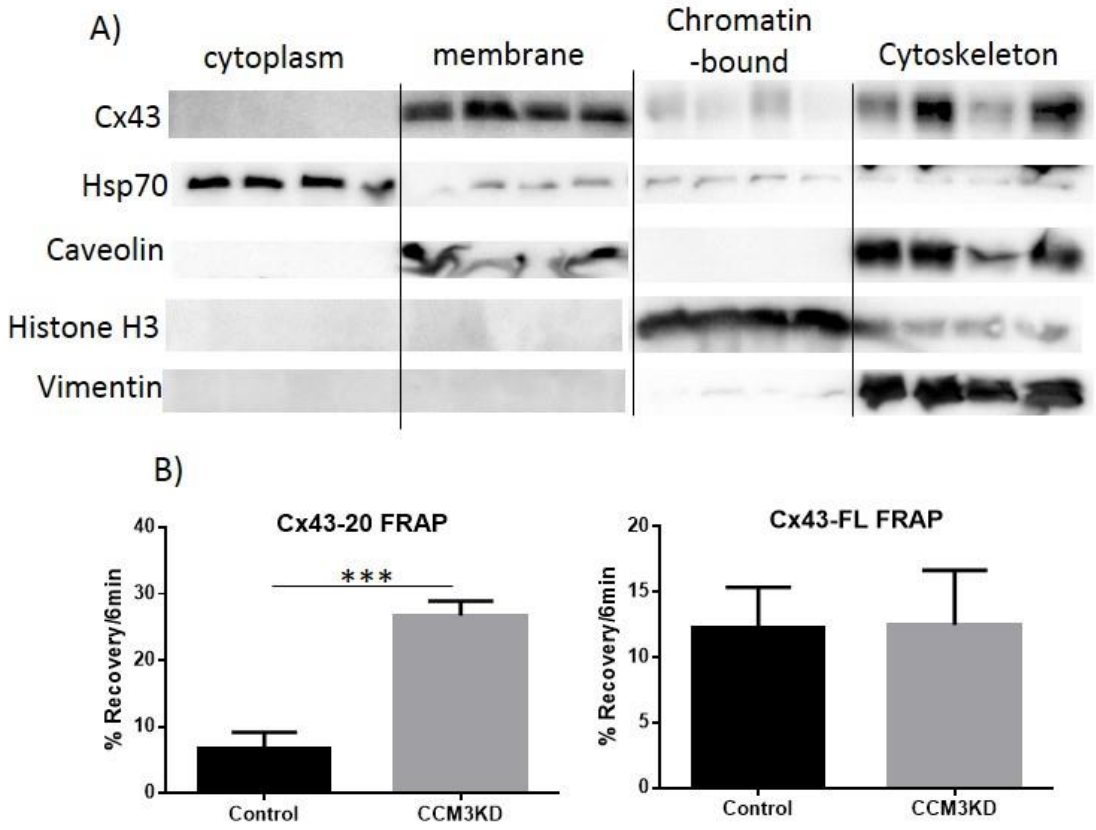

Figure 4.2.10. Cx43 localization is altered in Cx43 overexpressing cells. (A) Cell fractionation was performed with control, CCM3KD, full-length and 20kD Cx43 overexpressing (FL^{over}, 213^{over}) mBECs. In each cell type, Cx43 was localized to the membrane (Cav-1), chromatin-bound (Histone H3) and cytoskeletal (vimentin) fractions. CCM3KD and 213^{over} cells exhibited reduced full-length Cx43 content in the chromatin-bound fraction and higher full-length Cx43 content in the cytoskeletal fraction compared to control and FL^{over} cells. n=2 independent experiments. (B) Fluorescence recovery after photobleaching (FRAP) was performed with control and CCM3KD cells expressing AcGFP-tagged 20kD or full length Cx43 (20-Cx43, 43-Cx43). The mobility of 20-Cx43 in CCM3KD cells was significantly higher compared to controls, while 43-Cx43 displayed no difference in mobility between control and CCM3KD cells.

Given its localization to the chromatin-bound fraction and apparent transcriptional control of endogenous 43-Cx43, we examined whether 20-Cx43 may regulate the transcription of ZO-1 and claudin-5. Both CCM3KD and 213^{over} cells demonstrated significantly higher transcription of ZO-1 and claudin-5 compared to controls with no transcriptional elevation observed for ZO-1 or claudin-5 in FL^{over} cells (Fig. 4.2.11).

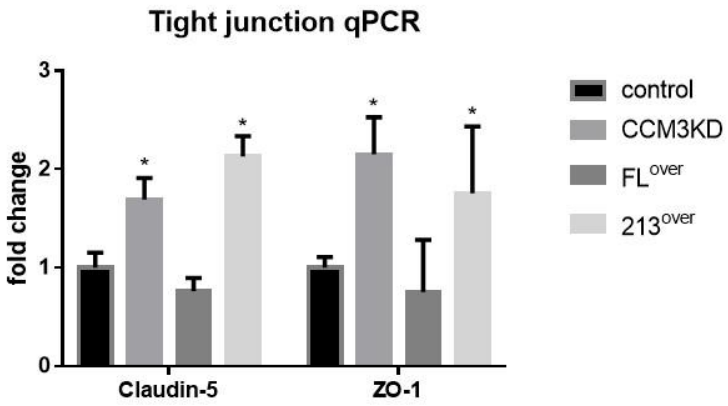

Figure 4.2.11. TJ transcripts are elevated by 20-Cx43 overexpression. The expression of claudin-5 and ZO-1 transcript was evaluated in control, CCM3KD, FL^{over} and 213^{over} mBECs using qPCR. This analysis revealed a significant increase in claudin-5 and ZO-1 transcription in CCM3KD and 213^{over} cells compared to control cells, and a small, but significant decrease in claudin-5 transcription in FL^{over} cells compared to controls. n=3 independent experiments, *p<0.05 compared to control cells.

Finally, we performed several gene arrays to determine if 20-Cx43 was capable of regulating the expression of genes in addition to claudin-5 and ZO-1. In the first set of experiments, gene expression changes in control, CCM3KD, FL^{over} and 213^{over} mBECs was examined using the SABiosciences Endothelial Cell Biology and Signal Transduction PathwayFinder arrays (Fig. 4.2.12). When analyzing the results, we were particularly interested in identifying genes that were changed in more than one group compared to controls. Significant overlap between CCM3KD, FL^{over} and 213^{over} transcriptional changes compared to controls was observed. Interestingly, while FL^{over} mBECs produced no unique overlapping transcripts with CCM3KD mBECs that were not also altered in 213^{over} mBECs, 213^{over} mBECs had several overlapping transcriptional changes with CCM3KD mBECs that were not altered in FL^{over} mBECs. This suggests that 20-Cx43, not 43-Cx43, is the principal driver of transcriptional changes in CCM3KD mBECs. Given our observations of both gene transcriptional changes as well as changes to Cx43 content in the chromatin-bound fraction in 20-Cx43 overexpressing cells, we sought to determine whether overexpression of 20-Cx43 can regulate gene transcription in a chromatin-modification dependent manner. Analysis of gene

expression in control and 213^{over} mBECs using the Epigenetic Chromatin Modification Enzyme gene expression array from SABiosciences revealed many transcriptional changes in epigenetic modifying enzymes (Fig. 4.2.13).

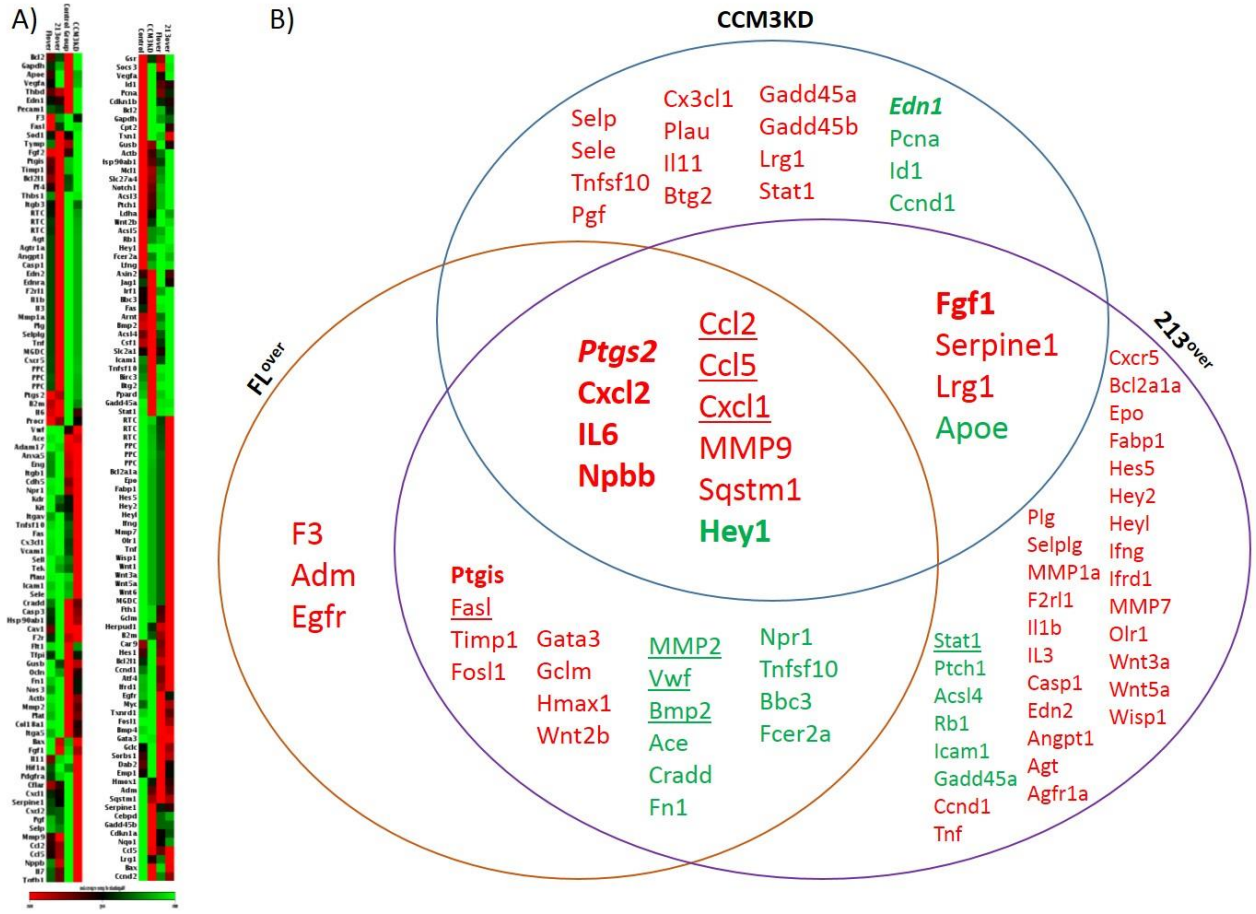

Figure 4.2.12. CCM3KD and Cx43 overexpression result in overlapping transcriptional changes. (A) Cluster grams of gene expression in control, CCM3KD, FL^{over} and 213^{over} mBECs using arrays detecting genes involved in endothelial cell biology (left) or signal transduction (right). (B) Venn diagrams of genes changed in CCM3KD (top circle), FL^{over} (left circle) and/or 213^{over} (right circle) mBECs compared to control mBECs. Red genes indicate expression greater than control; green genes indicate expression less than control. Underlined genes represent genes whose transcription was increased >4 fold in one group compared to control. Bold fonts represent genes whose transcription was changed by >4 fold in 2 or more groups compared to control. Italicized genes represent genes whose transcription was changed >8 fold in at least one group compared to control.

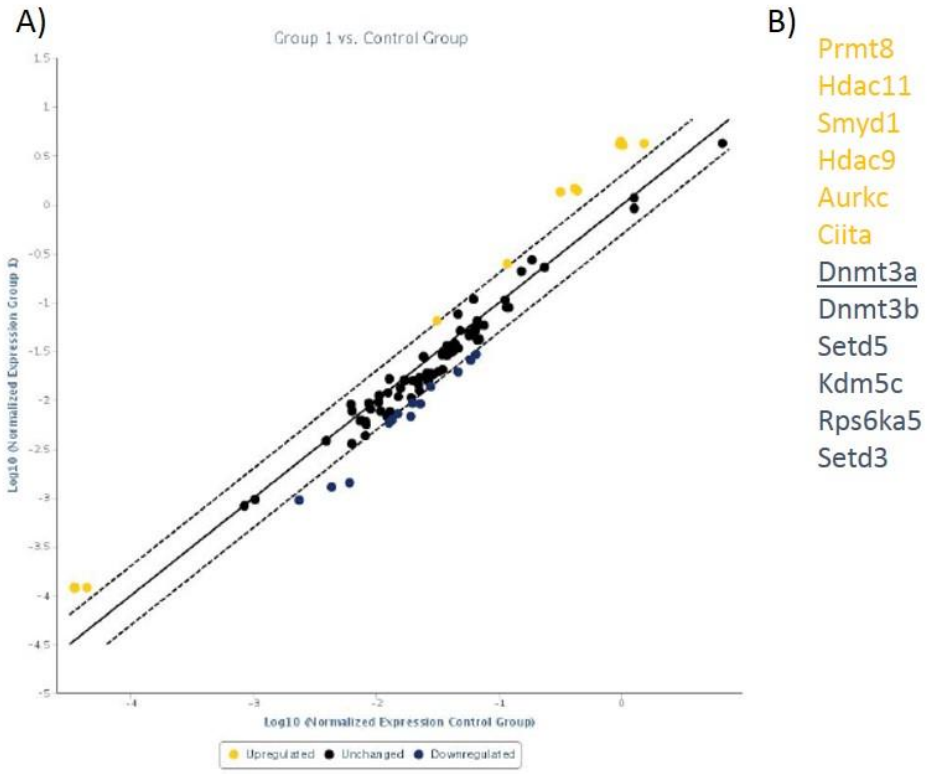

Figure 4.2.13. 20-Cx43 overexpression regulates the transcription of epigenetic modification enzymes. A) Scatter plot of gene expression changes in 213^{over} compared to control mBECs. Black dots represent genes whose expression have <2-fold change between control and 213^{over} mBECs. Yellow dots represent genes whose expression has increased >2-fold in 213^{over} mBECs compared to control mBECs. Blue dots represent genes whose expression has decreased >2-fold in 213^{over} mBECs compared to control mBECs. B) List of gene transcription changes > 2-fold in 213^{over} compared to control mBECs; increased (yellow) or decreased (blue). Underlined genes represent genes whose transcription was altered >4 fold compared to control.

2.3 Discussion

Studies of the origin and function of Cx43 lower molecular weight isoforms are only beginning to emerge in the literature. The expression of 20-Cx43 has never been addressed in the context of BBB permeability and has not been quantified in fCCM3. In the present study, we have observed 1) 20-Cx43 expression is increased in CCM3KD cells, 2) 20-Cx43 likely arises from translation at M213, 3) overexpression of 20-Cx43 recapitulates many molecular events observed in CCM3KD cells, including Cx43-associated functions and effects on TJ organization and permeability and 4) 20-Cx43 may contribute to CCM3KD phenotypes through direct regulation of gene expression.

A central question in the literature is whether 20-Cx43 arises from enzyme-driven cleavage of the C-terminal tail, internal translation at M213, or an alternative, yet to be described mechanism. We have ruled out the possibility of MMP2, 7, or 9 cleavage as the main driver of 20-Cx43 existence, at least in the context of CCM3KD cells. Previous *in vitro* studies have shown via surface plasmon resonance imaging that MMP7 directly binds to the C-terminal tail of Cx43 and separately, that *in vitro* enzyme reactions with Cx43 and MMPs2, 7 and 9 result in production of several C-terminal cleavage products. These studies have utilized antibodies directed towards the upper-C-terminal tail (252-270) and lower C-terminal tail (372-382) and demonstrate cleavage occurs between those upper and lower portions. Two principal observations in our test of MMP inhibition is that 1) we did not observe the re-appearance of other C-terminal products of varying molecular weight, which would be expected given the multiple cleavage sites reported for MMP-Cx43 interaction, and 2) we did not observe a change to either the expression level of 20-Cx43 nor the ratio of 43-Cx43 to 20-Cx43 expression. Expression of 20-Cx43 would be expected to significantly decrease with MMP inhibition if it's production was dependent on MMP activity, and we would expect a concurrent increase in 43-Cx43 if that pool of Cx43 is no longer being depleted by MMP cleavage. It is possible that other MMPs may be important for Cx43 cleavage or that MMP cleavage of Cx43 is cell type or context dependent and our conditions did not meet the criteria to induce such events.

Our strongest data that 20-Cx43 arises from internal translation is the observation that exogenous expression of a Cx43 construct with N-terminal truncation, such that the open reading frame begins at M213, produces an increase in appearance of the band at 20-Cx43 that we observe in CCM3KD cells. We were surprised to observe that 213^{over} cells had increased expression of full-length Cx43 (43-Cx43). This effect has not previously been described in the literature. Several possibilities could explain this observation, including that 20-Cx43 post-translationally increases 43-Cx43 translation or pro-longs its half-life, or that 20-Cx43 increases the availability of 43-Cx43 transcript. We determined that the latter case was true using primers sets designed to amplify the C-terminal - endogenous and exogenous 20-Cx43

transcript - or the N-terminus, which could only be due to transcription of endogenous protein given that the 213 construct transcript does not include the sites for N-terminal primer annealing. It is still possible that 20-Cx43 also acts in other ways to increase 43-Cx43 cellular content, including control of its half-life. Future experiments, including quantification of 43-Cx43 half-life in control and 213^{over} cells using translation inhibitor cycloheximide, will further define how 20-Cx43 increases 43-Cx43 content. How 20-Cx43 expression is increased in CCM3KD cells is also subject to future study. Previous work has suggested that the internal translation of 20-Cx43 is dependent on the Mnk1/2 pathway (13). Intriguingly, Mnk1/2 is downstream of ERK1/2, the latter of which has been shown to have increased basal activity in CCM3KD cells by a STRIPAK-dependent mechanism (14). Whether inhibition of ERK1/2 can reduce 20-Cx43 expression in CCM3KD cells will be the subject of future study.

We demonstrate that overexpression of 20-Cx43 results in many of the same functional phenotypes observed in CCM3KD cells, including elevated GJIC, HC activity and importantly, reduced monolayer permeability. In Chapter 2, we observed that Cx43 GJ plaques in CCM3KD cells disrupted the incorporation of ZO-1 into TJ structures. Similarly, we observe that overexpression of 20-Cx43 significantly shortens ZO-1 TJ fragment length, suggesting a similar mechanism by which permeability is decreased in both CCM3KD and 213^{over} cells. While ZO-1 protein expression was decreased in CCM3KD, FL^{over} and 213^{over} cells, it is most intriguing that only 20-Cx43, and not 43-Cx43, overexpression recapitulates the TJ transcript profile of CCM3KD cells. Both claudin-5 and ZO-1 transcripts were significantly elevated in CCM3KD and 213^{over} cells, with no significant increases in FL^{over} cells. The increase in transcript with a decrease in protein is not surprising for CCM3KD cells, given previous work has demonstrated that the regulation of TJ protein content by CCM3 occurs in a post-translational mechanism (14). The similarities in transcript profile between CCM3KD and 213^{over} cells, and not FL^{over} cells, is the first observation to suggest a 43-Cx43-independent function within CCM3KD cells and one that may have significant outcomes given its ability to regulate transcriptional events.

In addition to the observation that 20-Cx43 regulates claudin-5 and ZO-1 transcription, we also demonstrate for the first time that 43-Cx43 is incorporated into the chromatin-bound fraction of mBECs. Furthermore, we observe that CCM3KD and 213^{over} cells both have depleted 43-Cx43 in this fraction. Only one study to our knowledge has indicated a direct interaction with a nuclear protein that affects transcription (15). That study, performed in a lung cancer cell line, demonstrated that Cx43 can localize to the nucleus when bound to A-kinase anchoring protein 95 (AKAP95) and this interaction and localization to the nucleus enables cell cycle progression. Whether gene expression was altered by localization of the Cx43-AKAP95 complex to the nucleus was not examined. Given that 43-Cx43 localizes to the chromatin-bound fraction, chromatin immunoprecipitation experiments will provide further information and is the subject of future study.

Analysis of gene expression of genes regulating endothelial biology as well as genes involved in signal transduction revealed that several overlapping genes have altered transcription in CCM3KD, FL^{over} and 213^{over} compared to control mBECs, as well as additional overlap between CCM3KD and 213^{over} compared to control mBEC gene transcription. Nearly all genes with altered transcription in all three groups compared to controls had a greater than 4-fold change compared to controls, while genes with altered transcription in only one or two groups did not have such robust changes. Ccl2, Ccl5, Cxcl1, Cxcl2, Il6, Npbb, and Ptgs2, all robustly increased in all three groups compared to controls, are regulators of angiogenesis and inflammation. Given that these genes are increased by overexpression of 43-Cx43 or 20-Cx43 alone, it is likely that elevated Cx43 in CCM3KD cells directly or indirectly contributes to the elevation of these transcripts. Inflammation and angiogenesis have both been implicated in the pathogenesis of fCCM (16, 17). Inflammation in general is a known contributor to increased barrier permeability (18). Whether these genes are specifically regulated by Cx43 GJs or represent additional mechanisms by which Cx43 contributes to fCCM pathology will need to be explored. Finally, we observed a robust decrease in Hey1 for all groups compared to controls. Hey1 is a transcription factor and direct target of Notch, a

regulator of vasculogenesis in development (19). It has been shown that decreased Notch signaling can be observed in CCM3KD cells and it is suggested that this promotes angiogenesis (20, 21). This also supports our data showing robust increases in genes regulating angiogenesis. How 43-Cx43 or 20-Cx43 regulates Notch signaling is not known.

Analysis of epigenetic modification enzyme transcription revealed approximately 4-fold decreases in DNA methyl transferases 3a and 3b (DNMT3a, DNMT3b) in 213^{over} mBECs compared to control mBECs. *Dnmt3a* mutations that reduce DNMT3 activity are prevalent in patients with acute myeloid leukemia (AML) and *in vitro* work has demonstrated the necessity of DNMT3 for the differentiation of hematopoietic stem cells (22, 23). Studies of CCM1KO mice have suggested that loss of CCM1 results in an endothelial to mesenchymal transition (EndMT) and while EndMT has not thoroughly been addressed in fCCM3, a decrease in the pro-differentiation regulator DNMT3 suggests that loss of a differentiated state should be examined in CCM3KD mBECs (24). It is also interesting to note that both Cx43 and DNMT3 play important roles in bone homeostasis. As discussed in the introduction, N-terminal mutations in Cx43 in humans causes ODDD, in which patients have malformed bones in the cranial and cephalic regions (25). Cx43 knockout mice have impaired osteoblast differentiation (26-28). Intriguingly, DNMT3 knockout mice also display abrogated osteoclastogenesis but no study has linked the Cx43 and DNMT3 pathways (29). Our gene array results suggest that Cx43 directly or indirectly regulates DNMT3 and suggests a mechanism through which Cx43 can regulate gene expression and cell differentiation state. Examining the effects of DNMT3 in brain endothelial cells, particularly in CCM3KD cells will be informative.

Currently, it is difficult to determine whether the functional effects we observe with 20-Cx43 overexpression are due to direct 20-Cx43 effects or indirectly through its modulation of 43-Cx43 expression. Future experiments will employ a strategy where endogenous transcription can be controlled. One approach would include the use of shRNA directed to the 3'UTR of Cx43 such that endogenous protein level can be controlled by the concentration of shRNA employed. Another approach would be the

use of an alternative cell line that does not express endogenous Cx43 and use double transfections of 43-Cx43 and 20-Cx43 constructs. If the expression of 43-Cx43 can be kept constant and remain unaltered in 213^{over} cells compared to control cells, we can begin to address whether functional effects result from direct action of 20-Cx43 on particular pathways or indirectly by its ability to transcriptionally regulate 43-Cx43 and increase its protein expression. A companion approach will include the use of a Cx43 M213A construct already available in the lab in which the start codon for 20-Cx43 has been mutated. By transfecting cells with both 3'-UTR Cx43 shRNA and the Cx43 M213A construct, we can produce cells expressing only 43-Cx43 and lower molecular weight isoforms that do not include 20-Cx43.

In conclusion, we have observed striking functional overlap between CCM3KD mBECs and mBECs overexpressing 43-Cx43 and 20-Cx43. Given the recent implications for Cx43-driven permeability defects in the BBB (discussed in detail in the Chapter 2 discussion), studies addressing how Cx43 may regulate brain endothelial biology are of the utmost importance. Based on our findings, 20-Cx43 represents an important target to pursue in fCCM3, especially given its ability to recapitulate TJ defects observed in CCM3KD cells. Future studies will focus on extending the analysis of 20-Cx43 function in brain endothelial cells to its regulation of gene expression.

4.4 Materials and Methods

4.4.1 Cx43 construct cloning

Flag-tagged Cx43 expression constructs were produced to facilitate study of Cx43 overexpression. For full length Cx43 (FL^{over}), the entire ORF of Cx43 was cloned into Clontech's flag vector. To produce the 20kD isoform according to the internal translation hypothesis, methionine (M) 213 was used as the start codon, such that the entire ORF coding for M213-I382 was cloned into flag tag vector (213^{over}). To produce a 20kD isoform according to the cleavage event hypothesis, the entire ORF between AA243-382 was cloned, with addition of a Met start codon prior to residue 243 to facilitate expression, into a flag tag vector. Constructs were transfected into mBECs using TorpedoDNA transfection reagent (ibidiUSA).

4.4.2 20kD isoform validation

Antibodies directed towards the N- or C-terminus of Cx43 were used to confirm that the 20kD band identified on western blots is indeed the C-terminus of Cx43. The N-terminus-directed antibody recognizes AA107-118 (Cxn-6, GeneTex), while the C-terminus-directed antibody (3516, Cell Signaling) recognizes the C-terminal tail.

MMP2, 7 and 9 inhibition studies were performed using Batimastat. Control or CCM3KD mBECs (see chapter 2 methods for knockdown protocol) were treated with 100nM Batimastat for 1hr. Cells were harvested and full cell lysates were analyzed via western blot to confirm C-terminal Cx43 expression.

4.4.3 Cell fractionation

Cell fractionation was performed using the Subcellular Protein Fractionation Kit for Cultured Cells (Pierce). Fractionation was performed according to kit instructions for 3 independent experiments each for control, CCM3KD, FL^{over} and 213^{over} cells. Fraction purity was determined using the following antibodies: cytosol, HSP70; membrane, Caveolin-1; chromatin-bound fraction, Histone H3; cytoskeleton, vimentin.

Cx43 Gap Junction Intracellular Communication (GJIC) and Hemichannel (HC) activity assays, Transendothelial Electrical Resistance (TEER) assays, and FRAP and FRET analysis were performed as described in Chapter 2 Materials and Methods Sections.

4.4.4 Gene arrays

RNA from control, CCM3KD, FLover or 213over mBECs was harvested using the RNeasy Mini Kit (SABiosciences). As recommended, 0.5μg of RNA was reverse transcribed for each gene array plate using the RT^2 First Strand kit (SABiosciences). Finally, the following gene arrays were performed according to the manufacturer's instructions: Endothelial Cell Biology (PAMM-015Z), Signal Transduction PathwayFinder (PAMM-014Z) and Epigenetic Chromatin Modification Enzymes (PAMM-085Z) (SABiosciences). Analysis was performed using the SABiosciences PCR array analysis services.

4.5 References

1. Leithea E, Mesnilb M, Aasen T. (2017) The connexin 43 C-terminus: A tail of many tales. *Biochimica et Biophysica Acta (BBA) – Biomembranes*.

2. Solan JL and Lampe PD. (2009) Connexin43 phosphorylation: structural changes and biological effects. *Biochem. J.* 419:261–272.

3. Lampe, P. D., Cooper, C. D., King, T. J. and Burt, J. M. (2006) Analysis of connexin43 phosphorylated at S325, S328 and S330 in normoxic and ischemic heart. *J. Cell Sci*. 119: 3435–3442

4. G.E. Morley, J.F. Ek-Vitorin, S.M. Taffet, M. Delmar. (1997) Structure of connexin43 and its regulation by pHi *J. Cardiovasc. Electrophysiol*. 8: 939–951

5. Cottrell, G. T., Lin, R., Warn-Cramer, B. J., Lau, A. F. and Burt, J. M. (2003) Mechanism of v-Src- and mitogen-activated protein kinase-induced reduction of gap junction communication. *Am. J. Physiol. Cell Physiol.* 284:C511–C520

6. Maass K, Shibayama J, Chase SE, Willecke K, Delmar M. (2007). C-terminal truncation of connexin43 changes number, size, and localization of cardiac gap junction plaques. *Circ Res*. 101:1283-91.

7. Smyth JW and Shaw RM. (2013) Autoregulation of Connexin43 Gap Junction Formation by Internally Translated Isoforms. *Cell Reports* 5:611–618

8. De Bock M, Wang N, Decrock E, Bultynck G and Leybaert L. (2015) Intracellular Cleavage of the Cx43 C-Terminal Domain by Matrix-Metalloproteases: A Novel Contributor to Inflammation? *Med Inflamm*. Article ID 257471.

9. H.T. Xu, Q.C. Li, Y.X. Zhang, Y. Zhao, Y. Liu, Z.Q. Yang, E.H. Wang. (2008) Connexin 43 recruits E-cadherin expression and inhibits the malignant behaviour of lung cancer cells. *Folia Histochem Cytobiol* 46:315–321

10. M. Ionta, R.A. Ferreira, S.C. Pfister, G.M. Machado-Santelli. (2009) Exogenous Cx43 expression decrease cell proliferation rate in rat hepatocarcinoma cells independently of functional gap junction. *Cancer Cell Int*. 9: 22

11. E. McLachlan, Q. Shao, H.L. Wang, S. Langlois, D.W. Laird. (2006) Connexins act as tumor suppressors in three-dimensional mammary cell organoids by regulating differentiation and angiogenesis. *Cancer Res* 66:9886-9894.

12. Kameritsch P, Pogoda K, Pohl U. (2012) Channel-independent influence of connexin 43 on cell migration. *Biochimica et Biophysica Acta (BBA) – Biomembranes*. 1818: 1993–2001.

13. Dreas A, Mikulski M, Milik M, Fabritius CH, Brzózka K, Rzymski T. (2017). Mitogen-activated protein kinase (MAPK) interacting kinases 1 and 2 (MNK1 and MNK2) as targets for cancer therapy: recent progress in the development of MNK inhibitors. *Curr Med Chem*. 24

14. Stamatovic SM, Sladojevic N, Keep R, Andjelkovic AV (2015) PDCD10 (CCM3) regulates brain endothelial barrier integrity in cerebral cavernous malformation type 3: role of CCM3-ERK1/2-cortactin cross-talk. *Acta Neuropathol* 130:731–750.

15. Chen X, Kong X, Zhuang W, Teng B, Yu X, Hua S, Wang S, Liang F, Ma D, Zhang S, Zou X, Dai Y, Yang W & Zhang Y. (2016) Dynamic changes in protein interaction between AKAP95 and Cx43 during cell cycle progression of A549 cells. *Sci Reports*. 6:21224.

16. Zhu Y, Wu Q, Xu JF, et al. (2010) Differential angiogenesis function of CCM2 and CCM3 in cerebral cavernous malformations. *Neurosurg Focus.* 29:E1.

17. Retta SF and Gladingc AJ. (2016) Oxidative stress and inflammation in cerebral cavernous malformation disease pathogenesis: Two sides of the same coin. *Int J Biochem Cell Biol*. 81: 254–270.

18. Varatharaj A and Galea I. (2017) The blood-brain barrier in systemic inflammation. *Brain Behav. Immun*. 60: 1-12.

19. Fischer A, Schumacher N, Maier M, Sendtner M, Gessler M. (2004) The Notch target genes Hey1 and Hey2 are required for embryonic vascular development. *Genes Dev*. 18:901-11.

20. Wüstehube J, Bartol A, Liebler SS, Brütsch R, Zhu Y, Felbor U, Sure U, Augustin HG, Fischer A. (2010) Cerebral cavernous malformation protein CCM1 inhibits sprouting angiogenesis by activating DELTA-NOTCH signaling. *Proc Natl Acad Sci U S A.* 107:12640-5.

21. You C, Sandalcioglu IE, Dammann P, Felbor U, Sure U, Zhu Y. (2013) Loss of CCM3 impairs DLL4-Notch signalling: implication in endothelial angiogenesis and in inherited cerebral cavernous malformations. *J Cell Mol Med*. 17:407-18.

22. Ley TJ, Ding L, Walter MJ, McLellan MD, Lamprecht T, Larson DE, et al. (2010) DNMT3A mutations in acute myeloid leukemia. *N Engl J Med*. 363: 2424–33.

23. Challen GA, Sun D, Jeong M, Luo M, Jelinek J, Berg JS, Bock C, Vasanthakumar A, Gu H, Xi Y, Liang S, Lu Y, Darlington GJ, Meissner A, Issa JP, Godley LA, Li W, Goodell MA. (2012) Dnmt3a is essential for hematopoietic stem cell differentiation". *Nat Gen*. 44: 23–31.

24. Maddaluno L et al., (2013) EndMT contributes to the onset and progression of cerebral cavernous malformations. *Nature* 498:492–496.

25. Laird DW. (2014) Syndromic and non-syndromic disease-linked Cx43 mutations. *FEBS Lett*. 588:1339-48.

26. Lecanda F, Warlow PM, Sheikh S, Furlan F, Steinberg TH, and Civitelli R. (2000). Connexin43 deficiency causes delayed ossification, craniofacial abnormalities, and osteoblast dysfunction. *J. Cell Biol*. 151, 931–944.

27. Chaible LM, Sanches DS, Cogliati B, Mennecier G, Dagli MLZ (2011).Delayed Osteoblastic Differentiation and Bone Development in Cx43 Knockout Mice. *Toxicologic Pathol*. 39:1046-1055.

28. Sternlieb M, Paul E, Donahue HJ, and Zhang Y. (2012). Ablation of connexin 43 in osteoclasts leads to decreased in vivo osteoclastogenesis. *J. Bone Miner. Res.* 27:S53.

29. Challen GA, Sun D, Jeong M, Luo M, Jelinek J, Berg JS, Bock C, Vasanthakumar A, Gu H, Xi Y, Liang S, Lu Y, Darlington GJ, Meissner A, Issa JP, Godley LA, Li W, Goodell MA. (2012) Dnmt3a is essential for hematopoietic stem cell differentiation. *Nat Gen*. 44: 23–31.

Chapter 5: Conclusions, Future Directions and Final Remarks

5.1 Conclusions and Future Directions

The work in this dissertation describes our efforts to characterize the role of Cx43 in familial Cerebral Cavernous Malformations Type III and in the regulation of BBB permeability at large. In Chapter 2, we identified the overexpression of Cx43 in CCM3KD mBECs and pericytes and described that overactive GJIC and HC activity can be observed in CCM3KD mBECs. We demonstrated a striking rescue of CCM3KD monolayer permeability with GAP27-mediated inhibition of Cx43 GJIC. The characterization of Cx43 GJIC in the regulation of permeability in CCM3KD cells was extended to show that aberrant accumulation of Cx43 GJ plaques prevents proper distribution of ZO-1 to TJ structures and results in downstream consequences for the incorporation of claudin-5 into the TJs. In Chapter 3, we extended our evaluation of Cx43 in fCCM3 to a murine model based on the two-hit hypothesis of fCCM. In the course of our mouse studies, we established the important point that lesion permeability occurs prior to hemorrhage and that lesion permeability is a predictor of hemorrhage. Immunofluorescence study of lesion sections demonstrated that Cx43 expression is elevated in all lesion maturation stages and particularly high in developing, permeable lesions, adding weight to our findings in Chapter 1 – that elevated Cx43 expression is a direct contributing factor to loss of BBB integrity. Finally, in Chapter 4, we extended our analysis of Cx43 to mBEC biology outside of fCCM3 with the goal of determining what aspects of Cx43 overexpression were contributing factors to fCCM3 pathology. We demonstrate that the C-terminal Cx43 isoform of 20kDa likely arises from internal translation and that overexpression of 20-Cx43 in mBECs recapitulates many aspects of fCCM3 pathology observed in Chapter 2. Finally, we introduce the novel concept that elevated 20-Cx43 may directly regulate gene expression in mBECs.

To our knowledge, no previous study has provided a mechanistic description of how Cx43 may regulate BBB integrity and no study has examined Cx43 in fCCMs. Additionally, while many studies have examined the effect of ZO-1 on Cx43 GJ plaque stability and GJIC, no study has examined whether an opposite regulation exists by which Cx43 GJs can influence ZO-1 organization (1-3). Indeed, we have uncovered a novel mechanism by which accumulation of GJs plaques in CCM3KD cells leads to the preferential accumulation of ZO-1 at Cx43 GJs plaques and lack of ZO-1 incorporation into TJs. It is of interest for future study how Cx43 influences ZO-1 localization. In published studies, ZO-1 accumulates at Cx43 GJ plaque perimeter and signals plaque internalization (3). One hypothesis is that the internalization machinery of CCM3KD cells is incapable of internalizing the Cx43-ZO-1 complex, thus both Cx43 and ZO-1 continue to accumulate into the plaque. However, we observed with FRET analysis that Cx43 and ZO-1 interaction at the membrane is reduced, thus another potential explanation is that the signal regulating ZO-1 localization to Cx43 GJs for degradation are functional, but phosphorylation events guiding the Cx43-ZO-1 complex formation are absent, preventing their complexing and eventual degradation. This also would explain accumulation of ZO-1 at Cx43 plaques and is supported in part by our observation that GAP27-mediated inhibition of Cx43 GJIC reduces Cx43 GJ plaque size and is reported elsewhere to induce a conformational change in Cx43. Overall, the Cx43 regulation of ZO-1 is important given that targeting Cx43 degradation pathways may represent an alternative method outside of GAP27 treatment to inhibit Cx43 plaque formation and re-establish ZO-1 localization to TJs in fCCM3.

An initial goal of this dissertation was to address the question of what cell types of the NVU contribute to fCCM3 pathology. Endothelial cells are accepted to be the central cell type of origin for *ccm3* loss of function mutations and this is supported by mouse studies demonstrating that neuronal- and glial-specific CCM3KO mice have no disease penetrance (though they do have other pathologies including enlarged brains) (4-7). However, how the crosstalk between $ccm3^{-/-}$ endothelial cells and $ccm3^{+/-}$ pericytes and astrocytes promotes disease progression is still unknown. Cx43 was initially selected for study due to

its ability to directly link all cell types of the NVU. We demonstrate that Cx43 is also elevated in CCM3KD pericytes and GJIC between CCM3KD mBECs and CCM3KD pericytes remains intact and is observationally increased (Chapter 2) and that Cx43 is at minimum, expressed in lesion pericytes of *ccm3*$^{+/-}$*p53*$^{-/-}$ mice. A more refined study of Cx43 GJIC between mBECs and pericytes as well as more quantitative analysis of Cx43 expression levels in pericytes of *ccm3*$^{+/-}$*p53*$^{-/-}$ mice is of interest for future study. In particular, it is of great interest to examine the extent to which injury can be propagated from *ccm3*$^{-/-}$ mBECs to surrounding mBECs, pericytes and astrocytes. Other studies have demonstrated the ability of dying cells to kill surrounding cells via transfer of harmful molecules through Cx43 GJIC (8). In addition, Cx43 HC-dependent calcium waves have also been implicated in distant cell injury, thus increases to Cx43 HC activity in CCM3KD cells may represent an additional mechanism by which injury can be propagated from ccm3$^{-/-}$ cells to healthy cells (9, 10). The number of *ccm3*$^{-/-}$ cells required for lesion initiation is not known, however, if Cx43 GJs can truly propagate injury, the number of initiating cells required may be quite low, and may provide an explanation for new lesion appearance throughout the lifetime of an fCCM patient when it is unlikely to acquire second hits in multiple neighboring cells. Alternatively, Cx43 GJIC may facilitate the passage of toxic agents to genetically healthy cells that incite a second-hit. Finally, we observed that Cx43 expression was most robustly elevated in CCM3KD cells compared to CCM1- or CCM2KD cells. Cx43-mediated propagation of injury may explain why fCCM3 disease is the most aggressive subtype.

Another novel finding of this dissertation was the elevated expression of 20-Cx43 and its characterization in mBEC biology. Importantly, we observed similar functional behavior of CCM3KD and 213^{over} mBECs, including increased GJIC and HC activity, decreased monolayer permeability, TJ transcription and Cx43 depletion from the chromatin-bound fraction. Gene expression arrays indicated that 43- and 20-Cx43 overexpression cause transcriptional changes to genes also altered by CCM3KD. In particular, angiogenic and inflammatory pathways were elevated in CCM3KD, FL^{over} and 213^{over} mBECs

compared to control mBECs, and 20-Cx43 overexpression altered the expression of chromatin modification enzymes. Future studies will validate these findings as well as extend the study of altered transcripts to cell culture and mouse models to form a more cohesive picture of how 43- and 20-Cx43 regulate CCM3 pathogenesis. Further study of 20-Cx43 is difficult given the lack of available techniques for its study. Given that 20-Cx43 arises from internal translation, and thus the same transcript as full-length Cx43, transcript-depleting methods cannot be employed to knockdown 20-Cx43 without affecting 43-Cx43 expression. The same problem exists with techniques employing antibodies against the C-terminal tail of Cx43, such as immunoprecipitation and IHC of endogenous protein, given that the amino acid sequences are identical. It is not known if 20-Cx43 confers a different structure than the C-terminus of 43-Cx43, however, that may represent an opportunity for 20-Cx43-specific antibody development. While we successfully employed the strategy of using an N-terminal and C-terminal Cx43 antibody in the confirmation of the C-terminal origin of 20-Cx43 via Western blotting, we have not been successful in identifying N-terminal/C-terminal antibody pairings that are compatible with IHC. If new antibodies become available, N-terminal/C-terminal IHC comparison can be used to differentiate between 43-Cx43 and 20-Cx43 localization (regions where there is no co-staining of N- and C-terminal antibodies would be indicative of 20-Cx43 staining). Additional future strategies to study 20-Cx43 are discussed in the Chapter 4 discussion.

In an effort to identify disease mechanisms unique to fCCM3, we determined that Cx43 protein is also upregulated in CCM1KD and CCM2KD cells, however, to a much lesser extent than CCM3KD cells. Functional characterization of Cx43 in CCM3KD cells has indicated that future work into CCM3 pathways mediating Cx43 function should focus on events regulating the accumulation of GJ plaques. Two candidate pathways based on the literatures are a STRIPAK-PP2A-Cx43 pathway and STRIPAK-ERK1/2-Cx43 pathway. Previous work in the lab identified increased basal activation of ERK1/2 downstream of CCM3 and the STRIPAK complex and ERK1/2 is reported to phosphorylate Cx43 at inhibitory residues and inhibit the

internal translation pathway, both in opposition to Cx43 behavior in CCM3KD cells (11). However, these studies may represent cell type-specific pathways and thus are worth pursuing. Preliminary experiments not included in this dissertation examined whether ERK1/2 lies in the CCM3-Cx43 axis and demonstrated that ERK1/2 inhibition decreased 43-Cx43 and 20-Cx43 expression as well as GJIC, however, these results need to be validated with additional experiments. The STRIPAK resident phosphatase PP2A is also a promising candidate. It is reported in the literature to dephosphorylate Cx43 to promote trafficking to the membrane (12). Loss of CCM3 from the STRIPAK complex may result in over-activated PP2A in a mechanism similar to over-activated Mst4, such that instances of PP2A dephosphorylation of Cx43 in CCM3KD cells are higher than in control cells. An experiment examining PP2A inhibition and GJ plaque formation or GJIC will be informative to prove or disprove this hypothesis.

Additional mouse models may be helpful in future studies examining Cx43 in fCCM3. Cx43 knockout (Cx43KO) mice die shortly after birth due to cardiac defects, however $Cx43^{fl/fl}$ mice are available (13, 14). Conditional global and endothelial-specific Cx43 KO mice principally exhibit altered bone formation – consistent with human ODDD – and non-fatal cardiac pathologies including bradycardia (15, 16). It would be informative to determine whether induction of Cx43 deletion in a ccm3+/-p53-/-Cx43fl/fl mouse ameliorates lesion development or hyperpermeability. Brain endothelial permeability in Cx43KO mice has not been examined. Cx43 transgenic mice are also available, though with reduced post-natal viability due to cardiac malformations (17). As with Cx43KO mice, brain endothelial cell permeability has not been studied in Cx43 transgenic mice. Such studies would complement our *in vitro* work characterizing Cx43's role in brain endothelial biology. Additionally, while no 20-Cx43 transgenic mouse exists, the development of this mouse model would ultimately allow for characterization of 20-Cx43 overexpression in mice. In particular, a full length Cx43-deleted, 20-Cx43 transgenic model would enable identification of biological roles for 20-Cx43 without interference of 43-Cx43, presuming these mice are viable. Finally, it is important to note that CCM3KO mice are embryonic lethal due to cardiac defects, and while

cardiopathies are not described in human fCCM patients, these phenotypes add support to the regulation of Cx43 by CCM3.

Finally, the overall goal of this dissertation was to identify signaling pathways regulated by CCM3 that may represent a therapeutic target. Based on our results as a whole, we believe that targeting Cx43 expression, and particularly Cx43 GJIC, represents a potential therapeutic strategy for fCCM3. Immediate future experiments to validate the potential of Cx43 GJIC inhibitor GAP27 will examine the ability of GAP27 treatment to decrease *ccm3*$^{+/-}$*p53*$^{-/-}$ lesion burden, permeability and hemorrhage. We are hopeful that the GAP27 or derivative peptides will be effective, as they have the advantage of targeting the extracellular loop of Cx43, potentially allowing it to be a more feasible option given that it does not require cellular uptake.

5.2 Final remarks

The pursuit of this dissertation has resulted in the identification of novel disease mechanisms in fCCM3 and has introduced Cx43 GJs as central components to brain endothelial barrier occlusion. We have laid an intellectual and technical foundation for the future study of Cx43 in fCCM3 and additional cerebrovascular pathologies.

5.3 References

1. Toyofuku T, Yabuki M, Otsu K, Kuzuya T, Hori M, Tada M (1998) Direct Association of the Gap Junction Protein Connexin-43 with ZO-1 in Cardiac Myocytes. Journal of Biological Chemistry 273:12725–12731.

2. Giepmans BN, Moolenaar WH (1998) The gap junction protein connexin43 interacts with the second PDZ domain of the zona occludens-1 protein. Current Biology, 8:931-934.

3. Segretain D, Fiorini C, Decrouy X, Defamie N, Prat J, Pointis G (2004) A proposed role for ZO-1 in targeting connexin 43 gap junctions to the endocytic pathway. Biochimie 86:241–244.

4. Chan AC, Drakos SG, Ruiz OE, Smith AC, Gibson CC, Ling J, Passi SF, Stratman AN, Sacharidou A, Revelo P, Grossmann AH, Diakos NA, Davis GE, Metzstein MM, Whitehead KJ and Li DY. (2011) Mutations in 2 distinct genetic pathways result in cerebral cavernous malformations in mice. *J Clin Invest*. 121:1871–1881

5. He Y, Zhang H, Yu L, Gunel M, Boggon TJ, Chen H and Min W. (2010) Stabilization of VEGFR2 Signaling by Cerebral Cavernous Malformation 3 Is Critical for Vascular Development. *Science Signaling* 3**:**ra26.

6. Louvi A, Chen L, Two AM, Zhang H, Min W, Gunel M (2011) Loss of cerebral cavernous malformation 3 (Ccm3) in neuroglia leads to CCM and vascular pathology. Proceedings of the National Academy of Sciences 108:3737–3742.

7. Louvi A, Nishimura S and Günel M. (2014) Ccm3, a gene associated with cerebral cavernous malformations, is required for neuronal migration. *Development* 141:1404-1415.

8. Lin JH, Weigel H, Cotrina ML, Liu S, Bueno E, Hansen AJ, Hansen TW, Goldman S and Nedergaard M. (1998) Gap-junction-mediated propagation and amplification of cell injury. *Nat Neurosci* 1(6).

9. De Bock M, Wang N, Decrock E, Bol M, Gadicherla AK, Culot M, Cecchelli R, Bultynck G, Leybaert L. (2013) Endothelial calcium dynamics, connexin channels and blood–brain barrier function. *Prog Neurobiol* 108:1–20.

10. Zhang J, O'Carroll SJ, Henare K, Ching LM, Ormonde S, Nicholson LF, Danesh-Meyer HV, Green CR. (2014) Connexin hemichannel induced vascular leak suggests a new paradigm for cancer therapy. *FEBS Letters* 588:1365–1371.

11. Stamatovic SM, Sladojevic N, Keep R, Andjelkovic AV (2015) PDCD10 (CCM3) regulates brain endothelial barrier integrity in cerebral cavernous malformation type 3: role of CCM3-ERK1/2-cortactin cross-talk. *Acta Neuropathol* 130:731–750.

12. Wu J, Taylor RN, Sidell N (2013) Retinoic Acid Regulates Gap Junction Intercellular Communication in Human Endometrial Stromal Cells Through Modulation of the Phosphorylation Status of Connexin 43. Journal of Cellular Physiology 228: 903–910.

13. Reaume AG, De Sousa PA., Kulkarmi S, Langille BL, Zhu D, Davies TC, Juneja SC, Kidder GM, Rossant J (1995). Cardiac malformation in neonatal mice lacking connexin43. *Science* 267: 1831–834.

14. Ya J, Erdtsieck-Ernste EB, de Boer PA, van Kempen MJ, Jongsma H, Gros D, Moorman AF, Lamers WH (1998). Heart defects in connexin43-deficient mice. *Circ Res* 82:360–66.

15. Liao Y, Day KH, Damon DN, Duling BR (2001). Endothelial cell-specific knockout of connexin 43 causes hypotension and bradycardia in mice. *Proc Natl Acad Sci U S A*. 98:9989-94

16. Chaible LM, Sanches DS, Cogliati B, Mennecier G, Dagli MLZ (2011).Delayed Osteoblastic Differentiation and Bone Development in Cx43 Knockout Mice. *Toxicologic Pathol*. 39:1046-1055.

17. Ewart JL, Cohen MF, Meyer RA, Huang GY, Wessels A, Gourdie RG, Chin AJ, Park SM, Lazatin BO, Villabon S, Lo CW. (1997) Heart and neural tube defects in transgenic mice overexpressing the Cx43 gap junction gene. *Development* 124:1281-92.